

AD-A107 455

NAVAL POSTGRADUATE SCHOOL MONTEREY CA

F/G 20/9

A COMPUTER ANALYSIS OF THE PLASMA-BOUNDARY LAYER BEHAVIOR OVER --ETC(U)

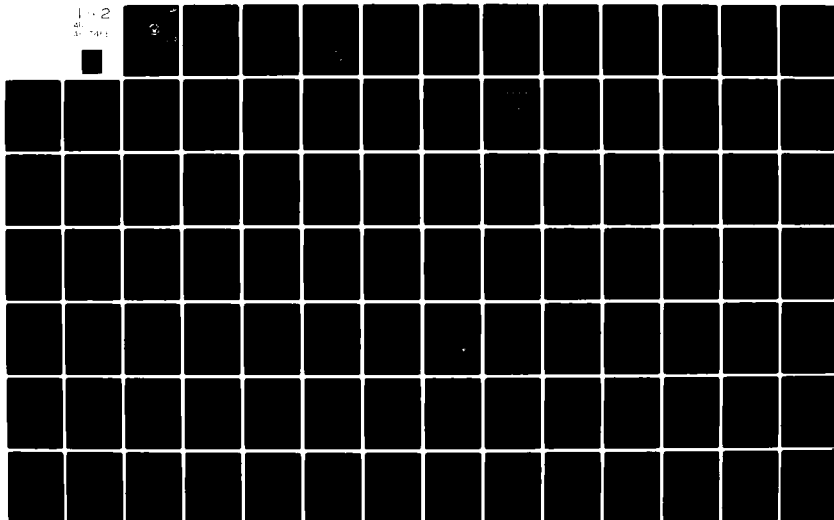
JUN 81 S T VAN BROCKLIN

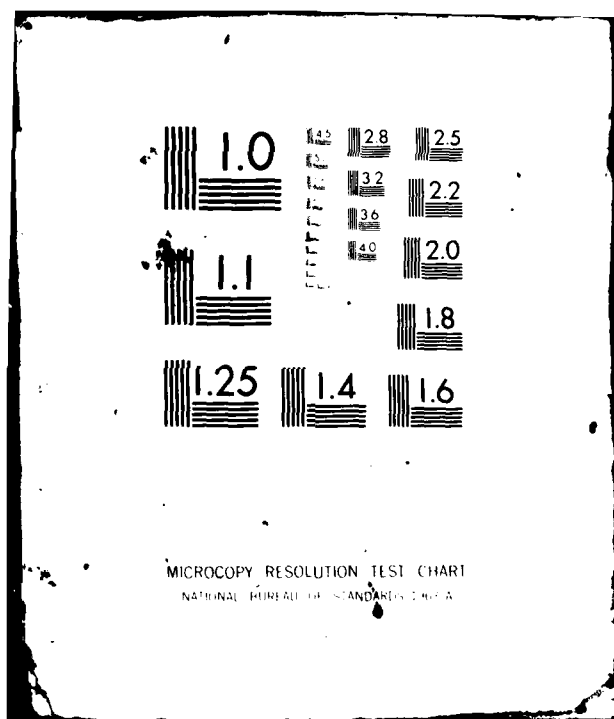
UNCLASSIFIED

NL

1-2

41
3-7411





AD A107455

NAVAL POSTGRADUATE SCHOOL
Monterey, California

LEVEL



DTIC
ELECTE
NOV 19 1981
S D

THESIS

A COMPUTER ANALYSIS OF THE PLASMA-BOUNDARY LAYER
BEHAVIOR OVER A POSITIVE ELECTRODE

by

Stephen Ted Van Brocklin

June 1981

Thesis Advisor:

O. Biblarz

Approved for public release; distribution unlimited

DTIC FILE COPY

81 11 18 029

UNCLASSIFIED

SECURITY CLASSIFICATION OF THIS PAGE (When Data Entered)

REPORT DOCUMENTATION PAGE		READ INSTRUCTIONS BEFORE COMPLETING FORM
1. REPORT NUMBER	2. GOVT ACCESSION NO.	3. RECIPIENT'S CATALOG NUMBER
	ADA107453	
4. TITLE (and Subtitle)		5. TYPE OF REPORT & PERIOD COVERED
A Computer Analysis of the Plasma-Boundary Layer Behavior Over a Positive Electrode .		Engineer's thesis June 1981
		6. PERFORMING ORG. REPORT NUMBER
7. AUTHOR(s)		8. CONTRACT OR GRANT NUMBER(s)
Stephen Ted Van Brocklin		Master's thesis
9. PERFORMING ORGANIZATION NAME AND ADDRESS		10. PROGRAM ELEMENT, PROJECT, TASK AREA & WORK UNIT NUMBERS
Naval Postgraduate School Monterey, California 93940		
11. CONTROLLING OFFICE NAME AND ADDRESS		12. REPORT DATE
Naval Postgraduate School Monterey, California 93940		June 1981
		13. NUMBER OF PAGES
		159 (12) 160
14. MONITORING AGENCY NAME & ADDRESS (if different from Controlling Office)		15. SECURITY CLASS. (of this report)
Naval Postgraduate School Monterey, California 93940		
		16a. DECLASSIFICATION/DOWNGRADING SCHEDULE
16. DISTRIBUTION STATEMENT (of this Report)		
Approved for public release; distribution unlimited		
17. DISTRIBUTION STATEMENT (of the abstract entered in Block 20, if different from Report)		
18. SUPPLEMENTARY NOTES		
19. KEY WORDS (Continue on reverse side if necessary and identify by block number)		
anode regions electron beam discharge electrical lasers sheath and ambipolar regions electrode boundary layers		
20. ABSTRACT (Continue on reverse side if necessary and identify by block number)		
A stable numerical procedure for solving the coupled, nonlinear equations of electron and ion conservation and electrical potential (Poisson's equation), is described. A two-dimensional model with periodic active sites on a flat plate is utilized to obtain both qualitative and quantitative results which clearly illustrate the self-generating sheath and ambipolar regions adjacent to a non-emitting electrode. The active sites are characterized as voltage sources and by electron densities depressed from both the non-active wall and the free-stream values.		

DD FORM 1 JAN 73 1473

EDITION OF 1 NOV 65 IS OBSOLETE
S/N 0102-014-6601

UNCLASSIFIED

SECURITY CLASSIFICATION OF THIS PAGE (When Data Entered)

UNCLASSIFIED

SECURITY CLASSIFICATION OF THIS PAGE/When Data Entered

Various cases of species density at the nonactive wall are evaluated. Recombination/ionization plays an important role in establishing the boundary layer behavior in the ambipolar region and in the dimensionality of the problem formulation. Application is for Nitrogen gas at one amagat in pulsed discharge of about 50 micro-seconds in duration.

Results clearly demonstrate the boundary layer nature of the species density at the electrode. A sheath length of 38 microns about a 35-volt active site and 5-20 microns along the non-active portion of the electrode is established. Joule heating is determined to be not important.

Accession For	
NTIS GRA&I	<input checked="checked" type="checkbox"/>
DTIC TAB	<input type="checkbox"/>
Unannounced	<input type="checkbox"/>
Justification	
By	
Distribution/	
Availability Codes	
Dist	Avail and/or Special
A	

Approved for Public Release, Distribution Unlimited

A Computer Analysis of
the Plasma-Boundary Layer Behavior
Over a Positive Electrode

by

Stephen Ted Van Brocklin
Lieutenant Commander, United States Navy
B.S., Clarkson College, 1969
M.S., University of West Florida, 1971
M.S., Naval Postgraduate School, 1980

Submitted in partial fulfillment of the
requirements for the degree of

AERONAUTICAL ENGINEER

from the
NAVAL POSTGRADUATE SCHOOL
June 1981

Author

Steph Ted Van Brocklin

Approved by:

Oscar Bublary

Thesis Advisor

F. Schmirer

Second Reader

M. F. P. L. P.

Chairman, Department of Aeronautics

William M. L. L.

Dean of Science and Engineering

ABSTRACT

A stable numerical procedure for solving the coupled, nonlinear equations of electron and ion conservation and electrical potential (Poisson's equation), is described. A two-dimensional model with periodic active sites on a flat plate is utilized to obtain both qualitative and quantitative results which clearly illustrate the self-generating sheath and ambipolar regions adjacent to a non-emitting electrode. The active sites are characterized as voltage sources and by electron densities depressed from both the non-active wall and the free-stream values. Various cases of species density at the nonactive wall are evaluated. Recombination/ionization plays an important role in establishing the boundary layer behavior in the ambipolar region and in the dimensionality of the problem formulation. Application is for Nitrogen gas at one amagat in a pulsed discharge of about 50 micro-seconds in duration.

Results clearly demonstrate the boundary layer nature of the species density at the electrode. A sheath length of 38 microns about a 35-volt active site and 5-20 microns along the non-active portion of the electrode is established. Joule heating is determined to be not important.

TABLE OF CONTENTS

I.	INTRODUCTION-----	10
A.	BACKGROUND-----	10
B.	REVIEW OF PREVIOUS WORK-----	13
C.	OBJECTIVES OF THE PRESENT STUDY-----	18
II.	PROBLEM FORMULATION-----	21
A.	GOVERNING EQUATIONS-----	21
B.	BOUNDARY CONDITIONS-----	23
C.	PARAMETERS OF THE DISCHARGE MEDIUM-----	25
III.	PROBLEM SOLUTION-----	27
A.	PROBLEM SIMPLIFICATION (PHYSICS)-----	27
B.	WORKING EQUATIONS-----	33
C.	NUMERICAL METHODOLOGY-----	34
IV.	RESULTS-----	38
A.	GENERAL DISCUSSION-----	38
B.	EFFECTS OF NET PRODUCTION-----	40
C.	DISCUSSION OF RESULTS-----	43
V.	CONCLUSIONS AND RECOMMENDATIONS-----	78
A.	REVIEW OF ASSUMPTIONS-----	78
B.	PHYSICAL CONCLUSIONS-----	79
C.	NUMERICAL CONCLUSIONS-----	82
D.	RECOMMENDATIONS-----	83
APPENDIX A: CHARACTERISTIC PARAMETERS-----		85

APPENDIX B:	DEVELOPMENT OF THE PRODUCTION TERM-----	91
APPENDIX C:	NUMERICAL SOLUTION METHOD-----	95
APPENDIX D:	DESCRIPTION OF COMPUTER PROGRAMS-----	102
APPENDIX E:	COMPUTER PROGRAM LISTINGS-----	108
	LIST OF REFERENCES-----	154
	INITIAL DISTRIBUTION LIST-----	157

TABLE OF SYMBOLS

English Letters And Symbols

A	matrix of coefficients (Eq. C10)
C_{1-3}	non-dimensionalizing terms (Eqs. 6, 7 and 8)
D_s	diffusion coefficient of species-s
E	electric field
e	electron charge ($1.602 \cdot 10^{-19}$ coulombs)
f	namely $f(x) \dots$ a function of x (App. C)
J	current (amps/m ²)
J	Jacobian (Eq. C5)
k	Boltzmann's constant ($1.38 \cdot 10^{-23}$ V-coul/°K)
L	characteristic diffusion length
l_p	characteristic production length
n^*, N	stationary density state (App A, Sec C)
n_s	number density of species-s (m ⁻³)
p_s	pressure of species-s ($p_s = n_s k T_s$)
Re	Reynolds number
s	subscript denoting electron or ion species
T_s	temperature of species-s
u	velocity vector
v_d	drift velocity (Sec. III.A.1)
\bar{v}_s	average thermal velocity (App A, Sec C)
v_∞	free-stream velocity in the y-direction

Z degree of ionization ($Z=1$ in this study)
 z column vector of solution set ϕ, n_e, n_i

Greek Characters and Symbols

α thermal diffusivity (Sec. III.A.3)
 α_i recombination rate coefficient (App. B)
 β ratio of electron to the background gas temperature
 δ velocity boundary layer thickness (Sec. III.A.3)
 ϵ_0 permittivity of free space (8.854×10^{-12} F/m)
 λ_s characteristic sheath length
 μ_s mobility of species-s
 ν dynamic viscosity (Sec. III.A.3)
 ν_i ionization rate coefficient (App. B)
 ϕ voltage potential (volts)
 Φ functional defined in App. C, to be minimized.
 τ characteristic time
 τ_p characteristic net production time
 ∞ refers to the free-stream condition
 ∇ mathematical gradient operator
 Σ mathematical summation
 \wedge "caret" indicating a non-dimensional term
 Δ "delta" indicating a small increment or change

ACKNOWLEDGEMENTS

I extend my gratitude to Professor O. Biblarz, who as my thesis advisor and friend, provided expert assistance, guidance and inspiration. With his direction and special counsel the objectives of this work were met and are compiled in these pages.

I wish also to thank Professor A.W. Cooper of the Physics Department; who, beyond his own very busy schedule found time to provide individual tutoring and background for my thesis. To Professor F.R. Schwirzke, also of the Physics Department, I extend my gratitude for his academic assistance and for his inspiration to follow on work.

Finally, I reserve special mention to my wife Connie and our two sons, Andy and Mark; who, while competing with the computer for my attention, provided the necessary moral support to complete the job.

I. INTRODUCTION

A. BACKGROUND

Losses at the electrode boundary regions play an important role in high energy density molecular gas flow lasers. Of particular interest to this study is the Carbon-Dioxide glow-discharge plasma, of which Nitrogen is the principal energy bearing constituent.

The main energy loss mechanisms in a collision dominated plasma are found in the sheath and ambipolar regions. The sheath voltage loss occurs directly as a result of Debye shielding, which creates a space charge layer abutting an electrode or wall. The ambipolar losses are associated with ambipolar diffusion, relating to the charged species density being less than the free-stream or equilibrium density. This loss exists even in the absence of current flow.

An initial premise of probe theories that takes account of collisions between charged particles, atoms and molecules, is that the plasma is quasi-neutral up to a certain distance from the probe and that the electric fields are localized within a narrow sheath region adjacent to the surface of the probe. The problem of making the transition

from the quasi-neutral solution to the sheath solution was usually resolved through matching techniques. The description of a collision dominated sheath together with the quasi-neutral ambipolar region presents an imposing set of coupled nonlinear partial differential equations, for which there exists no known exact solution. This study reports a numerical method that describes the sheath and ambipolar regions in a self-consistent fashion.

In the hydrodynamic approximation (i.e., collision dominated), the dimensions of the space charge region " λ_s " (the sheath length) is larger than the mean free path " λ " of the species particles. Additionally the sheath characteristic length is very much smaller than the characteristic length of the plasma boundary layer. This puts our study in the collisionally thin sheath region, [Ref. 1].

However, the plasma is not considered to be in thermal equilibrium. In fact for plasmas in thermal nonequilibrium, the electron temperature is governed by the electron energy equation, which includes the effects of the electron energy-conduction and electric field as well as collisional energy exchange between electrons and heavy-gas particles. The consideration of negligible energy exchange during collisions (thermally frozen) does not generally result in a

constant electron temperature (T_e); particularly in the sheath region, even if other properties such as the ion temperature (T_i) are constant. Therefore the electron energy equation is necessary even in the case of the thermally frozen situation.

An ionizer/sustainer discharge pumped laser requires that relatively high E/n values be distributed as uniformly as possible throughout the bulk of the gas medium. The electrode regions however represent a substantially higher and more inhomogeneous E/n which may impose an instability on the remainder of the discharge. In the region of the electrode, the E/n is significantly higher than the undisturbed plasma. In this region the elevated electron temperature, which is a direct function of the sustainer field, will increase ionization, which could lead to arcing and breakdown.

In the so-called vacuum arc [Ref. 2], anode spots appear under certain operating conditions. These anode spots are of practical importance, having been also observed in high density plasmas [Ref. 3]. They are typically micron or sub-micron sized protrusions on the electrode surface, which act to "focus" the electric field and current stream lines. Primary consideration here is with the anode.

B. REVIEW of PREVIOUS WORK

1. Physics

Most work on sheath phenomena is embodied in "probe" theory investigations, where the effects of the electrode (probe) locally disturb the quiescent plasma. Such work is relevant to this study since the anode is essentially a heavily biased probe in contact with the plasma, which is quiescent within the sheath region.

Analyses of electrostatic probes in collision dominated plasmas were originally done by assuming that a quasi-neutral diffusion controlled region extended to within one mean free path of the probe where it was matched to the edge of the free fall-sheath. No provision was made for a transition region between the two regimes [Ref. 4].

Shultz and Brown [Ref. 5] studied the transition from a collisionless to collision dominated sheath through charged species collection with a spherical probe. Postulating different physical models for cases ranging from a collisionless sheath to a sheath with many collisions, semi-empirical formulas were obtained in each instance. Several other authors attempted matching the solution in the collision dominated region directly to that of the free-fall sheath using variational principles.

The previously mentioned techniques can be criticized, because in each of these methods something was forced to fit. In other words, at least one derivative was discontinuous at some artificially imposed boundary, thereby raising doubt as to the validity of the results.

The first systematic analysis of probes in collision dominated plasmas were carried out by Cohen [Ref. 6] and Su and Lam [Ref. 7], who assumed the continuum equations valid throughout the plasma, including to the probe surface. As a consequence of these analyses, both the sheath and the quasineutral regions appeared naturally from the diffusion equations in the limit as the ratio of probe size to Debye length approached infinity. The continuum model removed the concern about forcing sets of equations to match at the edge of an arbitrarily assumed sheath. These authors restricted the problem to an isothermal plasma, but as will be shown here, the electron temperature may vary significantly in the neighborhood of the probe for most discharges of interest.

Radbill [Ref. 8] quasilinearized the continuum equations, and solved with numerical integration, obtaining results that agreed with those of Cohen where comparison could be made.

In the previous analyses, not only was the isothermal plasma assumed, but the plasma was so slightly ionized that only charge-neutral interactions needed to be taken into account. However, for highly nonequilibrium plasmas, charge-charge collisions play an important role [Refs. 9 and 10]. The effects of collisions between charged particles manifest themselves as volume ionization, volume recombination and the dependence of the transport coefficients on charged particle density and temperature and, therefore on position. Barad [Ref. 11] cites a specific example,

"If the electrons have a temperature of 2500 °K, then the ionization fraction equal to about 10^{-5} will result in charge-charge collisions occurring one-tenth as frequently as charge-neutral collisions. It is shown... that for such a degree of charge-charge interaction, significant effects are felt."

Chung, Talbot and Touryan [Ref. 1], in an extensive review of probe studies, state that no general solution is available for determining charge density and species temperature for probes small in comparison to the hydrodynamic boundary layer thickness.

Dolson [Ref. 12] investigated the nature and extent of the voltage drops in the vicinity of magnetohydrodynamic (MHD) non-emitting electrodes, in particular the losses attributable to the sheath. Under his conditions the nonexistence of a one-dimensional sheath solution is shown, and a

computer model with two-dimensional, periodic active sites representing a flat plate electrode is developed. With this model the effects of a magnetic field and Joule heating are studied and the results are compared with experimental observations reported by Argyropoulos (1973), and Sonju and Teno (1974), [Refs. 13, 14].

An extension of Dolson's work is reported in 1980 [Ref. 15], for application to ionizer/sustainer discharges. The role of electron pressure is introduced along with net ionization and recombination, which proves necessary in establishing truly boundary-layer behavior for the charged species profiles. Additionally, a modified Newton-Raphson computational procedure, which enables much faster solution convergence is formulated. That study demonstrates solutions with non-active wall densities depressed from the free stream density, a result Dolson did not accomplish. Results were for 10 volts of electrode potential fall, an increase from 5.0 volts reported by Dolson.

2. Computational Methods

The fundamental difficulty in the development of computational models for the prediction of plasma flow phenomena lies in the coupling of equations governing both the gasdynamic flow and the electromagnetic (EM) fields. Since

the flow fields can affect the EM fields (and vice-versa), the nonlinear partial differential equations must be solved simultaneously and the formulation of the problem becomes complicated. In the present study the flow properties are decoupled from the the charged species conservation equation and Poisson's Equation.

The approaches used in the solution of plasma flow phenomena are quickly reviewed below so as to point out the background of the the approach in this study. This problem is typical to those dealing with plasma-boundary layer phenomena. Approaches to solving the general plasma flow problems have consisted of the following;

- (a) One dimensional "influence coefficients."
- (b) One-dimensional closed form analytic solutions to ordinary differential equations.
- (c) Similarity transformation and closed form solutions to a modified differential equation in one- or two-dimensions.
- (d) One-, two-, or three-dimensional numerical solution to the uncoupled steady plasma flow phenomena equations.
- (e) One-, two-, or three-dimensional numerical solution to the coupled steady plasma flow phenomena equations

using either the magnetic induction equation or the elliptic equation governing the electric fields.

- (f) One-, two-, or three-dimensional transient numerical solution to the coupled plasma flow phenomena equations using either the magnetic induction or the elliptic equation.

Methods (a) through (c) are exact but are restricted to a narrow range of problems. Approaches (d) and (e) provide rapid convergence to a steady state solution but do not consider the transient behavior between the gasdynamic and electromagnetic fields, or often the strong coupling between the two sets of fields. Method (f) is most desirable since it treats a wide range of problems, but suffers from large computational times [Ref. 16]. The approach of this study is characterized as a method (e) approach.

C. OBJECTIVES OF THE PRESENT STUDY

The objective of this study is to demonstrate a numerical procedure which can model the physical behavior of a conducting fluid, as would be generated in the after-glow of an electron beam discharge laser, under the influence of electric forces. Calculations are performed in two dimensions, with a flat plate non-emitting electrode (anode) which has periodic active sites. These active sites

facilitate current constriction required to satisfy charge continuity, Ohm's law, and Poisson's equation. The physical model is idealized in Fig. 1.

The controlling equations are solved for the potential, the charged species density distributions, electron temperature and current in the vicinity of the electrode. The resulting computer programs generate sheath and ambipolar regions in a self-consistent fashion, using the same set of equations throughout the field. The size of the sheath and the voltage drop attributable to its shielding effects are investigated.

This work does not consider those phenomena that lead to the arc discharge, which results from thermal instabilities. The constriction at the anode is purely that required to satisfy continuity.

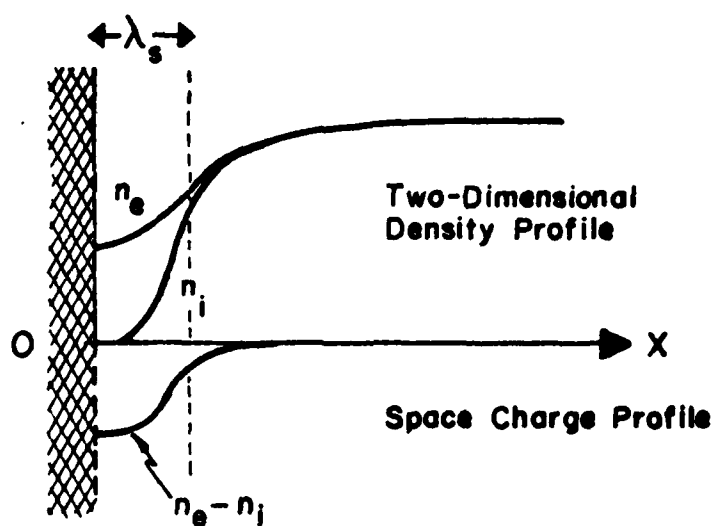
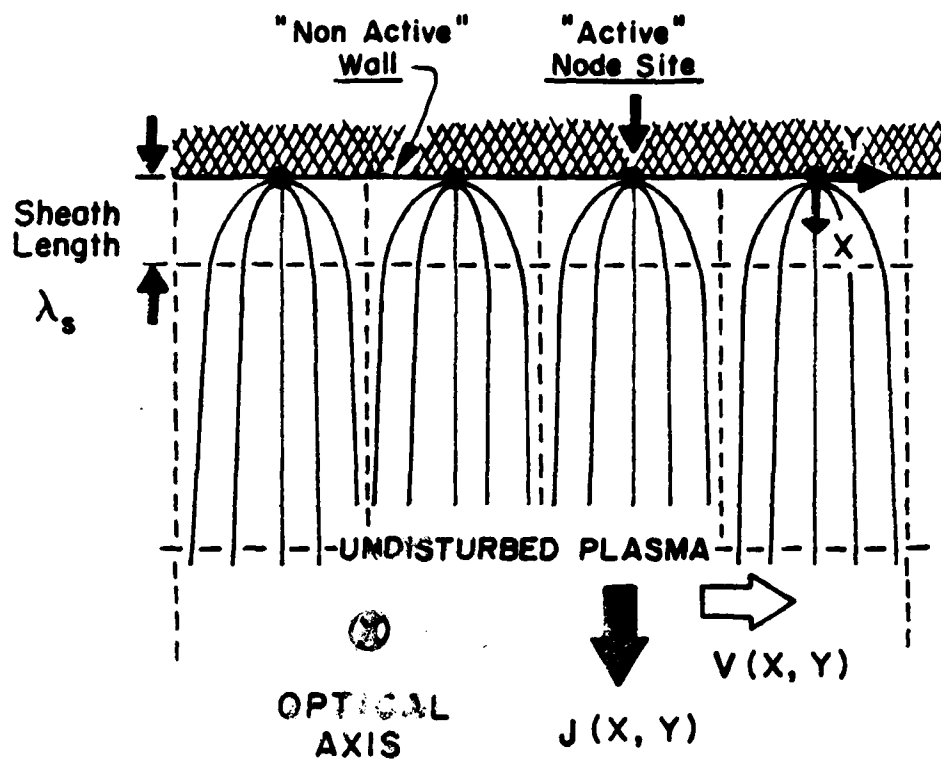


Figure 1

Two-Dimensional Model with Periodic Current Constriction.

II. PROBLEM FORMULATION

A. GOVERNING EQUATIONS

The governing equations that describe the electrode region portion of the plasma, consist of Poisson's equation, species conservation and electron energy equation, in addition to the overall continuity, momentum and energy equations of the plasma. These overall plasma equations are essentially those of the background gas since the plasma is weakly ionized (less than 0.01 %).

We have [Ref. 1];

Poisson equation...

$$\nabla^2 \phi = \frac{e}{\epsilon_0} (n_e - \sum z_i n_i) \quad (1)$$

electron conservation...

$$u \cdot \nabla n_e - \nabla \cdot \left[D_e \left(\frac{n_e}{p_e} \nabla n_e - \frac{e}{kT_e} n_e \nabla \phi \right) \right] = \dot{n}_e \quad (2)$$

ion conservation...

$$u \cdot \nabla n_i - \nabla \cdot \left[D_i \left(\frac{n_i}{p_i} \nabla p_i + \frac{e}{kT_i} n_i \nabla \phi \right) \right] = \dot{n}_i \quad (3)$$

In gas discharges, the electron energy distribution is known to be non-Maxwellian. In order to allow for non-Maxwellian distributions and still retain use of a temperature concept, an empirical fit to the calculated relation of electron temperature as a function of E/n is used in the representation of the electron temperature (see Sec. III.A). The concept of a "two-temperature" plasma is preserved but no restrictions are made on the energy distribution function of the electrons. In addition to the assumption of a functional dependence of the electron temperature upon E/n only, there is no representation of an external magnetic field and, in particular the internal or self-generated magnetic fields are not considered. The overall gas temperature is assumed constant and in equilibrium with the plasma ions. The bulk energy equation is assumed to have little bearing on this study, since there is negligible gas heating as discussed in Section III.A. This effectively uncouples overall energy consideration from the problem.

The electrodes serve the purpose of sustaining the E/n to pump the laser medium. No account is made of an external E-beam or other source of primary ionization. Simply, the medium may be considered to exist in an afterglow state.

The production term (i.e., the right hand side) in Eqns. (2) and (3) has been described utilizing measured and theoretical results of the rate coefficients for Nitrogen ionization and two-, and three-body recombination. The production term is expressed as;

$$\dot{n}_e = \gamma_i n_e - \alpha_1 n_e n_i - \alpha_2 n_e^2 n_i - \alpha_3 n_e n_i n_o \quad (4)$$

where " γ_i ," and " α_i " are respectively the ionization and recombination rate coefficients.

B. BOUNDARY CONDITIONS

In the customary boundary-value problem in fluid mechanics, a two-dimensional flat plate is assumed. A similar two-dimensional Cartesian description is used in the present work, which has been found to be the minimum suitable description for the problem posed, [Refs. 3, 12, 15]. No one-dimensional solution exists for the frozen flow of charges through a collisional sheath, since a Cartesian geometry in one dimension is devoid of the necessary geometric decrease of current density away from the electrode, as there would be in a cylindrical or spherical geometry.

Convection is considered negligible, as can be demonstrated by comparing fluid velocity with the drift velocity.

Electron and ion densities are determined at the plasma edge, knowing the state of the medium. A current balance can be used to establish the species densities resident at the active portion of the anode. An electrode voltage drop is determined from the properties of the medium; e.g., the effective ionization energies of the gas in particular. Since current constricts, there must be regions of the flat plate that receive no current. The inactive portion of the flat plate merits attention, especially in the regions adjacent to the active anode site. Species concentration along the inactive portion of the wall can vary, depending on the reactivity (catalytic properties) of the wall. There is a balance that can be established between the voltage variation normal to the wall, and the species concentration at the wall together with the species variation normal to the wall. A zero concentration of electrons and/or ions at the wall is an acceptable boundary-condition; which is to say that the wall acts as a perfect sink for the charged species. A detailed kinetic-theory analysis shows that there is in fact a lower bound to the electron and ion concentrations at the wall [Ref. 17]. In any case, there is no current into or out of the inactive wall, (see Fig. 1). This is discussed later in Sect. IV.

The remaining portion of the boundary conditions refer to the free stream medium, and are easily established.

C. PARAMETERS OF THE DISCHARGE MEDIUM

The application of this study is for molecular Nitrogen at one amagat, where the gas temperature is 273 °K. Other pertinent parameters follow;

Electric Field: 1.5 to 15 KV/cm.

Electron Density: 10^{+17} to 10^{+19} m^{-3} .

Electrode Voltage Drop: 35 volts.

The electron energy relation is, as mentioned, a curve fit from experimental results [Ref. 18], carried out by R.W. Compton and D.J. Sutton (1952). Since cross-section data for electrons in Nitrogen discharges are available [Ref. 19], the electron temperature and diffusion coefficient are readily determined, and representable as a function of E/n .

The ion temperature is assumed to follow that of the neutral gas. An electrode potential fall of about 35 volts may be assumed since it is the effective ionization energy for Nitrogen gas and, therefore, the anode fall [Ref. 20].

The cathode is more complicated to describe because of the requirement of surface electron emission. The cathode fall in cold cathodes is of the order of 250 volts, and is considerably less in thermionic cathodes. A proper

III. PROBLEM SOLUTION

A. PROBLEM SIMPLIFICATION (PHYSICS)

There are a number of simplifications that are incorporated in the problem description. Namely;

- Steady state conditions (within the pulse time).
- No magnetic fields.
- Negligible convection.
- Negligible Joule heating, $T_i = T_e = \text{constant}$.

However, specific account is made of;

- Ionization/recombination.
- Electron pressure.

These are discussed in part in this section.

1. Convection

The ambipolar region is the transition region from the sheath to the undisturbed plasma and can perhaps span the boundary layer. This fact requires some consideration of the presence of convective effects.

From the ion species conservation equation (Eq. 3), for example, we know that in the ambipolar region the last term of the left hand side is small compared to electric conduction. Now we need only to compare the convection with

the conduction, or simply the fluid velocity with the drift velocity.

$$v = v_{\infty} R_e^{-1/2} \approx 0.1 \text{ to } 1.0 \text{ m/sec}$$

where the Reynolds number (R_e) is 10^4 to 10^6 and the free stream velocity is 10 to 100 m/s. Now the drift velocity may be approximated by

$$v_d \approx \mu E_{\infty} = 10 \text{ to } 100 \text{ m/s}$$

for $E = 10^5$ to 10^6 V/m and the mobility $\mu = 10^{-4}$ m²/s/volt. Clearly, in the presence of a relatively strong interelectrode field, the contribution of ion convection due to a cross flow should be negligible. The geometrical orientation of the discharge with respect to the primary flow can thus become an important consideration.

2. Density Boundary Layer Formation Time

The charged-species density profiles change in a more complicated manner than either the voltage potential or the electric field. The magnitude of the ion and electron densities may change appreciably within the sheath; moreover, fractional analysis is risky because inflections are present in the profiles. A discussion pertaining to the stability of the ambipolar region and its boundary layer nature is presented in detail by Biblarz, et al., [Ref. 15]. However, Appendix A shows that the characteristic length of

the ambipolar region is of the order of the characteristic sheath length. Letting $L=5 \times 10^{-5}$ meters and the drift velocity as before, $v_d = 10$ to 100 m/s, a characteristic time for the formation of the density boundary layer would be 0.5 to 5.0 microseconds. It is reasonable that the ambipolar diffusion to the wall can establish itself well within the 50 microsecond pulse period of the electrodes.

3. Significance Of Joule Heating

For the present problem, joule heating can be shown not to be significant. In the vicinity of the active site, the average energy deposition rate per unit volume is shown to be approximately 4×10^8 watts/m³. The temperature of the Nitrogen gas at one amagat would be raised approximately 10°K in 2.6×10^{-6} sec. Allowing a 50×10^{-6} sec pulse period would raise the temperature of that region by approximately 20°K , or 7% .

Assume that the heat generated at the anode spot is carried away by thermal diffusion (conduction). Then for Nitrogen gas ($k=0.0267$ W/m- $^\circ\text{K}$, $\rho=1.138$ kg/m³, and $c_p=1043$ J/kg- $^\circ\text{K}$) the thermal diffusivity is;

$$\alpha = \frac{k}{\rho c_p} = 2.25 \times 10^{-5} \text{ m}^2/\text{sec}$$

A typical diffusion time would be (for, $\lambda_s = 4.4 \times 10^{-5}$ m);

$$\tau_d \approx \lambda_s^2 / \alpha \approx 0.86 \text{ millisec}$$

The "flush time" is the time required for clearing the lasing cavity of residue gases in preparation for the next pulse, and can be estimated as the gas flow rate divided by the flow length. Assuming $v = 100$ m/sec and $L = 10$ cm, the flush time would be;

$$FT = 0.1/100 = 1 \text{ millisecon}$$

Other factors considered, the inter-pulse period (time between pulses) would be larger, but even in a one millisecond period, there is just enough time to cool the anode spot.

The analysis so far has assumed a flow velocity at the surface to be the same as the bulk flow in the laser cavity. However a boundary layer exists-- probably turbulent, with a laminar sub-layer adjacent to the electrode for;

$$Re = x v_{\infty} / \nu = (0.1)(100)/(15.53 \times 10^{-6}) = 6.44 \times 10^5$$

The velocity boundary layer thickness would be 2.55 millimeters. Assuming a 1/7-th power profile, the velocity at a sheath length from the electrode would be:

$$v = v_{\infty} (\lambda_s / \delta)^{4/7} = 100 (4.4 \times 10^{-3} / 2.55 \times 10^{-3})^{4/7} = 56 \text{ m/sec}$$

A characteristic local flush time would be approximately 2 milliseconds, and much higher for a laminar velocity profile. These flush times can be quite large as the requirement to cool the Joule heated gas near the anode spot is

increased. The design flush time based on other factors may in fact be insufficient to clear enough of the Joule heated gas from the vicinity of the anode spot, enabling a build up of heated gas, which could lead to local enhanced ionization of the gas.

4. Electron Temperature

The electron temperature (T_e) is assumed to be a linear function of E/n as presented in Fig. 2, for the region of interest, namely $E/n = 0.5$ to 5.0×10^{-20} V-m². For the range of E/n considered, it is adequate to take the electron temperature as:

$$T_e = [A \cdot \log(E/n) + B] \cdot T_0 \quad (5)$$

where;

$$A = 12.1$$

$$B = 38.5$$

$$E/n \text{ is normalized to } 10^{-20} \text{ V-m}^2$$

The diffusion coefficients were determined from Brown [Ref. 18]. The drift velocities were obtained from plotted results, and since $\mu_y = v_d/E$, and $D_y = \mu_y k T_y / e$, (Einstein's relation), the diffusion coefficients are;

$$D_e = 0.0665 \text{ m}^2/\text{sec}$$

$$D_i = 8.0 \times 10^{-6} \text{ m}^2/\text{sec}$$

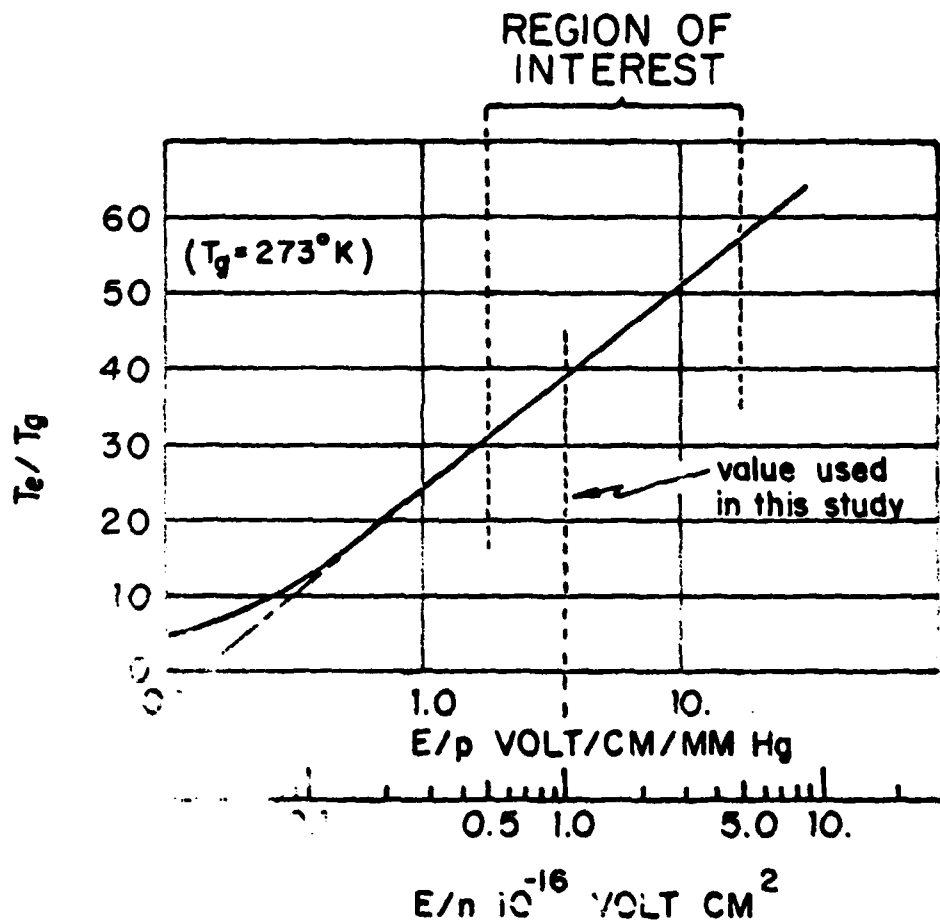


Figure 2

Ratio of Electron - Nitrogen gas Temperature
(Ref. 18)

B. WORKING EQUATIONS

Since convection is negligible, and assuming that the sustainer operates in the afterglow of an electron beam, the governing equations, namely Eqs. 1, 2 and 3, can be written as follows:

$$\nabla^2 \hat{\phi} = c_1 (\hat{n}_e - \hat{n}_i) \quad (6)$$

$$-\hat{\nabla} \cdot [\hat{\nabla} \hat{n}_e + \hat{n}_e \hat{\nabla} \theta / \theta - \hat{n}_e \hat{\nabla} \hat{\phi} / \theta] = c_2 \hat{n}_e \quad (7)$$

$$-\hat{\nabla} \cdot [\hat{\nabla} \hat{n}_i + \beta \hat{n}_i \hat{\nabla} \hat{\phi}] = c_3 \hat{n}_e \quad (8)$$

where;

$$\hat{n}_s = n_s / n_{e0} \quad \hat{\phi} = e\phi / kT_{e0}$$

$$\theta = T_e / T_{e0} \quad \beta = T_{e0} / T_0$$

$$c_1 = e\phi / kT_{e0} \quad c_2 = \lambda_s^2 n_{e0} / D_e \quad c_3 = c_2 D_a / D_i$$

The equations may now be applied to flat plate formulation as depicted in Fig. 3. It is convenient to drop the "h" for simplicity, but it is to be understood that all variables have been suitably non-dimensionalized.

We have Poisson's equation;

$$\frac{\partial^2 \phi}{\partial x^2} + \frac{\partial^2 \phi}{\partial y^2} = c_1 [n_e - n_i] \quad (9)$$

electron conservation equation;

$$\begin{aligned}
 c_1 n_e (n_e - n_i) + \left[\frac{\partial n_e}{\partial x} \frac{\partial \phi}{\partial x} + \frac{\partial n_e}{\partial y} \frac{\partial \phi}{\partial y} \right] - \frac{n_e}{\theta} \left[\frac{\partial \phi}{\partial x} \frac{\partial \theta}{\partial x} + \frac{\partial \phi}{\partial y} \frac{\partial \theta}{\partial y} \right] \\
 - \left[\frac{\partial \theta}{\partial x} \frac{\partial n_e}{\partial x} + \frac{\partial \theta}{\partial y} \frac{\partial n_e}{\partial y} \right] - \theta \left[\frac{\partial^2 n_e}{\partial x^2} + \frac{\partial^2 n_e}{\partial y^2} \right] \\
 + \frac{n_e}{\theta} \left[\left(\frac{\partial \theta}{\partial x} \right)^2 + \left(\frac{\partial \theta}{\partial y} \right)^2 \right] - n_e \left[\frac{\partial^2 \theta}{\partial x^2} + \frac{\partial^2 \theta}{\partial y^2} \right] = c_2 \theta \dot{n}_e
 \end{aligned} \tag{10}$$

ion conservation;

$$c_1 \beta n_i (n_e - n_i) - \beta \left[\frac{\partial n_i}{\partial x} \frac{\partial \phi}{\partial x} + \frac{\partial n_i}{\partial y} \frac{\partial \phi}{\partial y} \right] - \left[\frac{\partial^2 n_i}{\partial x^2} + \frac{\partial^2 n_i}{\partial y^2} \right] = c_3 \dot{n}_e \tag{11}$$

C. NUMERICAL METHODOLOGY

The nonlinear terms create problems in the computer analysis of the electron and ion species conservation equations, (Eqs. 10, 11). The Jacobi method includes all nonlinear terms on the "right hand side"; i.e., external to the coefficient matrix. Convergence to a solution is possible if these non-linear terms change slowly over each iteration. It was found by Dolson [Ref. 12] that the Jacobi method was

in fact unstable for the present set of equations and conditions. As a consequence of the failure of the Jacobi method, a quasi-Jacobi method was implemented, in which an estimate for each of the solution variables (ϕ , n_e , n_i) was computed. When the product of two variables is encountered, one variable is treated as a constant coefficient for each iteration. This means that the non-linear terms are retained in the coefficient matrix. The "constant" coefficients are updated after every iteration, thus altering the coefficient matrix. The conventional Jacobi method was found to converge only for low values of voltage potential at the electrode, whereas the quasi-Jacobi procedure provided converged solutions for approximately 5 volts. A discussion of these methods is provided in Appendix C as background for the development of the modified Newton-Raphson (MNR) method, which is used in the solution to Eqs. 1 through 4.

The nonlinear coupled partial differential equations (PDE), Eqs. 9, 10 and 11 are linearized to provide a set of linear algebraic equations, which must hold throughout the domain described as follows. The domain as illustrated in Fig. 3, is divided up into equal sided sub-areas whose vertices are the computational nodes at which the linearized

algebraic equations must hold. The wall is represented by seven (7) nodes, with the leftmost node being the location of the active site. The "y" direction extends from this active site along the wall. The "x" dimension perpendicular to the wall is represented by 25 nodes starting from each of the wall nodes. The solution to the PDE's is represented by the vector $z(x,y)$, or on the computational mesh as $z(i,j)$.

The boundary conditions have been discussed previously and are presented in Fig. 3. The boundary condition that there is no net current into the nonactive wall ($J_x=0$) is satisfied by the electron contribution to current only. This is justified since it can be shown that the electron contribution is approximately three orders of magnitude greater than the ion contribution to the total current.

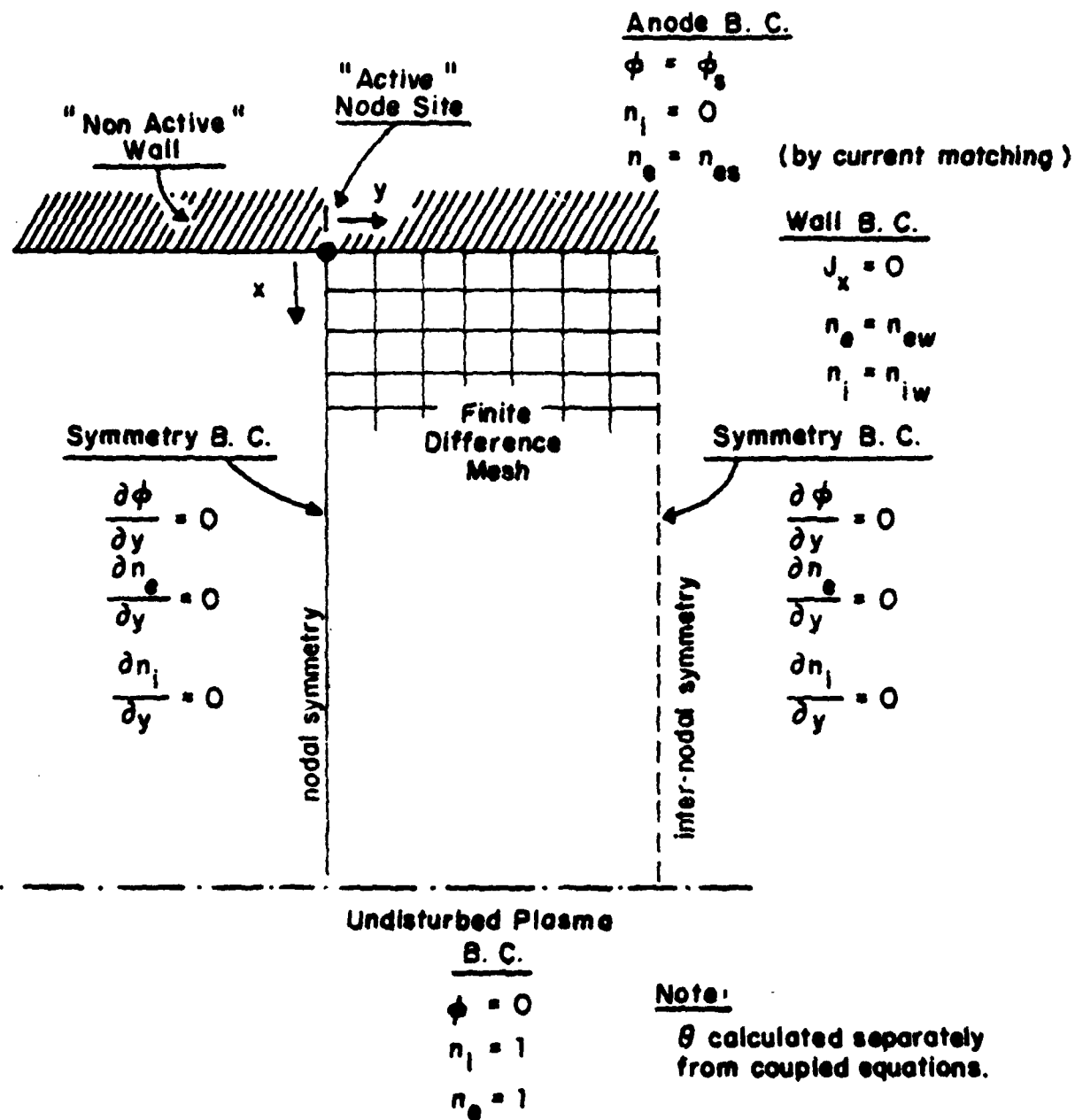


Figure 3

Boundary Conditions for Computational Method.

IV. RESULTS AND CONCLUSIONS

A. GENERAL DISCUSSION

Computer solutions are reported here for three cases presented in Table I. The active site voltage was 35 volts in each of the three cases. Included in this section are

TABLE I: Computer Solution Conditions

CASE	n_e (wall)	n_i (wall)	n_e (anode)	n_i (anode)
I	1.0	0.0	J-matched	0.0
II	"float"	0.0	not J-matched	0.0
III	"float"	"float"	not J-matched	0.0

also some pertinent results obtained at 10 volts to illustrate the effects the net production term has on the convergence to a boundary layer behavior for the species density and free stream electric field.

The solutions are depicted as oblique presentations of the potential, species density, space charge, net production, electric field and Joule heating distributions over the "x-y" coordinates defined in the problem formulation. Also included are two-dimensional plots of various terms along a "cut" or line perpendicular to the electrode wall,

starting at the active site, with some starting at the wall along the inter-nodal line of symmetry (see Fig. 3). The solutions are organized as Case I, II and III results, will be presented as Figs. 12, 13 and 14 respectively at the end of this section. The discussion of these results proceeds with additional figures which are interspersed in the text appropriately.

Table I presents various electron and ion boundary conditions along the wall some of which are "floated." By this term is meant that upon the completion of each numerical iteration, the electron (and/or ion) density at the nonactive portion of the wall is re-established by assigning it the value of a near neighbor away from the wall. This process is illustrated in Fig. 4.

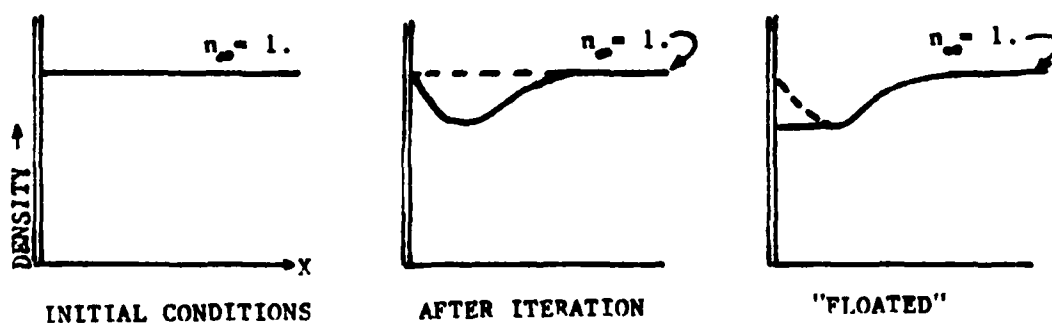


Figure 4

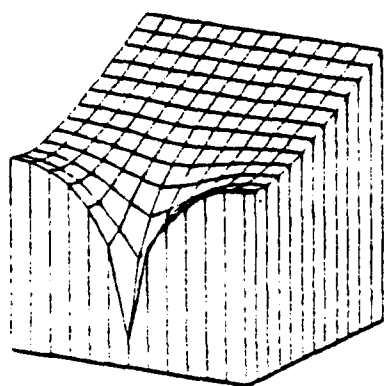
Description of "floating the Wall Boundary Condition.

The usual elliptic boundary value problem has well posed boundary conditions from a priori information. However, the nature of the problem in this study includes very little information as to the correct species wall density. It seems reasonable to set these densities to zero along the inactive portion of the electrode as previously mentioned in Sec. II.B. In this study the wall boundary conditions are "loosened" to facilitate "naturally occurring" and unpresuming species density profiles. The nature of the problem in effect, produces a self-consistent boundary condition.

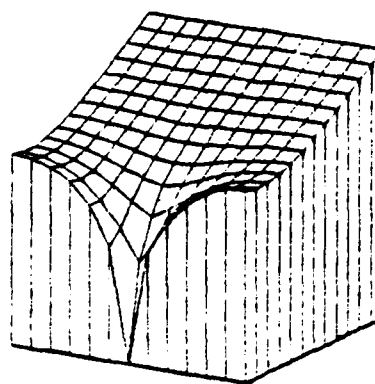
B. EFFECTS OF NET PRODUCTION

Earlier work [Ref. 15] reported limited results for a 10 volt active node site. Solutions for cases with and without the inclusion of the net production term have profound influences on the appearance of the charged species density profiles. Figures 5,6 and 7 illustrate the before and after effects of including the net production term. In both cases the wall boundary values for the species density was initialized at the free-stream value (i.e., 1.0), then allowed to "float" as described previously. The addition of the net production term brings about the boundary layer behavior of the densities of the electrons and ions is illustrated in Fig. 7. Efforts to attain converged solutions with the net

production term set to zero proved fruitless for active site potentials exceeding 10 volts.



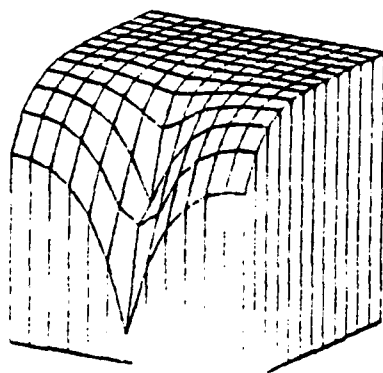
Electron Density
(a)



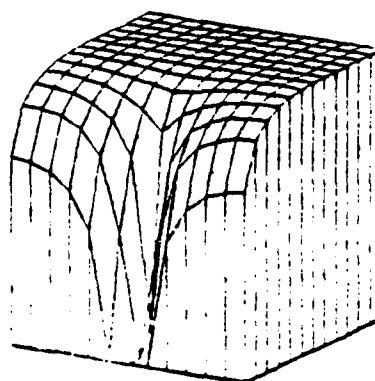
Ion Density
(b)

Figure 5

(a) Electron and (b) Ion density perspectives with the net production term set to zero. (10 volts)



Electron Density



Ion Density
(b)

Figure 6

(a) Electron and (b) Ion density perspectives with the net production term coupled. (10 volts)

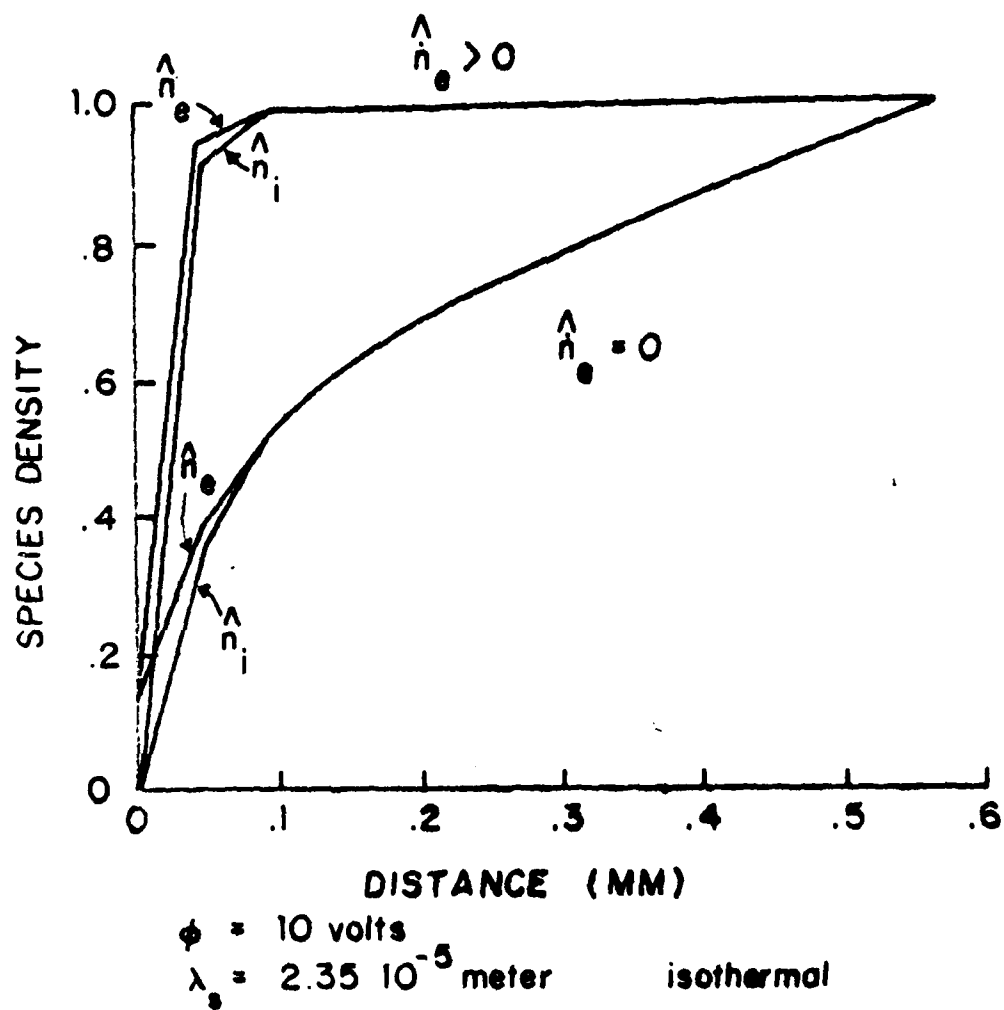


Figure 7
Influence of the net production term on the density profiles along a line perpendicular to the wall, extending from the active hole site, (10 volts).

C. DISCUSSION OF RESULTS

1. Voltage Potential

The voltage potential of the active node site ("the anode") in each of the cases presented was 35 volts. Figures 12-a, 13-a and 14-a will clearly illustrate sharp voltage spikes at the anode, and the "Laplacian" nature of the field far from the anode. The potential along the inactive wall varied from 12 volts at the farthest position from the anode to 17 volts just next to the anode. Similar profiles of the electric potential along the wall for the other cases are presented in Fig. 8. Figures 12-i, 13-i and 14-i will show the voltage potential variation along a line normal to the wall extending from the anode site.

Figure 9 illustrates a two-dimensional cut of the voltage potential along the inter-nodal symmetry line. Here it can be seen that the variation from the wall is shallow. It is important to point out that the electron temperature is directly related to the gradient of the voltage potential through Eq. 5. This fact has certain consequences which are discussed in the next section.

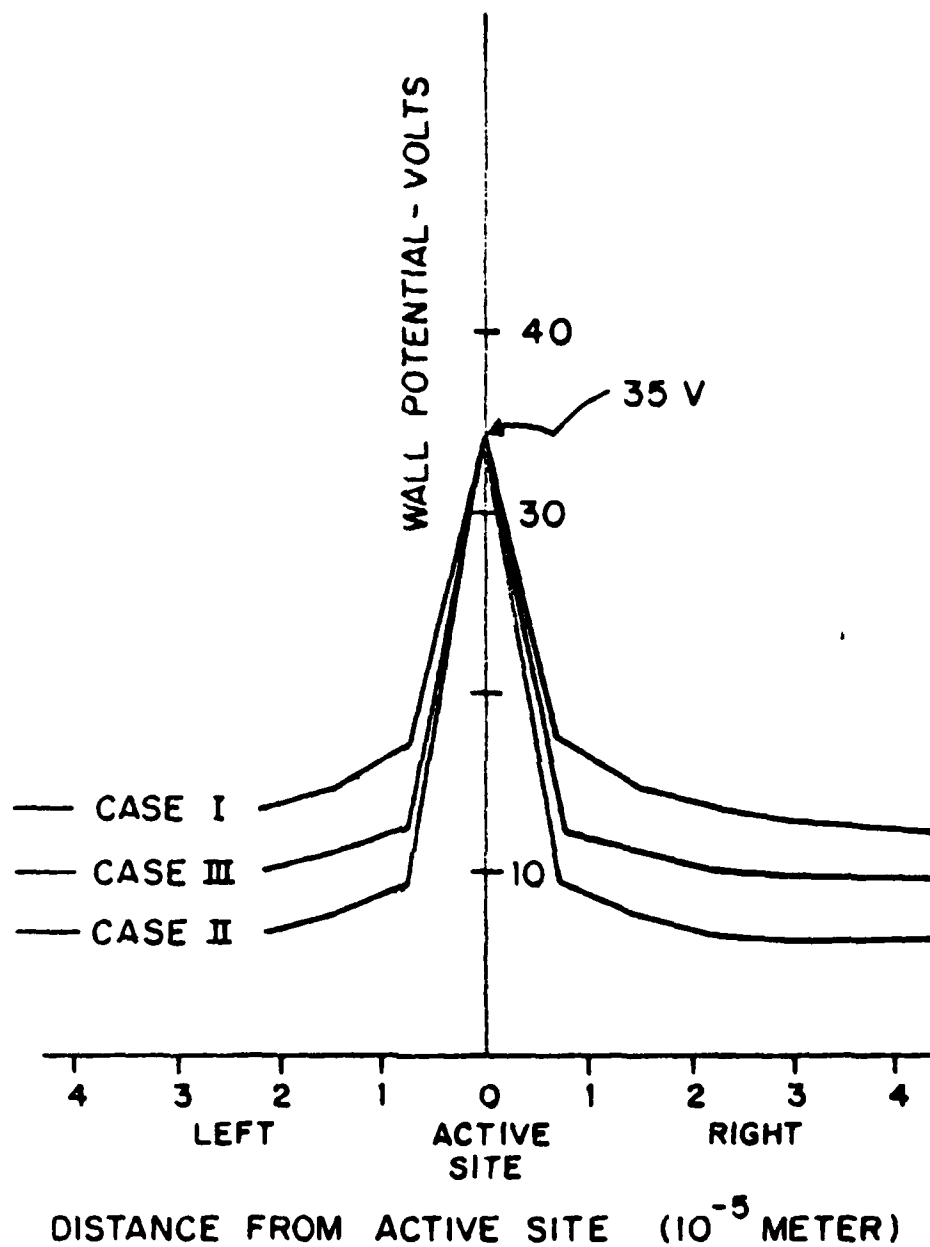


Figure 8
Voltage potential along the wall boundary (electrode)
for CASES I, II, and III.

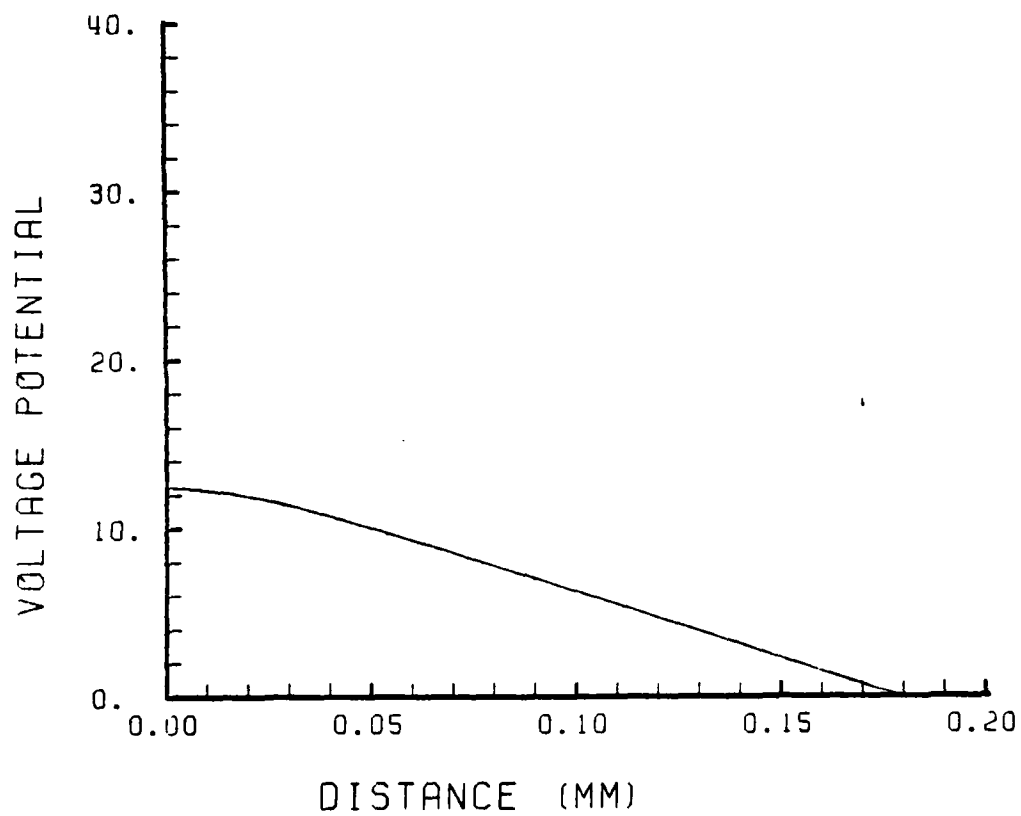


Figure 9
Voltage potential variation normal to the wall,
along the inter-nodal symmetry line, (CASE I)

2. Electron Energy

The electron energy will be presented in series -b of Figs. 12, 13 and 14, as oblique perspectives. The anode site temperature for Cases I, II and III are 2.1, 2.1 and 1.9 eV respectively. The description of the electron temperature is that of a linear function of the logarithm of the electric field. Any portion of the potential field that is "level" ($\text{grad } \phi = 0$) will necessarily generate a low or even negative (see Fig. 14-b) electron temperature. According to Fig. 2 and the discussion in Sec II.A.4, a negative temperature would occur below an E/n of 0.04×10^{-20} V-cm². This problem can be removed by setting a minimum value to the non-dimensional temperature field, nominally 0.13, corresponding to the minimum at the low end of E/n in Fig. 2.

The parameters of the discharge (Sec. I.C) require an electric field of 2.7×10^8 V/m (or, $\log[E] = 5.43$) at the free stream boundary, which corresponds to an electron temperature of 0.905 eV ($\theta = 1$). The temperature fields in all cases presented do not quite meet the free stream boundary requirements. The electric fields are insufficient to render proper results to the electron temperature profiles. Thus the free stream temperature boundary requirements are "forced" by slightly inflating the influence of the electric

field. The effect of forcing the temperature field in this way can also be looked at as "sliding" the linear representation of the temperature curve to higher values at constant E/n , (see Fig. 2). Figure 10 illustrates a case where a low electric field, here 0.8 kV/cm, results in a low electron temperature projecting toward the free stream ($\theta=0.62$). The low temperature is adjusted to meet the desired free stream value ($\theta=1.0$) by multiplying the electric field by a factor of 3.40. Figure 10 also illustrates an alternate method of meeting the free stream conditions by truncating the variation of temperature with a minimum value, namely the free stream boundary condition.

Both of the "forcing" techniques are used, but for different reasons. As long as the adjustment factor does not exceed an order of magnitude change in the electric field, then it is not objectionable in light of the simplified representation of the electron temperature. The adjustment requirements of the three cases reported in this study are between 3.0 and 5.0, with Case I using a factor of 10 to see the effects on the Joule heating. In Case I the non-dimensional temperature is artificially high at 1.4 eV at the free stream.

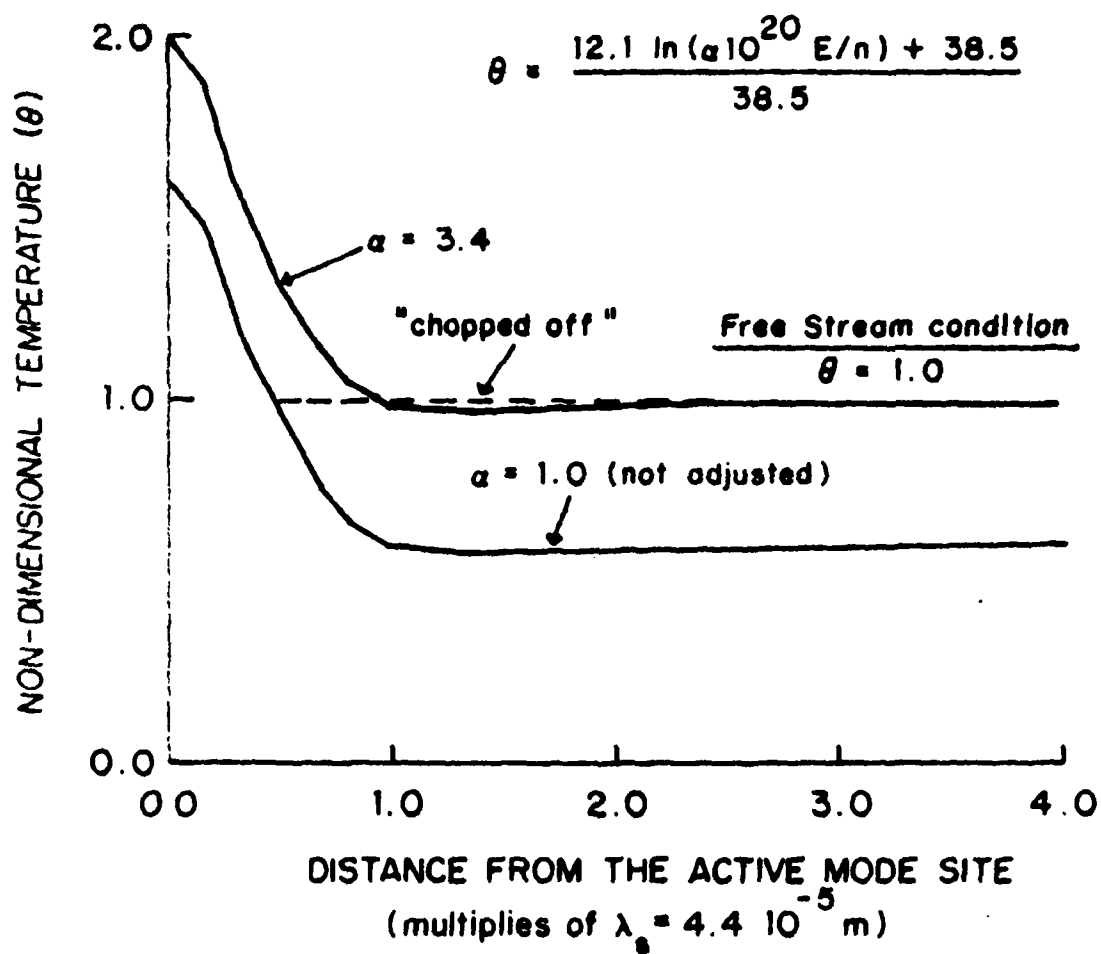


Figure 10
Electron temperature variation normal to the wall, along the nodal symmetry line; illustrating two methods of adjustment to "force" the free stream temperature conditions.

The electric field near the inter-nodal symmetry points of the wall are characteristically 2 orders of magnitude less than that of the free stream conditions. The resulting very low, even negative temperatures in Case III, Fig. 14-b, is "patched" using the truncation method previously discussed. Whether these low temperatures and the associated steep derivatives are physically reasonable, merits further investigation.

The temperature fields generated and presented as Figs. 12, 13, 14 series -b are the final result depictions. However, the temperature fields used in the solution process were adjusted and truncated as previously discussed to maintain solution convergence. An example of a "corrected" temperature field is presented in Fig. 14-c.

3. Electric Field And Joule Heating

The electric field and Joule heating distributions are generated from the primary voltage and electron density solutions, much in the manner as the temperature distribution was determined. In fact, the Electric field and the Joule heating distributions are similar in appearance to the temperature distributions. These distributions play no direct part in the solution scheme and thus being ancillary in nature were not "forced" to meet any a priori conditions.

The Joule heating term can be written as;

$$J \cdot E = [D_e n_{e\infty} k T_{e\infty} / \lambda_D^2] \cdot [\frac{n_e}{\phi} \nabla \phi - \nabla n_e] \cdot \nabla \phi$$

and thus is a rather straight-forward function of ϕ , n_e , and n_i . The ion contribution is shown to be negligible, since $D_e \gg D_i$. The Joule heat at the anode site is of order 10^6 and is 100 times that of the free stream values. Joule heating effects are negligible in the overall problem, as discussed in Sec. II.A.3, obviating the requirement for an energy equation.

4. Species Density Distribution

The solutions for the charged species density distributions are presented as oblique perspectives in Figs. 12, 13 and 14, series -e (electron density); series -f (ion density); and series -g (space charge density). Additionally the variation of these distributions normal to the wall along the active node symmetry line are presented in the series -j and -k figures. The oblique perspectives of the densities are reversed for clarity.

The electron and ion densities at the nonactive wall are a subject of interest in the literature, to which little information has been gathered on a firm basis. The results of this study suggest a slightly positive space charge at the inactive wall. Scrutiny of Case III results reveals, a

$2.2 \times 10^{16} \text{ m}^{-3}$ positive space charge number density, (or 3.5 milli-coulombs). Recall that Case III involved "floating" both of the charged species densities at the wall. In fact, close inspection of Case I and II reveals a positive space of similar magnitude but displaced slightly from the wall. The wall in these cases was set with a negative space charge as the boundary condition. The positive space charge along the wall is most predominant in the vicinity of the inter-nodal symmetry line, and whether the low temperature values in this region have significance, remains to be determined.

The active node site (anode) electron density in Case I ($2.4 \times 10^{17} \text{ m}^{-3}$) was determined so as to match the free stream current to the current constricting at the anode. In the results of Cases II and III the anode electron densities are chosen so as to provide a smooth variation extending outward from the active site.

5. Ionization/Recombination

The net ionization term is utilized in all cases; and was found necessary for (1) establishment of the charged particle density distributions, and (2) solution convergence for sheath lengths spanning more than one computational node spacing. The net production term is depicted in Figs. 12, 13 and 14 series -h. There is net ionization throughout the

solution domain. However as Case III demonstrates, there is a factor of 5 orders of magnitude greater ionization within the sheath region surrounding the anode site than at the free-stream edge. Cases I and II show ionization along the nonactive wall, simply because the ion density is zero, eliminating significant recombination, (see Eq. 4).

6. Current Description

Figure 11 is typical of the constricting nature of the current stream lines. The potential, electron density and the electron temperature are used to determine the "x-y" components of the current density. Using a "nearest neighbor" influence principal, a local derivative can be determined; from which a streamline can be "marched-out" in small increments. The profiles of all three cases are similar, the fact being that the current matching discussed previously will not affect the current streamline profiles. Figure 11 clearly demonstrates the satisfaction of the current constriction requirement necessary to permit solutions to the system of equations.

The current into the anode site in Case I is matched to the current entering at the free-stream boundary. This specifies the electron density at the anode site. However, in Cases II and III the current at the anode was only three

times the free-stream current. The current matching problem does not deserve serious complaint, since the problem description is simplified to two-dimensions and the current constriction is only required to satisfy continuity.

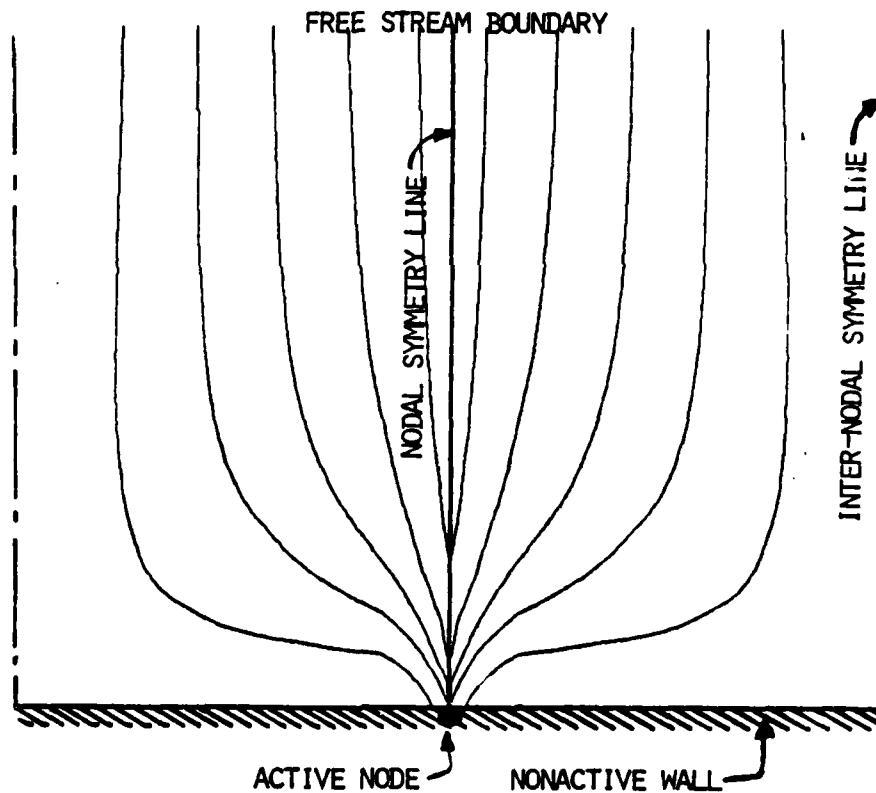


Figure 11
Two-dimensional depiction of the current stream line
constriction toward the active node site.

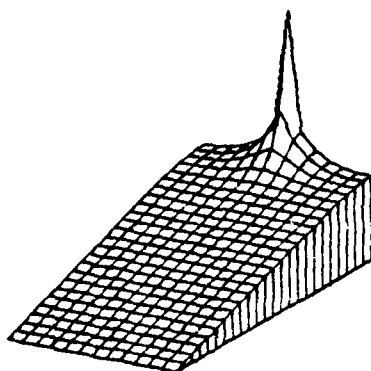


Figure 12-a
Oblique perspective of
Potential Field (CASE I)

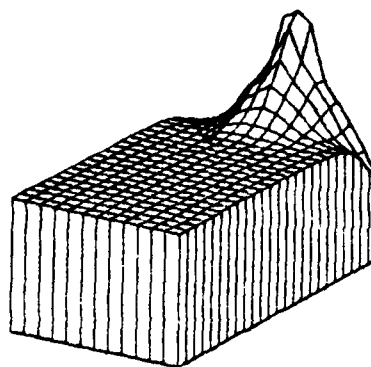


Figure 12-b
Oblique perspective of
Temperature field (CASE I)

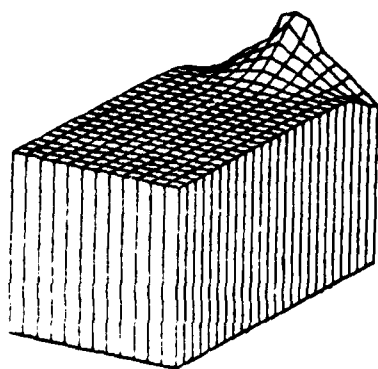


Figure 12-c
Oblique perspective of
log Electric Field (CASE I)

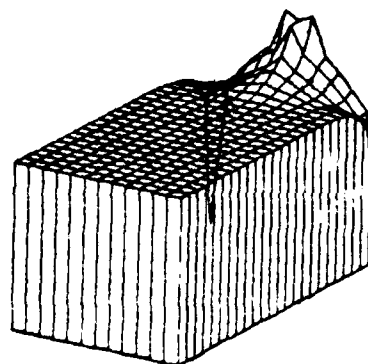


Figure 12-d
Oblique perspective of
log Joule Heat (CASE I)

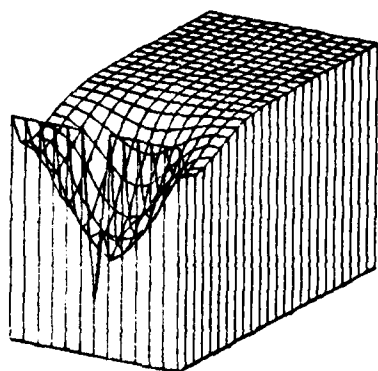


Figure 12-e
Oblique perspective of
Electron Density (CASE I)
(reversed perspective)

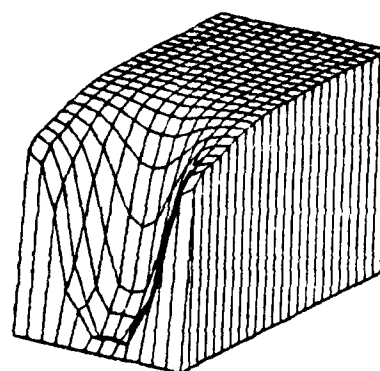


Figure 12-f
Oblique perspective of
Ion Density (CASE I)
(reversed perspective)

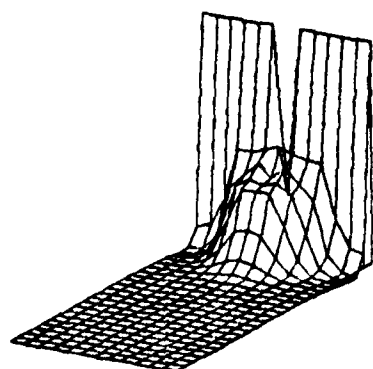


Figure 12-g
Oblique perspective of
Space Charge (CASE I)

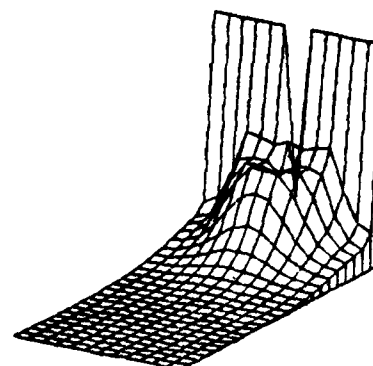


Figure 12-h
Oblique perspective of
Net Production (CASE I)

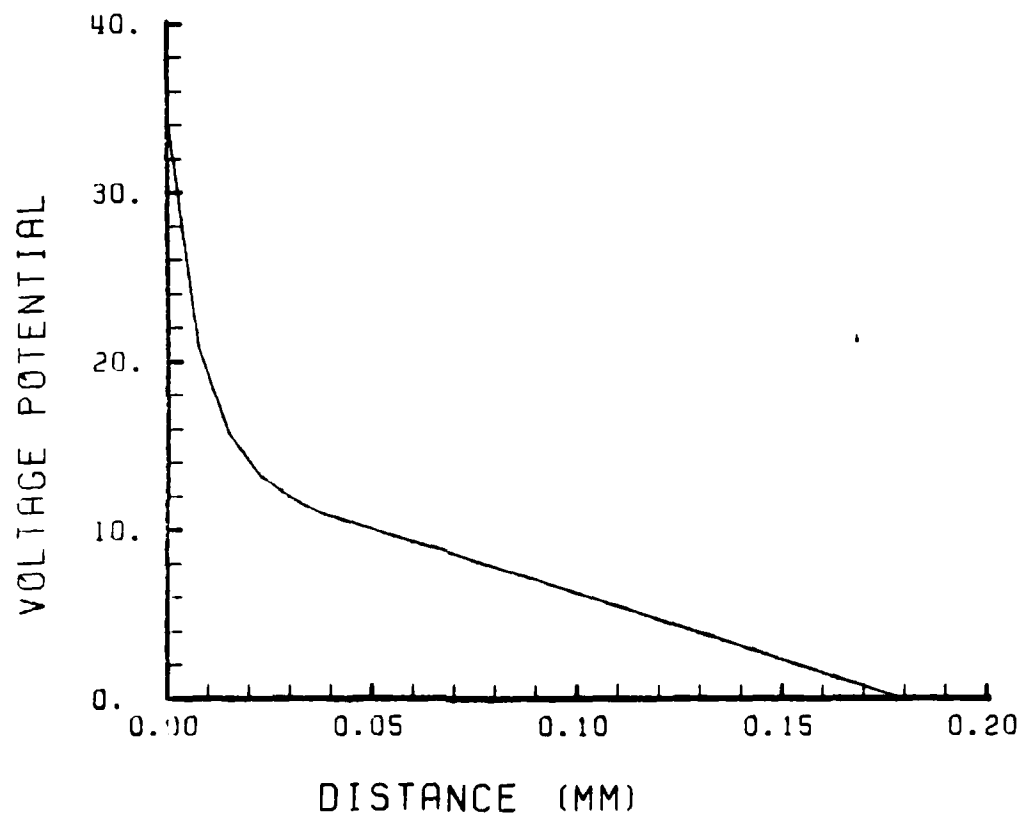


Figure 12-1
Presentation of the Voltage Potential
(CASE I) along a line normal to the wall,
extending from the active node site.

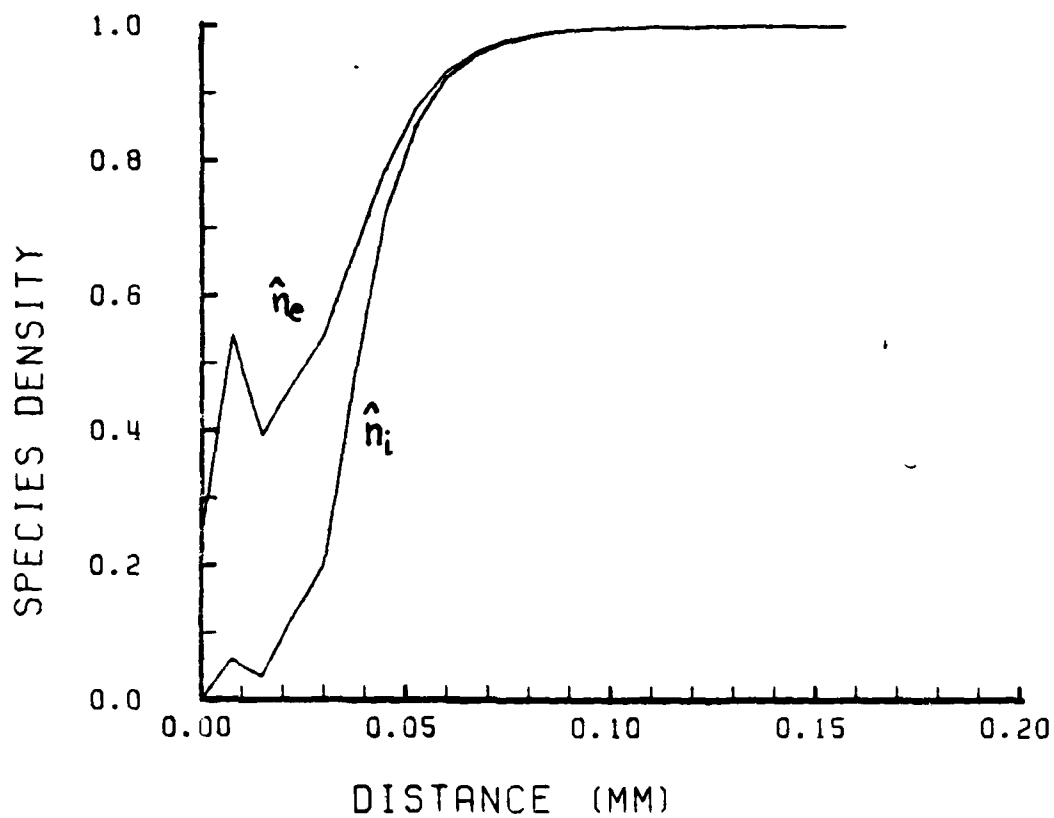


Figure 12-j
Presentation of Species Density
(CASE I) along a line normal to the wall,
extending from the active node site.

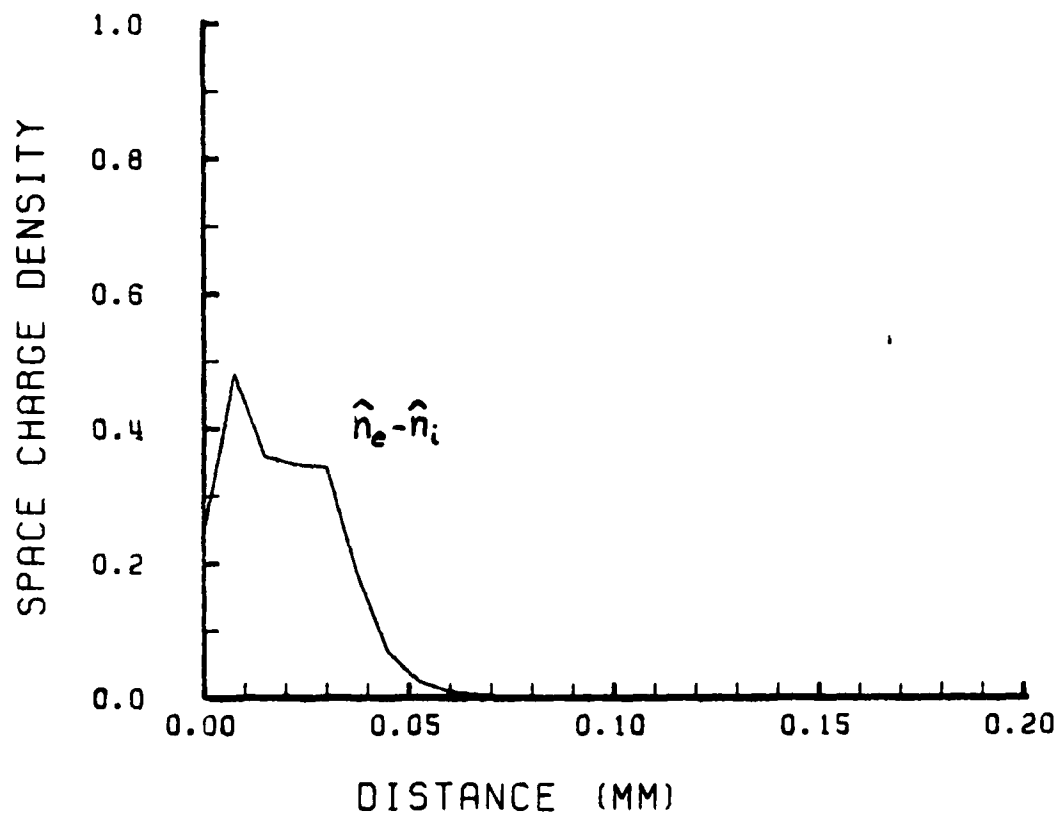


Figure 12-k
Presentation of the negative Space Charge Density
(CASE I) along a line normal to the wall,
extending from the active node site.

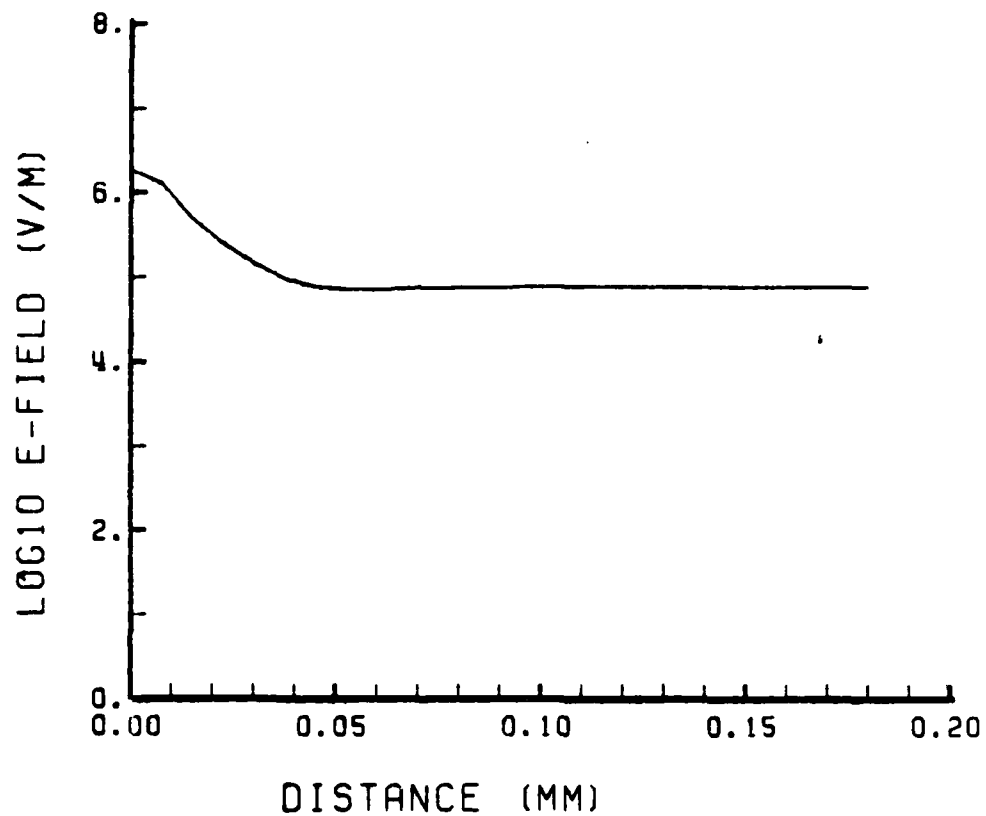


Figure 12-1
Presentation of the Electric Field
(CASE I) along a line normal to the wall,
extending from the active node site.
(logarithm scaled)

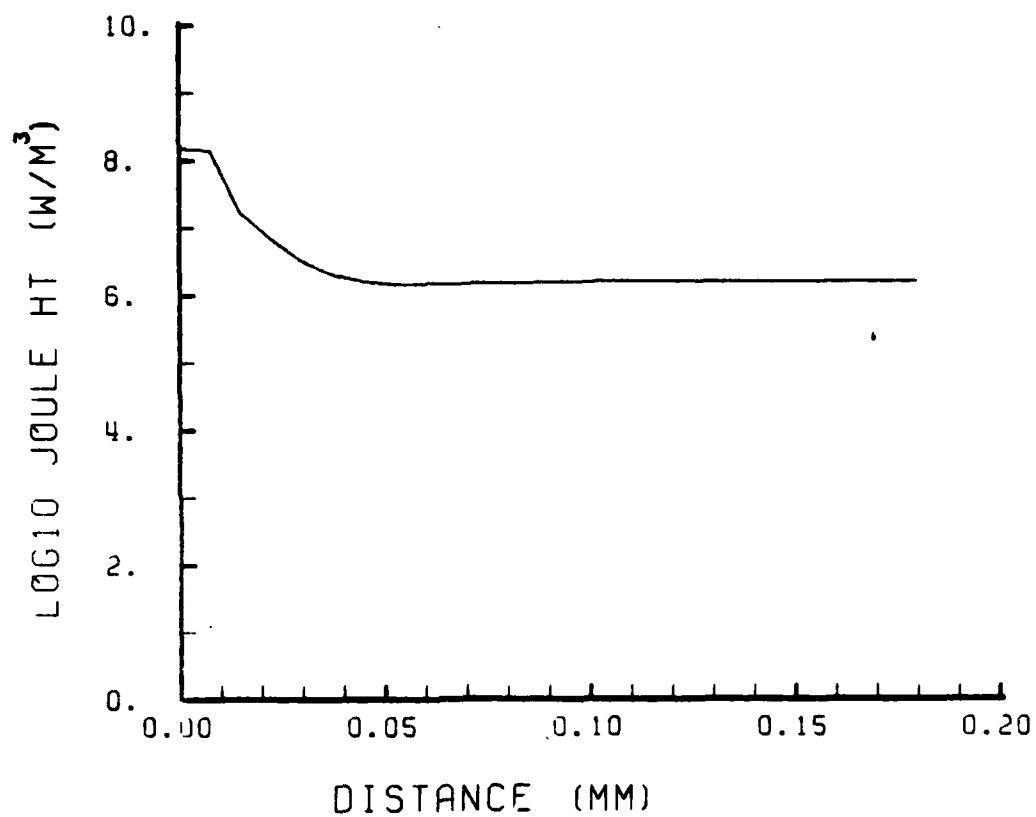


Figure 12-m
Presentation of the Joule Heating
(CASE I) along a line normal to the wall,
extending from the active node site.
(logarithm scaled)

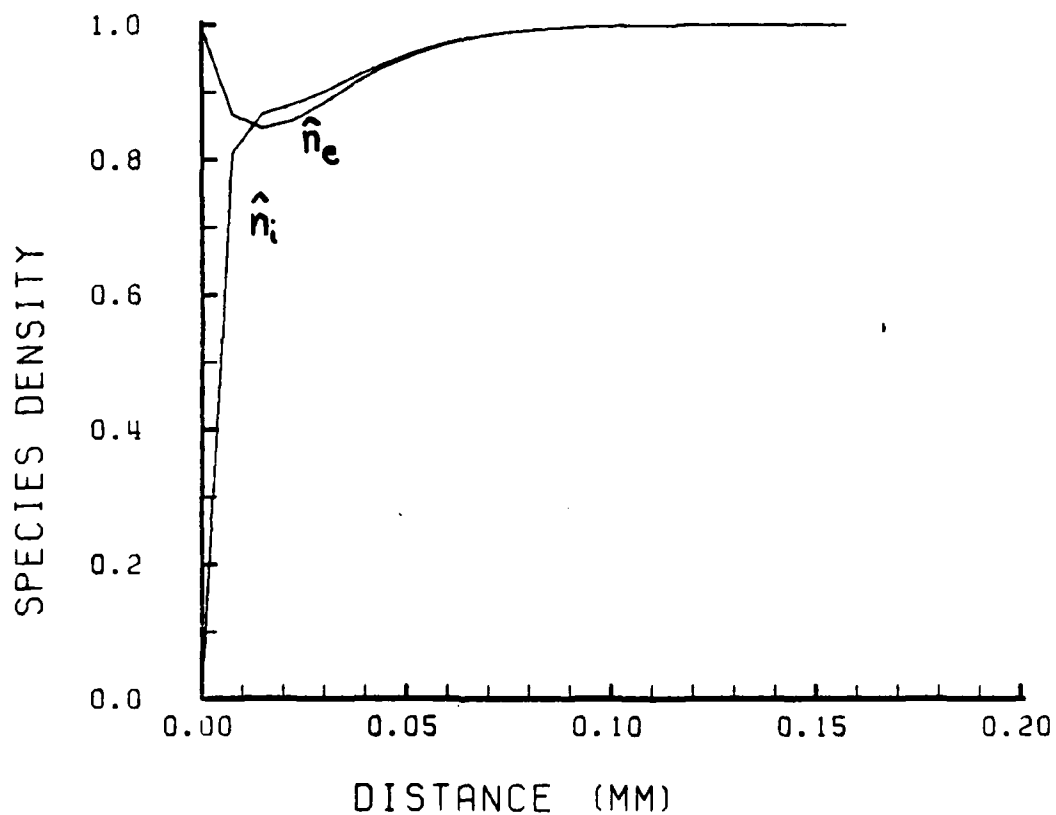


Figure 12-n
 Presentation of the Species Densities
 (CASE I) on a line normal to the wall,
 extending along the inter-nodal symmetry line.

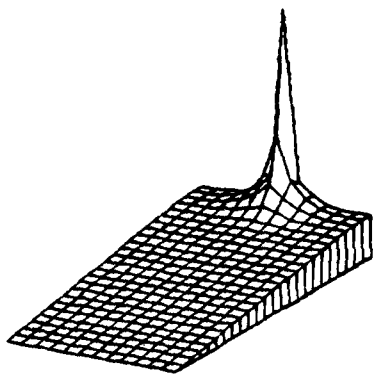


Figure 13-a
Oblique perspective of
Potential Field (CASE II)

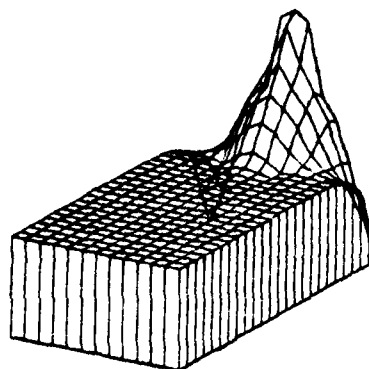


Figure 13-b
Oblique perspective of
Temperature field (CASE II)

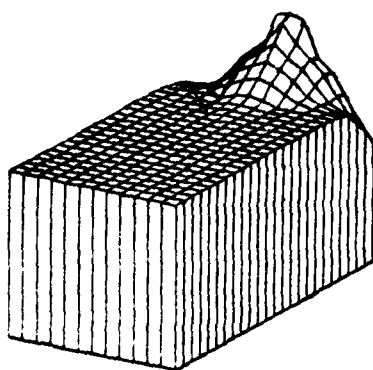


Figure 13-c
Oblique perspective of
log Electric Field (CASE II)

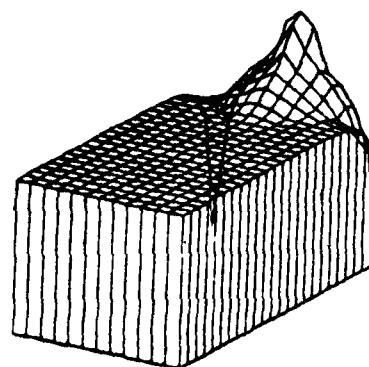


Figure 13-d
Oblique perspective of
log Joule Heat (CASE II)

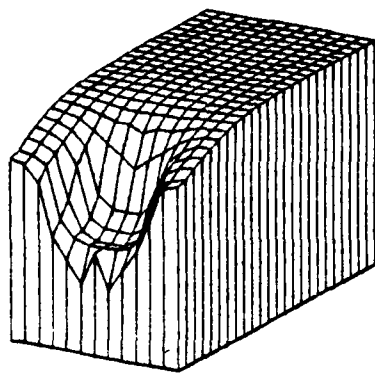


Figure 13-e
Oblique perspective of
Electron Density (CASE II)
(reversed perspective)

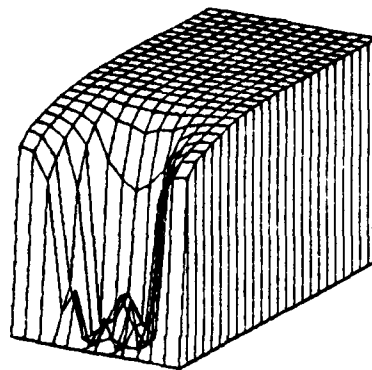


Figure 13-f
Oblique perspective of
Ion Density (CASE II)
(reversed perspective)

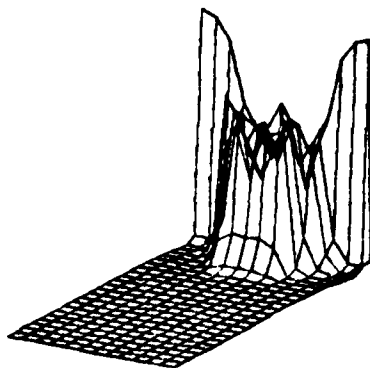


Figure 13-g
Oblique perspective of
Space Charge (CASE II)

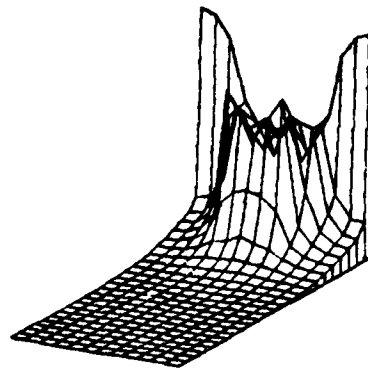


Figure 13-h
Oblique perspective of
Net Production (CASE II)

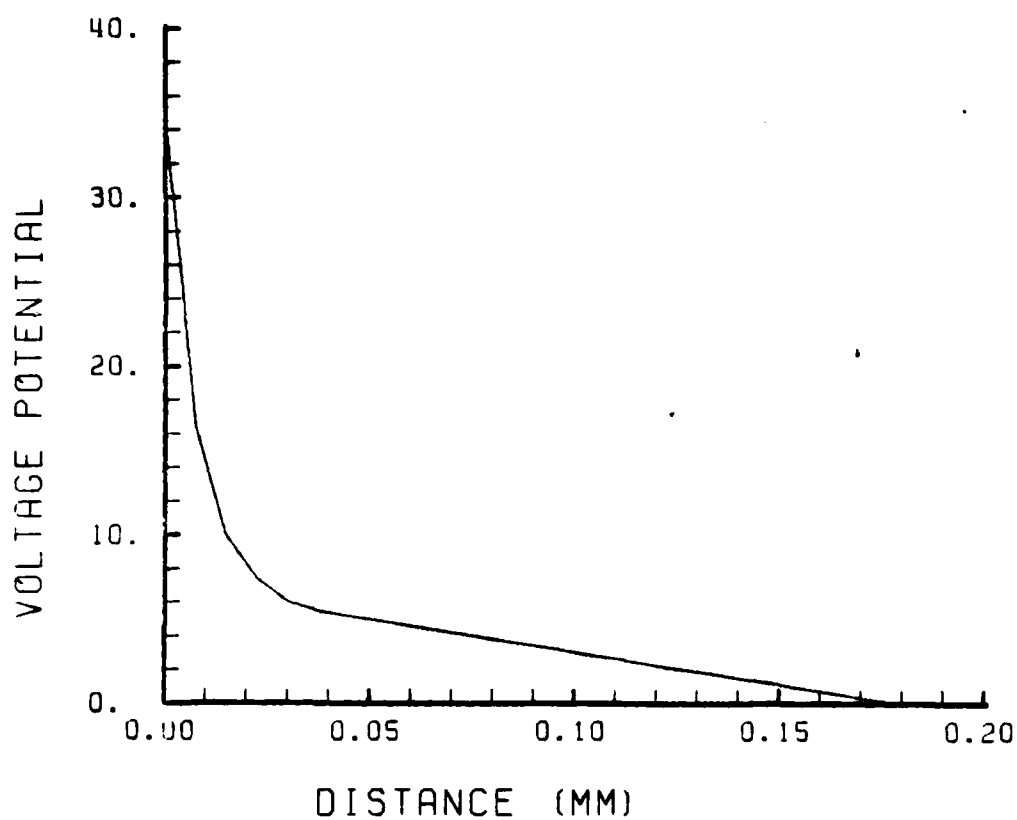


Figure 13-1
Presentation of the Voltage Potential
(CASE II) along a line normal to the wall,
extending from the active node site.

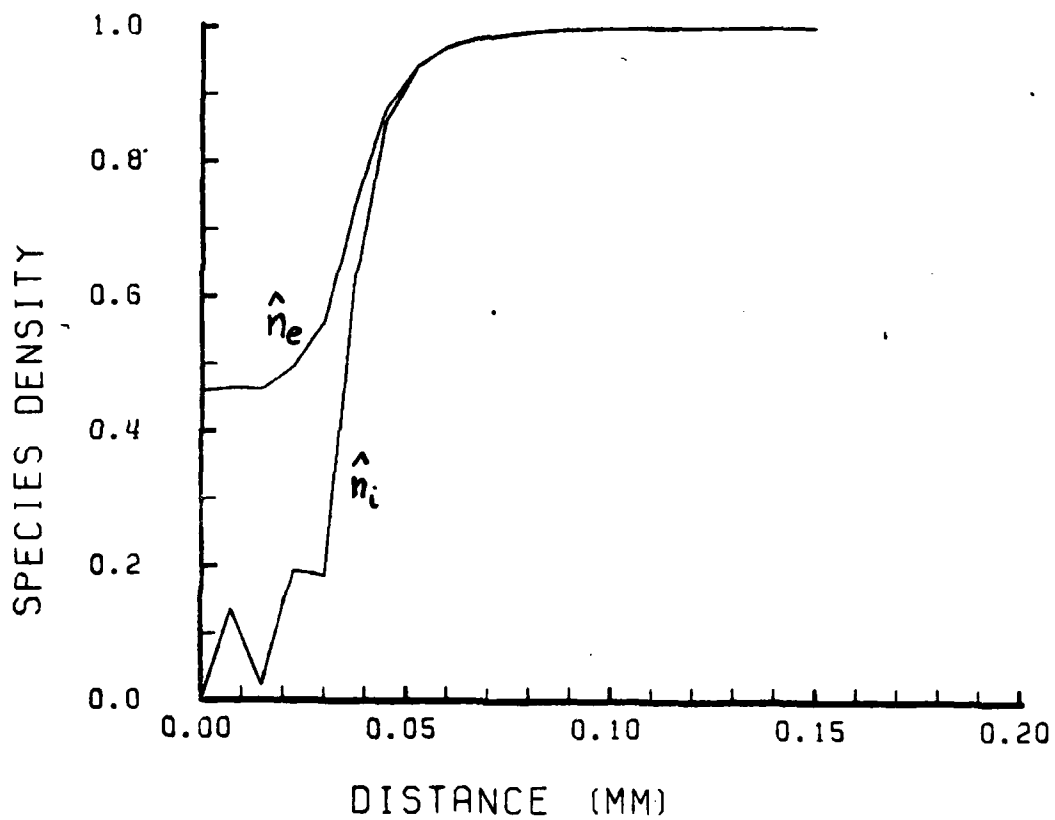


Figure 13-j
Presentation of Species Density
(CASE II) along a line normal to the wall,
extending from the active node site.

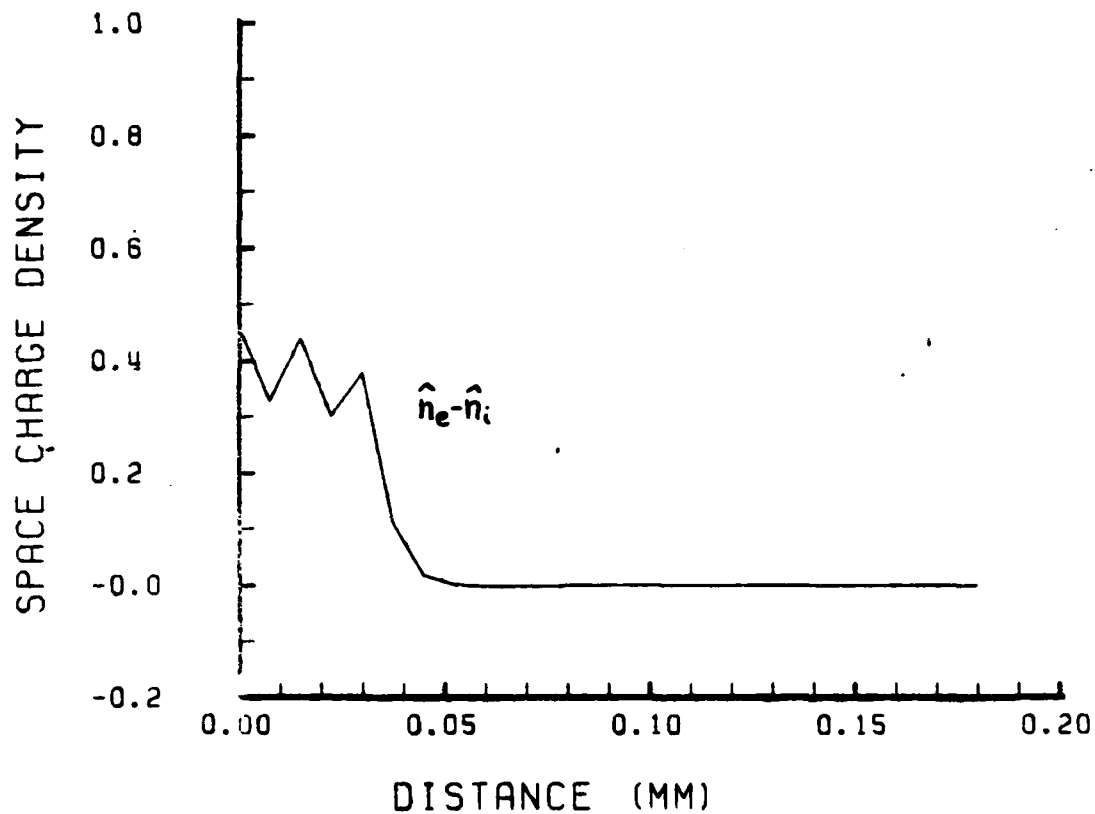


Figure 13-k
Presentation of the negative Space Charge Density
(CASE II) along a line normal to the wall,
extending from the active node site.

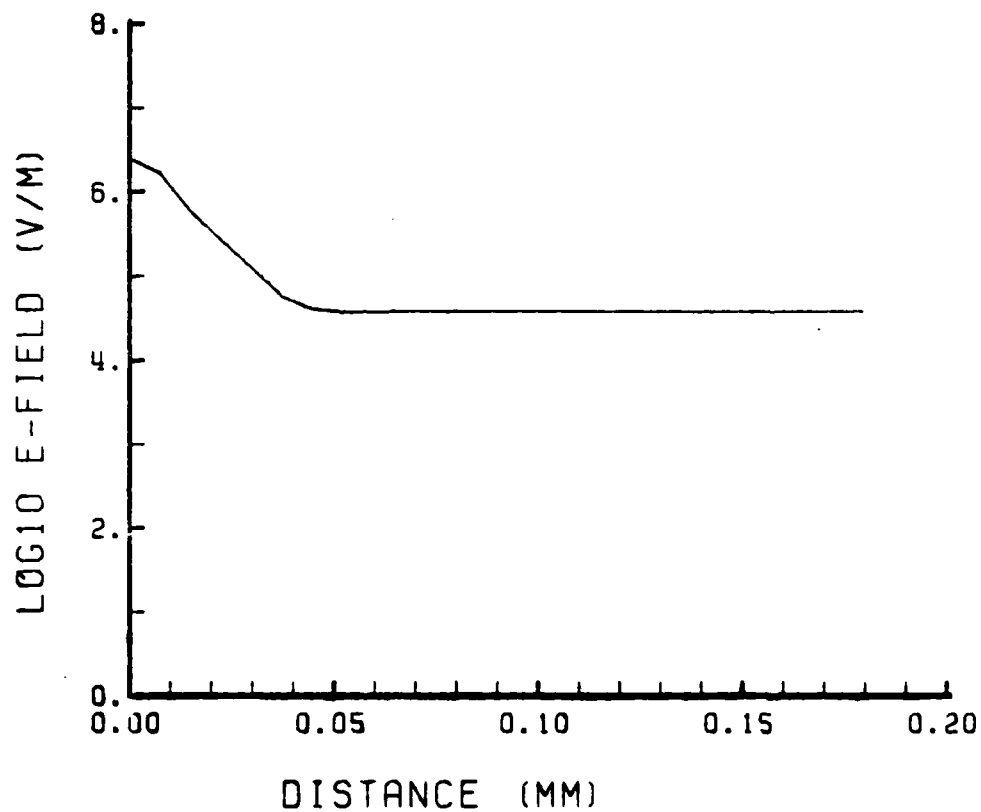


Figure 13-1
Presentation of the Electric Field
(CASE II) along a line normal to the wall,
extending from the active node site.
(logarithm scaled)

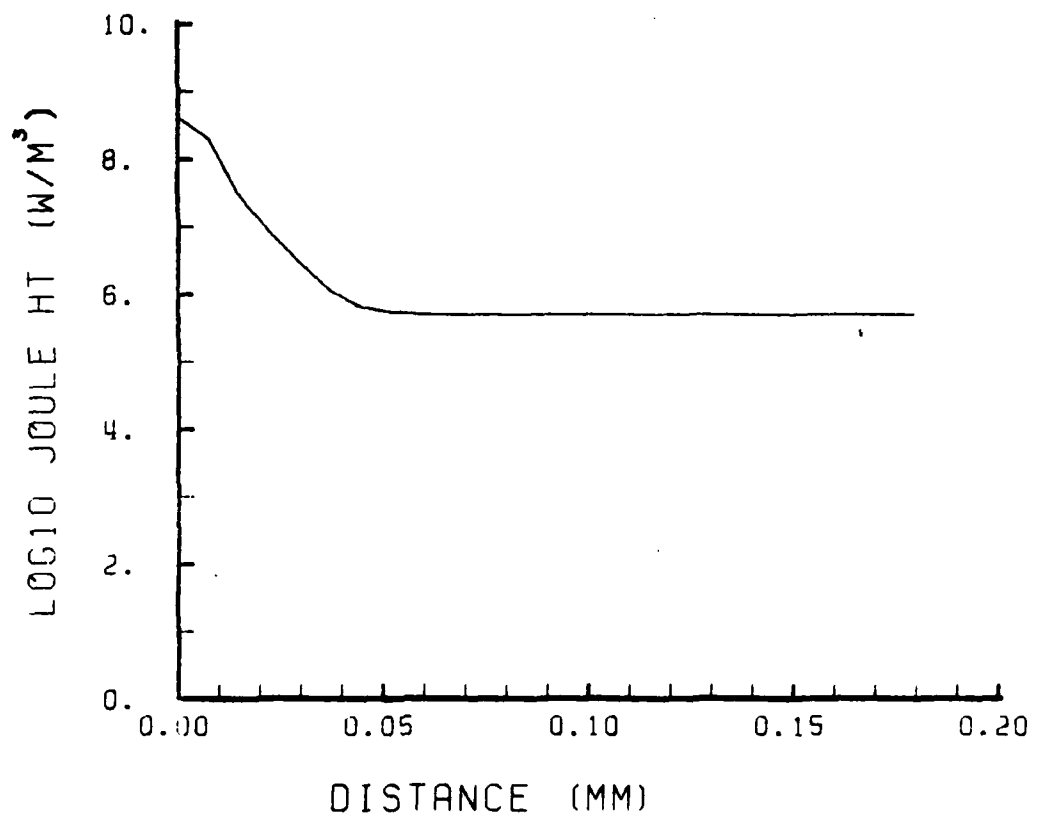


Figure 13-m
Presentation of the Joule Heating
(CASE II), along a line normal to the wall,
extending from the active node site.
(logarithm scaled)

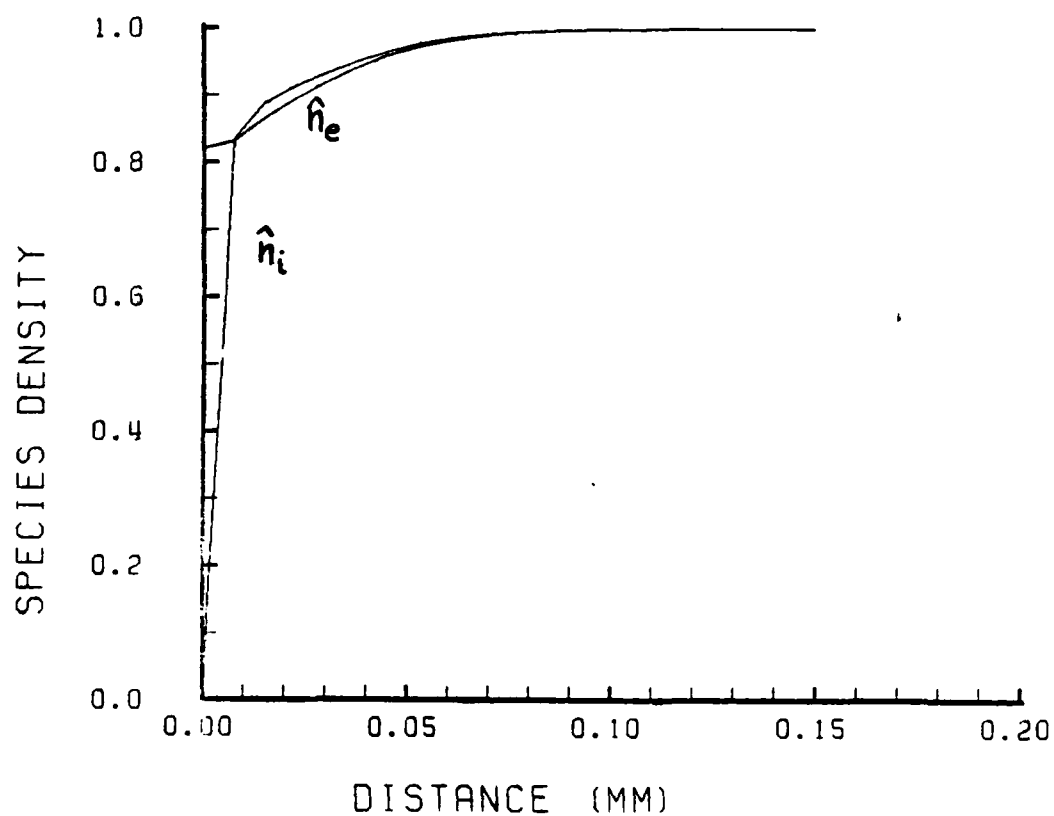


Figure 13-n
Presentation of the Species Densities
(CASE II) on a line normal to the wall
extending along the inter-nodal symmetry line.

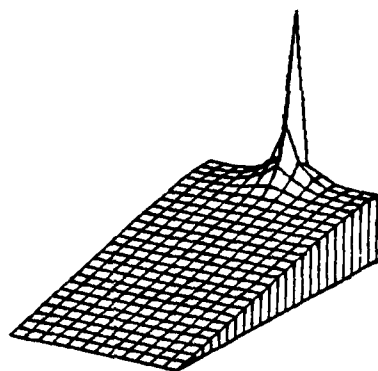


Figure 14-a
Oblique perspective of
Potential Field (CASE III)

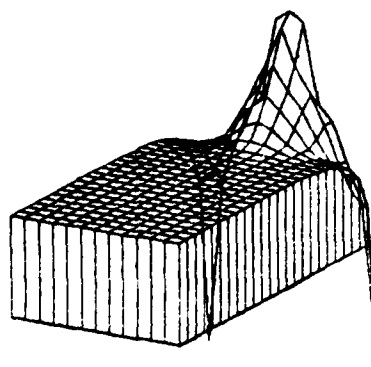


Figure 14-b
Oblique perspective of
Temperature field (CASE III)

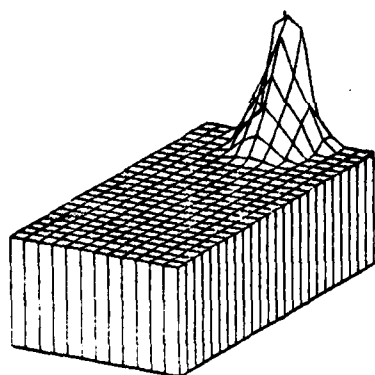


Figure 14-c
Oblique perspective of adjusted
Temperature Field (CASE III)

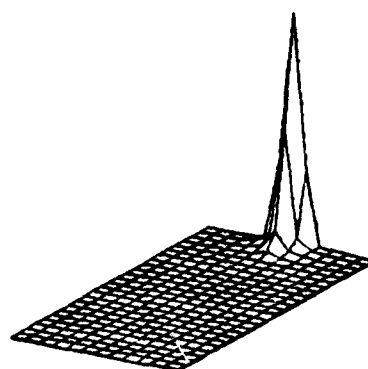


Figure 14-d
Oblique perspective of
Joule Heat (CASE III)

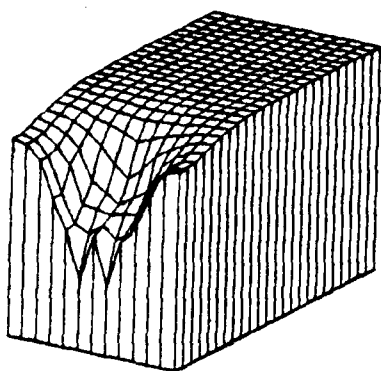


Figure 14-e
Oblique perspective of
Electron Density (CASE III)
(reversed perspective)

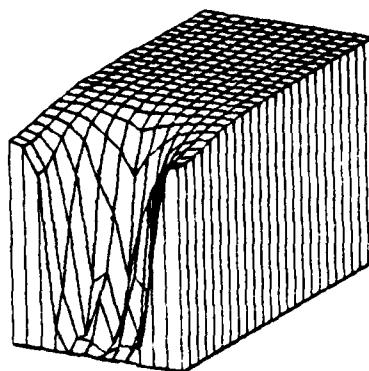


Figure 14-f
Oblique perspective of
Ion Density (CASE III)
(reversed perspective)

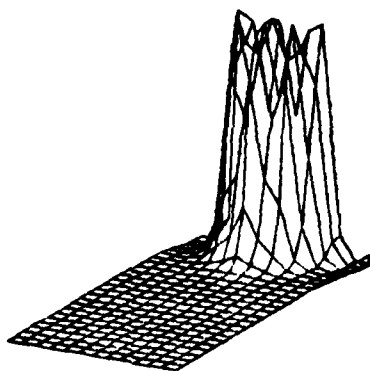


Figure 14-g
Oblique perspective of
Space Charge (CASE III)

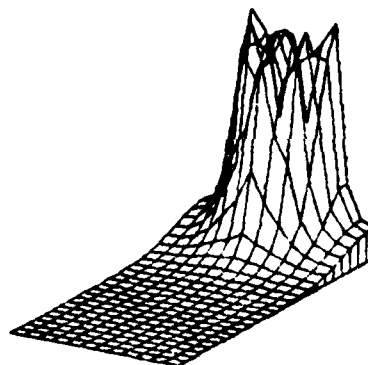


Figure 14-h
Oblique perspective of
Net Production (CASE III)

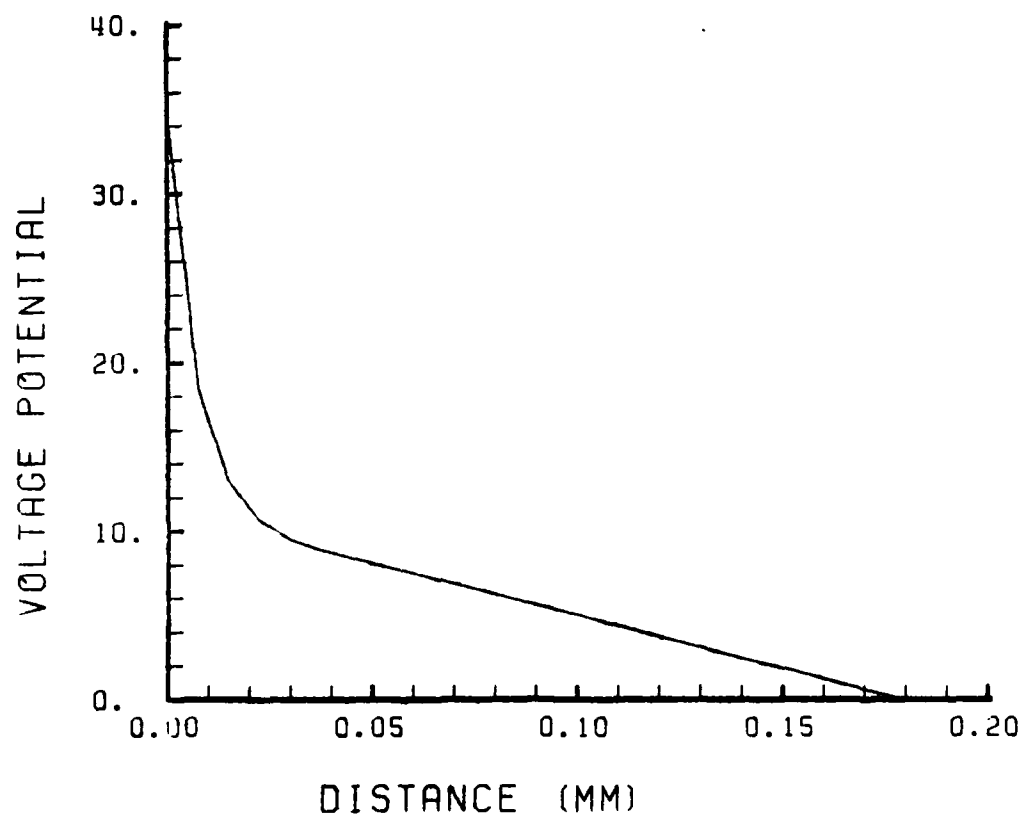


Figure 14-i
Presentation of the Voltage Potential
(CASE III) along a line norm to the wall,
extending from the active node site.

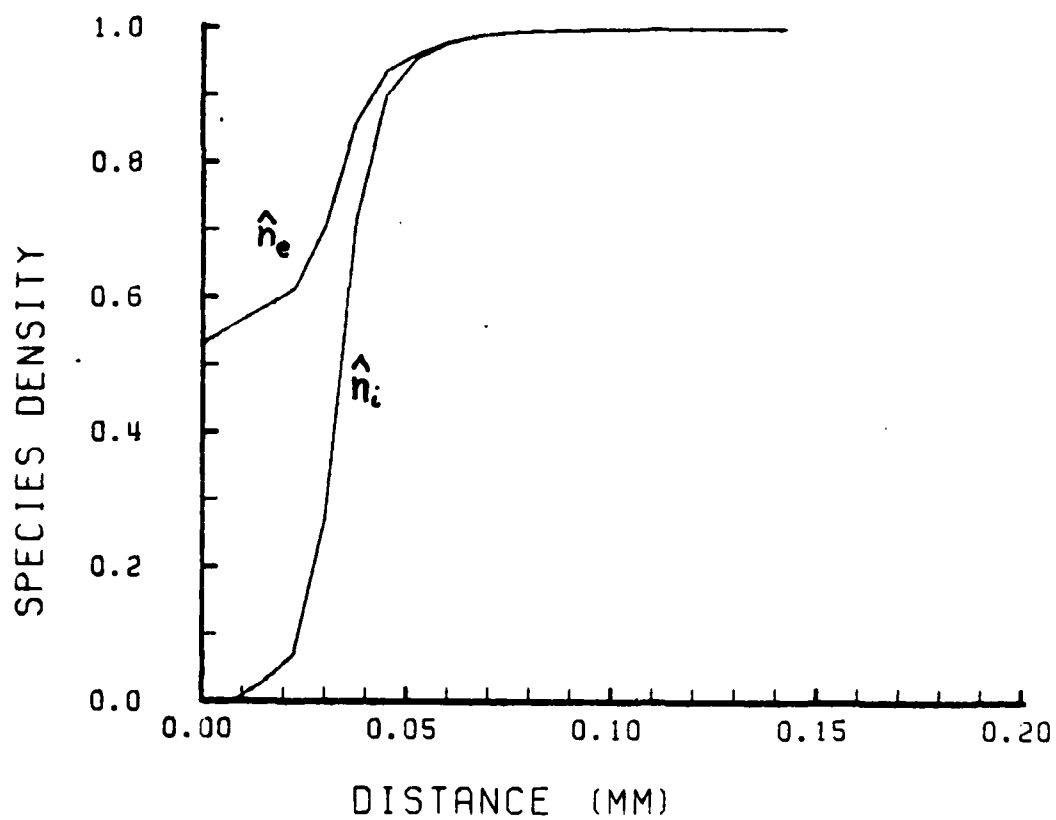


Figure 14-j
Presentation of Species Density
(CASE III) along a line normal to the wall,
extending from the active node site.

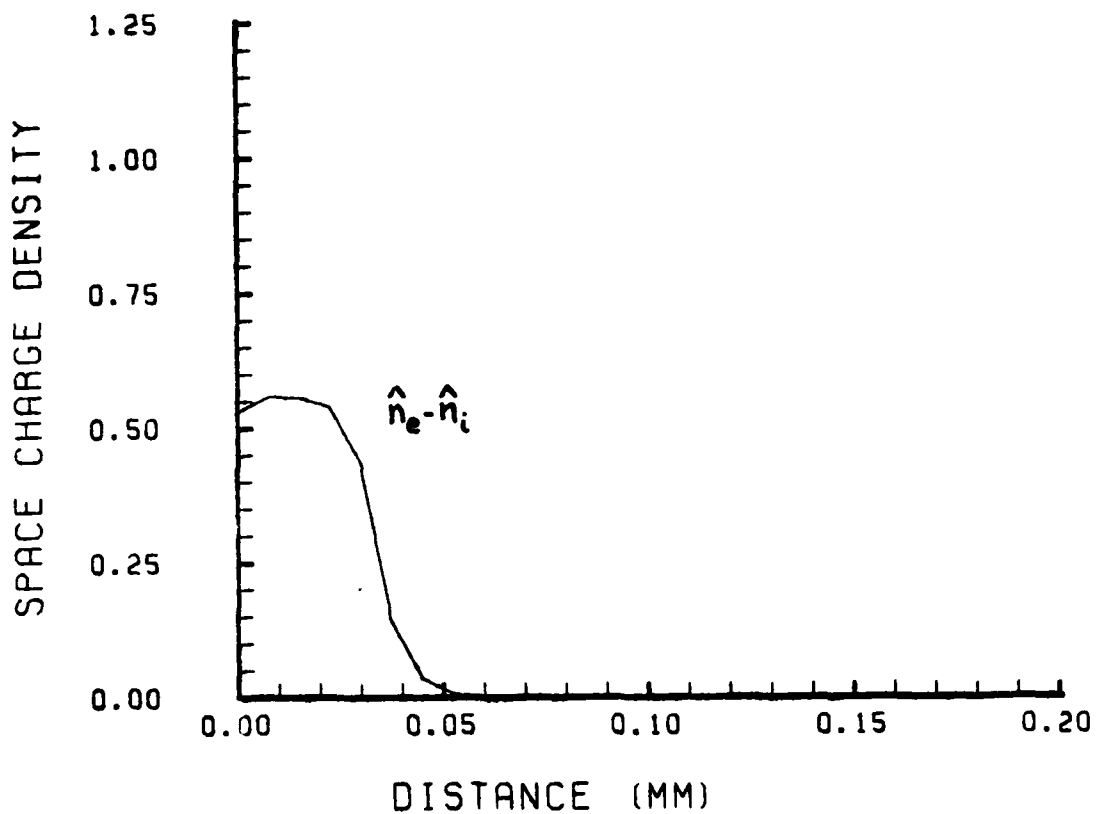


Figure 14-k
Presentation of the negative Space Charge Density
(CASE III), along a line normal to the wall,
extending from the active node site.

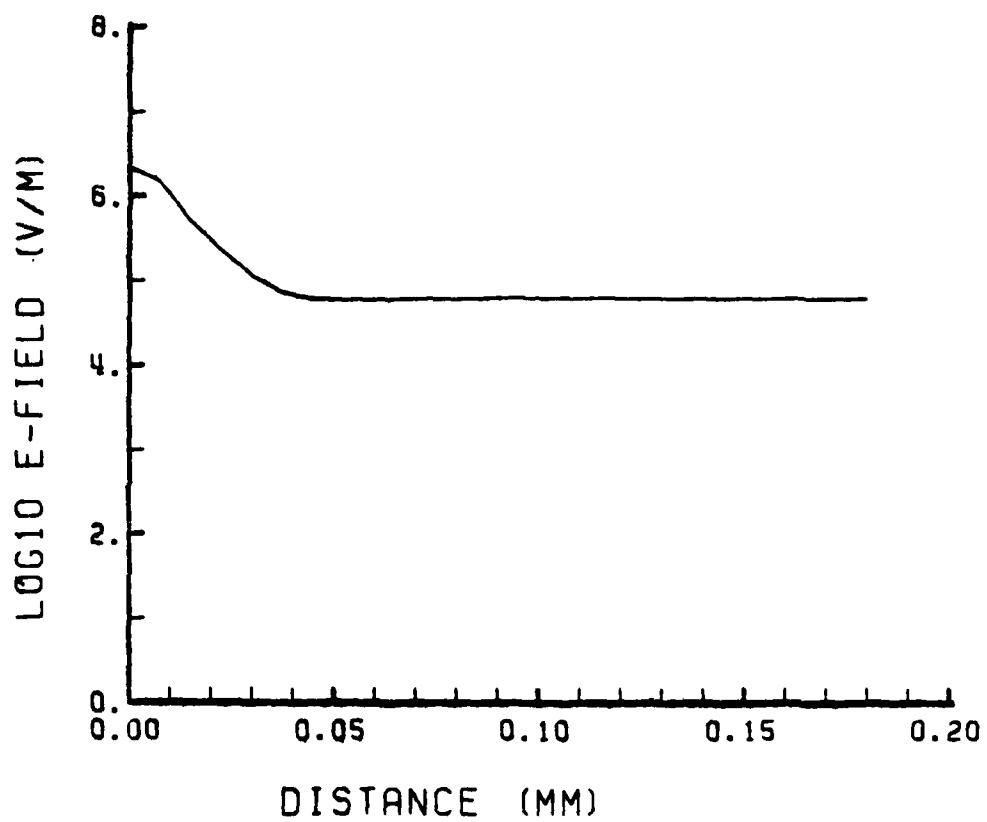


Figure 14-1
Presentation of the Electric Field
(CASE III), along a line normal to the wall,
extending from the active node site.
(logarithm scaled)

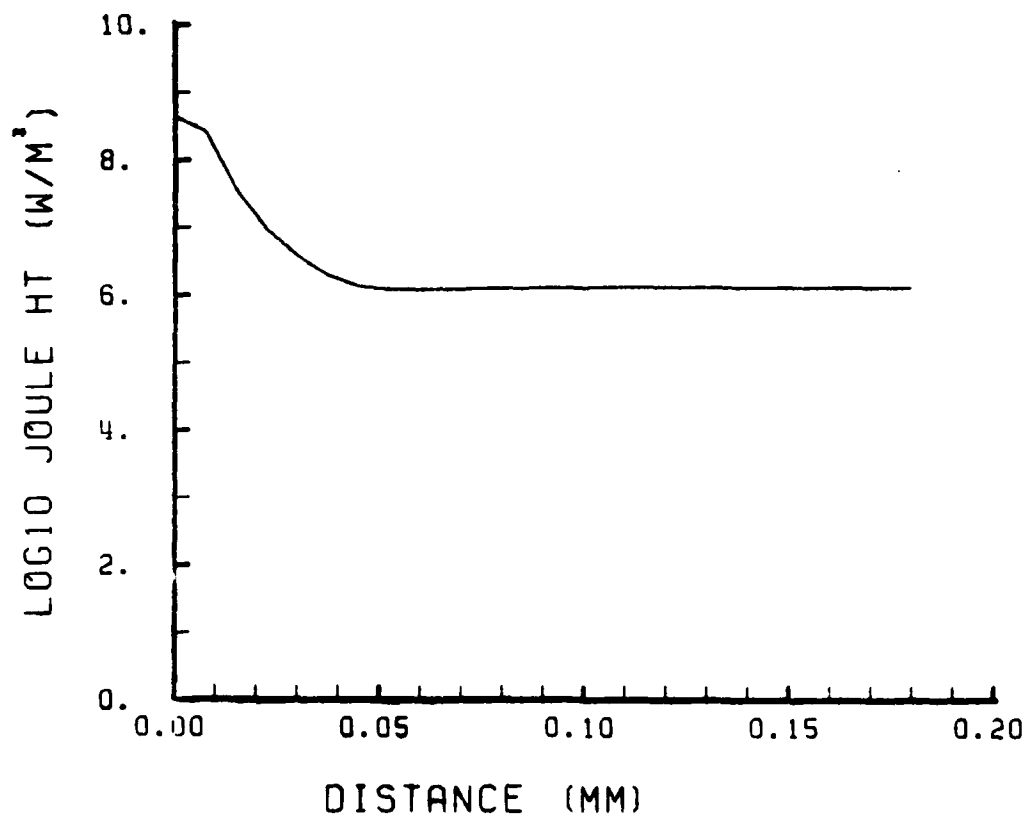


Figure 14-a
Presentation of the Joule Heating
(CASE III) along a line normal to the wall,
extending from the active node site.
(logarithm scaled)

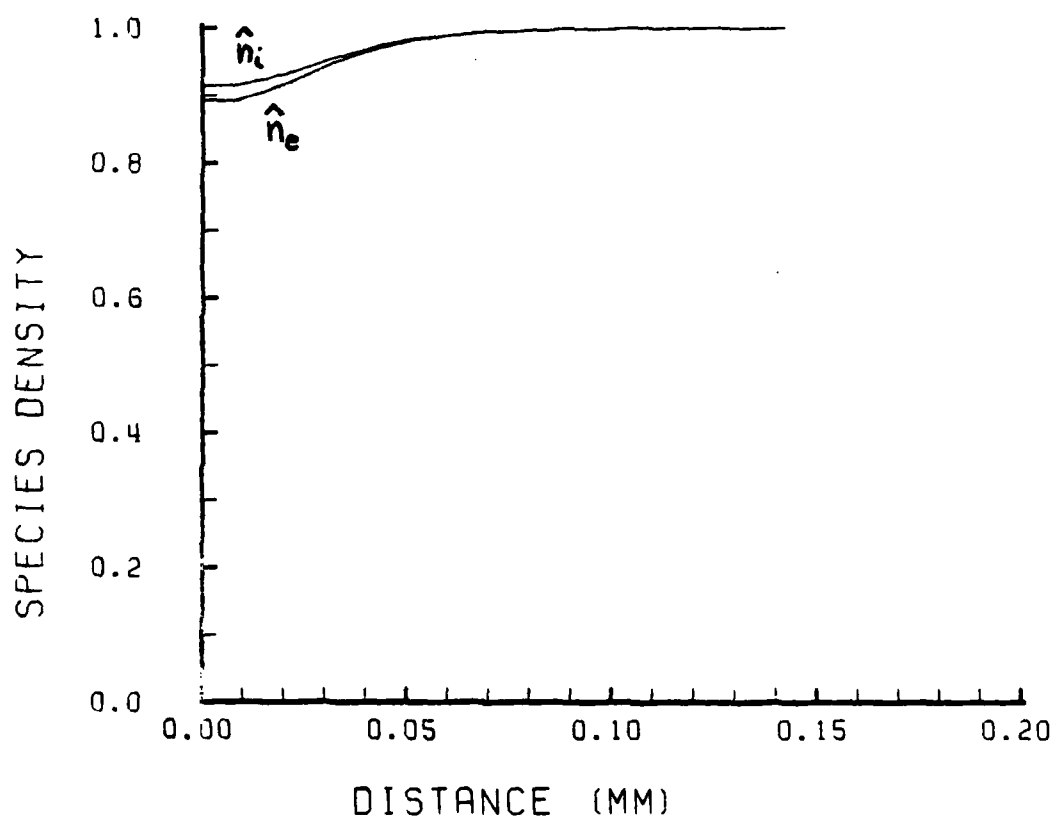


Figure 14-n
Presentation of the Species Densities
(CASE III) on a line normal to the wall,
extending along the inter-nodal symmetry line.

V. CONCLUSIONS AND RECOMMENDATIONS

A. REVIEW OF ASSUMPTIONS

In the development of this work several assumptions were made which the solution results later verified. The assumption of negligible convection effects is straight forward. The charged particle density boundary layer evolution time turns out to be small in relation to the pulse period; thus enabling consideration of the problem as a steady-state after-glow problem. The fact that the Joule heating of the gas is shown negligible, frees the formulation from an elaborate energy description. Since the electron temperature is a simple function of E/n , the problem can be further simplified. The solution proceeds with nominal values of the parameters of the discharge as discussed in Sec. II.B. Finally, the importance placed on the net production term is verified by the profound changes in the results including the fact that " \dot{n}_e " is necessary for the establishment of the charged-species boundary-layer behaviour. The analysis of App. B shows that an assumption of "frozen flow" would in fact be premature.

B. PHYSICAL CONCLUSIONS

The present model of the sheath and ambipolar region evolves from the assumptions of steady state, uniform ion temperature and constant diffusion coefficients. A summary of important results is presented in Table II.

TABLE II: SUMMARY OF IMPORTANT RESULTS

SUMMARIZED RESULTS	CASE I	CASE II	CASE III	(units)
sheath length	3.8	3.5	3.7	10^{-5} m
ambipolar length	4.5	3.5	3.7	10^{-5} m
E_{∞} (free-stream)	7.9	3.9	6.3	10^4 V/m
E_0 (anode)	1.9	2.5	2.2	10^4 V/m

The results show that a sheath develops as anticipated from theory and the proposed assumptions. The sheath characteristic length is consistent with that predicted by Debye shielding. Debye shielding of a flat plate predicts that the sheath length " λ_d " is 4.4×10^{-5} meters. For a point (or spherical) shielding the sheath length is 3.1×10^{-5} meters. The present study involves the shielding of a point voltage source situated on a surface charged plate. Since both two- and three-dimensional effects are inherent in the formulation, the resulting sheath lengths are quite reasonable.

As Table II shows, the size of the ambipolar region is of the same order as the sheath size. Here the ambipolar length is defined as the length extending from the edge of the sheath to the point at which 99% of the free-stream density is recovered. Finally, the sheath can be self-generating from a consistent set of equations without an overall energy equation.

The resulting electric fields at the free-stream boundary do not quite attain the desired 2.7×10^5 V/m presented in the problem formulation. These results fall short by the same factors required for the adjustment of the electron temperature field to meet the stated free-stream boundary requirements. It must be pointed out that the electric field is the required boundary condition. However, this boundary condition could be made to yield no reasonable results, and so the chosen boundary condition is $\phi = 0$.

The resulting electric fields at the active site in each of Cases I, II, or III was of two orders of magnitude higher than that of the free-stream. These electric fields are below that needed for breakdown of Nitrogen at one atmosphere, which is determined as, [Ref. 18];

$$E_0 = (E/p)p = (350 \text{ V/cm-torr}) \times (760 \text{ torr}) = 2.7 \times 10^5 \text{ V/m}$$

The requirement of strictly matched currents produces steep derivatives and inflections of the density profiles in the vicinity of the anode. A noticeable "spike" is evident in Fig. 12-j for example. Case II and III anode electron densities were established on more aesthetic grounds, where smoother appearing density profiles were generated. In these cases the anode current exceeded the free stream current by only a factor of 3.

The nonactive regions of the electrode (wall) far from the active site reveal a small positive space charge density amounting to approximately 2% of the free-stream density. The negative space charged sheath is 46% to 56% of the free-stream density.

Previous work [Ref. 12] of a similar problem reported no reasonable results for the case of a catalytic wall ($n_e = n_i = 0$). The results presented in this study demonstrate wall conditions of $n_i = 0$ and $n_e < 1$. Here, a noticeable positive space charge coexists with the large negative space charged sheath, without large inflections in either the voltage potential or densities.

The Case III study has both electron and ion wall conditions floated. The shape of these density distributions is quite symmetrical about the anode site in all directions.

One needs little imagination to visualize that the density profiles can be "wrapped" around the anode completely, in effect treating the anode as a whisker or protrusion into the plasma. However, the imagination must be tempered by the fact that it can only be a two-dimensional protrusion (e.g., a "blade").

The effect of the net production term has been previously discussed as one of the most important results of this study. The term is necessary for inclusion in the problem in order (1) to attain wall electron density values of less than the free-stream, (2) to produce the boundary-layer behavior of the species densities, and (3) to obtain converged solutions with voltages greater than 10 volts or computational node spacings of any order less than that of the sheath length.

C. NUMERICAL CONCLUSIONS

The Modified Newton-Raphson (MNR) method, presented to solve the particular set of coupled non-linear partial differential equations in this study, is a general method that can be applied to more sophisticated systems. The deficiency of the quasi-Jacobian method (discussed in Sec. III.C and App. C.) in dealing with non-linear terms is circumvented by an alternative linearizing scheme. Convergence is

rapid; however, the starting solution must not exceed 10 volts, must have zero net production, and must have a constant electron temperature during the first 2-3 iterations. After the solutions take their initial form at ten volts, the potential field is "amplified" and reinstated as a new starting solution. The final stages of the converging solution are carried out under the full influences of (1) floating wall densities, (2) variable electron temperature, (3) net production and (4) an active node site electron density being solved for through current matching.

The profiles of the space charge and net production distributions demonstrate erratic behavior at the first few computational nodes from the active site. This is believed to be caused by the linearization of the governing non-linear equations and has the appearance of truncation error when observed on an iteration to iteration basis. However, the remaining regions of the profiles are smooth.

D. RECOMMENDATIONS

This work succeeded in solving the problem in a two-dimensional environment. This fact necessarily limits the quantitative results since the current density decreases in only two dimensions. With the computational power of recent computers, it should prove worthwhile to make the next

advance as a three-dimensional problem rather than elaborate in the two-dimensional case. A three-dimensional scheme would render more realistic results of a quantitative nature because active spots are more likely to exist than active lines and because 3-D geometries require less voltage for a given current.

Specific recommendations other than the above include;

- Account for the ion contribution to the current boundary condition into the wall.
- Investigate the physical implications of the low electron temperature near the wall far from the anode site.
- Investigate the physical implications of the electron density "spikes" prevalent near the anode site.
- Make the wall temperature a valid boundary condition.
- Use a free-stream boundary condition of $E_\infty = 2.7 \times 10^5$ V/m, rather than zero potential. This would introduce desired results for pumping lasers.
- Include a more sophisticated electron temperature model, or verify the present one.
- Increase the computational mesh density.
- Study the general application limits of the MNR method.
- Investigate "n" in the role of making one-dimensional solutions possible (i.e., alter the reacting rates).
- Investigate whether the low electron temperatures and associated steep derivatives located along the wall between active sites have any physical implications, or result merely from inadequate problem formulation.
- Consider the electron-beam ionization in the solution to produce more realistic effects.

APPENDIX A

CHARACTERISTIC PARAMETERS

A. SHEATH LENGTH

The extent of the sheath is one of the most important characteristic lengths in this study. It is within the sheath that most of the potential drop occurs for a short discharge. Fortunately, the sheath length can be estimated rather easily from Poisson's equation, (Eq. A1)

$$\nabla^2 \phi = \frac{e}{\epsilon_0} (n_e - n_i) \quad (A1)$$

Let;

$$\hat{\phi} = \frac{e(\phi_0 - \phi_\infty)}{kT_{eo}} = \frac{e|\phi|}{kT_{eo}} \quad ; \quad \hat{n}_s = n_s / n_{eo} \quad (A2)$$

where " λ_s " is the characteristic sheath length; the subscript "o" indicates the value at the electrode and " " the value at the undisturbed plasma. After gathering the dimensional quantities on one side, Eq. A2 becomes;

$$\hat{\nabla}^2 \hat{\phi} = \frac{e n_{eo} \lambda_s^2}{\epsilon_0 |\phi|} [\hat{n}_e - \hat{n}_i] \quad (A3)$$

The characteristic sheath length " λ_s ", defined in this fashion, is used to non-dimensionalize the "del" operator in all directions. That is, independent of the dimensionality

of the problem, the sheath is effective over the characteristic length just defined. Now an estimate of the size of the sheath can be made by setting the grouping of dimensional quantities in Eq. A3 to be of the order one, namely;

$$\lambda = \left[\frac{\epsilon_0 |\phi|}{e n_{\infty}} \right]^{1/2} = \lambda_{D\infty} \left[\frac{e |\phi|}{k T_{e\infty}} \right]^{1/2} \quad (A4)$$

where " $\lambda_{D\infty}$ " is the Debye length in the undisturbed plasma.

Anticipated values are now established for the sheath length. Take for example a 35 volt anode potential, and a charge species density of 10^{17} to 10^{19} m^{-3} . These parameters define a sheath length of 1.4×10^{-4} to 1.4×10^{-5} meters.

As can be seen, a ten-fold increase in voltage would change " λ_s " by a factor of 3, rendering the nondimensionalization of the problem relatively insensitive to the chosen value of the voltage potential. That is to say the value of the sheath characteristic length as defined may be considered a reasonable estimate for the charge species densities exemplified.

The important implication here is that extreme care must be devoted to electrode surface preparation to preclude whiskers or flaws of a size comparable to " λ_s ". These protrusions would produce a focusing of the electric potential to create extremely high electric fields, which become sites

for initiation of breakdown. Protrusion growth has been observed to form in a time on the order of milliseconds. Many conditions are favorable to protrusion growth, dependent on the pre-breakdown and breakdown current profile, electrode composition (especially in the case of a thermionic cathode), surface purity and surface preparation [Ref. 21]. Some possibilities are;

- Electrode plastic flow or melting in an electric field due to micro-particle bombardment.
- Sticking of microparticles.
- Electron beam induced protrusion growth.

B. DIFFUSION LENGTH

If diffusion is a significant factor in this study then its contribution to the current would be;

$$J_x = D_e e \frac{\partial n_e}{\partial x} - D_i e \frac{\partial n_i}{\partial x}$$

or, since $D_e > D_i$, and using Einstein's relation, or $D/\mu_e = kT_e/e$;

$$J_x \approx e D_e \frac{\partial n_e}{\partial x} = \mu_e k T_e \frac{\partial n_e}{\partial x}$$

making the equation unit free (through fractional analysis);

$$\frac{JL}{e D_e n_{e0}} = \frac{\partial n_e}{\partial x} \sim \text{ORDER}[1] \quad (A5)$$

If the right side of Eq. A5 is of the order one, (the nondimensional density gradient is a maximum of 1) then "L" may be estimated as;

$$L \approx eD_e n_e / J \approx 3.7 \times 10^{-6} \text{ m}$$

for the values;

$$n_e = 10^{18} \text{ m}^{-3}$$

$$D_e = 0.0665 \text{ m}^2/(\text{V} \cdot \text{sec})$$

$$J_e = \mu_e \cdot n_e \cdot \nabla \phi = \mu_e \cdot e \cdot n_e \cdot n_e \cdot (E/n) \approx 2.88 \times 10^3 \text{ A} \cdot \text{m}^{-2}$$

Since $\lambda_D > L$, then any role attributed to diffusion should be visible within the sheath. The E/n within the thin sheath is of course greater than the E/n at the free stream ($10^{20} \text{ V} \cdot \text{m}^2$), which decreases the local value for "L" still further.

Another approach is to assume a one-dimensional solution to the charged species conservation equations, which can only be done outside of the sheath, i.e., in the ambipolar region. The ion conservation equation may be written;

$$\dot{n} = \nabla \cdot J = e \nabla \cdot [\nabla n \nabla \phi - D \nabla n] \quad (\text{A6})$$

Since it can be shown (next section) that the production term can be approximated as;

$$\dot{n} \approx \nu_i n - \alpha n^2$$

then for the stationary condition of no net production;

$$\nu_i = \alpha N$$

Nondimensionalizing Eq. A6, it can be shown that the

characteristic diffusion length "L" is;

$$L = \sqrt{D/\kappa N} = 2. \times 10^{-6} \text{ meters}$$

which is of the same order of magnitude as the characteristic sheath length.

C. IONIZATION/RECOMBINATION LENGTH

Analysis of the production term (Eq. 4) reveals that for Nitrogen the three-body (electron) collisional recombination rate (α_2) is small in relation to the other terms, (see App B.). In any case the net production term is;

$$\dot{n}_e = \nu_i n_e - \alpha_1 n_e n_i - \alpha_3 n_e n_i n_e \quad (A7)$$

In the steady state the net production term is zero, and as is done in Appendix B, the relation becomes;

$$\dot{n}_e = (\alpha_1 + \alpha_3 n_e) \cdot (n^+ - n_e) \cdot n_e$$

substituting the value of $0.17 \times 10^{-11} \text{ m}^3/\text{sec}$, and $(n^+ - n_e) \approx 10^{16}$, we can estimate the characteristic production time to be $\tau_p = 5.88 \times 10^{-7} \text{ sec}$.

To establish a meaningful characteristic length, the average thermal velocity will be used since it represents the principal transport velocity of the medium.

$$l_p = \tau_p \cdot \bar{v}_e = 5.88 \times 10^{-7} \cdot 3.2 \times 10^8 = 1.88 \times 10^{-6} \text{ m}$$

The characteristic length for net production is a factor of four larger than the sheath length ($\lambda_s = 4.4 \times 10^{-7} \text{ m}$). The

conclusion which can be made from this (fractional) analysis is that the net production is significant within the overall region of interest, including the sheath itself.

D. FROZEN FLOW

When a process relaxation time " τ_p " is long compared with the time that a fluid particle spends in a given region, the flow is said to be "frozen" in this region. By this term one means that a reaction process may be neglected, as far as influencing the flow is concerned, and the species involved treated as chemically inert, [Ref. 22]. In the opposite limit, where " τ_p " is very small relative to " τ_f " the characteristic flow time, the flow is said to be in "equilibrium." For the recombination rates given in this section, " τ_p " = 6×10^{-7} and " τ_f " = 4.0×10^{-7} seconds. Here flow time is defined as the sheath characteristic length divided by the drift velocity. Thus the flow is not "frozen" as far as chemical reaction, but we must consider that the electron and ion species are not in thermal equilibrium.

APPENDIX B

DEVELOPMENT OF THE PRODUCTION TERM

The net production term is defined as the difference between ionization and recombination rates. Whenever a neutral atom or molecule loses one or more of its electrons, ionization has occurred. Recombination is the process wherein positive ions and electrons combine to form neutral atoms or molecules. It is simply reverse ionization. If the net production is zero then ionization and recombination are equal. The net production term is the right side of Eqs. 2 and 3, the expression for which is developed here.

This work considers only three types of recombination

- (1) Dissociative - the electron recombines with a molecular ion $(AB)^+$, and the recombination energy goes into dissociating the molecule and increasing the kinetic energy of the resulting products. The process is described as;



- (2) Three-body (electron) - the energy released in the recombination process is carried off by a third body which is an electron. The process is described as;



- (3) Three-body (heavy) - the recombination energy is carried off by a third body which is a heavy particle such as an atom or molecule. The process is described as;



This study does not consider other recombination mechanisms such as radiative or dielectric recombination, since they are generally of low significance in relation to the just described processes. The ions are limited to singly positive ions. No account is made for intermediate or excited states as this requires a detailed balancing which is beyond the scope of this work. Additionally, no account is made of attachment.

Rewriting Eq. 4 for simplicity of discussion;

$$\dot{n}_e = \gamma_i n_e - \alpha_1 n_e n_i - \alpha_2 n_e^2 n_i - \alpha_3 n_e n_i n_o \quad (B1)$$

where each " α_i " refers to the recombination coefficients for dissociation, three-body (electron) and three-body (heavy), respectively.

The recombination coefficients depend upon the ionic species involved. Some general but representative values [Ref. 22] follow;

$$\begin{aligned} \alpha_1 &= 10^{-13} \text{ m}^3/\text{sec} \\ \alpha_2 &= 9 \times 10^{-14} \text{ m}^3/\text{sec} \\ \alpha_3 &= 2 \times 10^{-13} \text{ m}^3/\text{sec (air)} \end{aligned}$$

Hinnov and Hirschberg [Ref. 23] developed a relation for three-body (electron) recombination coefficients as a function of electron temperature (T_e) and density, valid for energies less than 0.25 eV.

$$\alpha_2 = 1.09 \times 10^{-20} n_e T_e^{-9/2} \text{ m}^3/\text{sec}$$

where the electron temperature is °K. Gurevich and Pitaenski [Ref. 24] extended this development to obtain;

$$\alpha_2 = 2.13 \times 10^{-20} n_e T_e^{-9/2} \ln A \text{ m}^3/\text{sec}$$

where;

$$\ln A = 1.24 \times 10^7 (T_e^3/n_e)^{-0.5}$$

At 1.0 eV these coefficients are 5.6×10^{-21} and 1.05×10^{-10} m^3/sec respectively. A simplification of the later expression for α_2 is valid from energies of 0.1 to 10.0 eV and $n_e = 10^{-18} \text{ m}^{-3}$;

$$\alpha_2 = 0.032 x T^{-4.3}$$

Brown [Ref. 18: p.197] gives a value for the dissociative recombination coefficient;

$$\alpha_1 = 1.5 \times 10^{-12} \text{ m}^3/\text{s}$$

The ionization coefficient can be determined from considering that there is no net production in the free stream, i.e., far from the electrode. Here;

$$0 = \nu_i N - \alpha_1 N^2 - \alpha_2 N^3 - \alpha_3 N^2 n_e \quad (\text{B2})$$

where "N" is the stationary state. Solving for and substituting into Eq B1 gives;

$$\dot{n}_e = n_e (N - n_i) (\alpha_1 + \alpha_2 n_e) + \alpha_3 n_e T_e^{-3/2} (N^2 - n_e n_i) \quad (B3)$$

where;

$$\alpha_1 = 1.5 \times 10^{-12} \quad (\text{from Ref. 18})$$

$$\alpha_2 n_e = 1.09 \times 10^{-20} \quad (\text{from Ref. 23})$$

$$\alpha_3 n_e = 2.0 \times 10^{-13} \quad (\text{from Ref. 22})$$

The net production term is the relation, suitably non-dimensionalized, that appears in the computer subprogram "RTSIDE."

APPENDIX C
NUMERICAL SOLUTION METHOD

A. GENERAL DISCUSSION

There are two basic approaches used in solving a nonlinear system of equations, such as posed in this study. A given method can usually be classified as one of the ascent (or descent) or more commonly referred to as gradient methods, or as one of the Newton methods. The method applied in this study and by Dolson [Ref. 12] is one of the Newton methods. A brief review of both methods will be presented to facilitate development of the particular method employed in this study.

Let the nonlinear system of equations be written as;

$$\begin{aligned} f_1(x_1, x_2, \dots, x_n) &= 0 \\ &\dots \\ f_n(x_1, x_2, \dots, x_n) &= 0 \end{aligned} \tag{C1}$$

or in vector form for convenience;

$$f(\vec{x}) = 0 \tag{C2}$$

In the descent method the problem is posed in such a way so as to form a function which is zero at any solution and positive otherwise. A typical such function would be;

$$\phi(x_1, x_2, \dots, x_n) = \sum_{i=1}^n |f_i|^2 \quad (C3)$$

so that the problem is reduced to finding a minimum of ϕ , which also happens to be the value zero. In solving problems by this method, an initial guess to the solution must be provided, call it $x^{(1)}$. Then a direction d is determined so as to point to a better solution, $x^{(2)}$. This direction is often chosen to be the gradient of $\phi(x)$. The operation $-\text{grad } \phi(x)$ is the direction in which $\phi(x)$ decreases most, and is locally the best direction in which to reduce $\phi(x)$.

$$d = -\text{grad } \phi(x)$$

so that;

$$x^{(2)} = x^{(1)} - a \cdot \text{grad } \phi(x^{(1)})$$

where "a" is chosen to be an appropriate step size. A problem is encountered at local minima of $\phi(x)$, which needs to be avoided. One must also use the step "a" in such a manner as to control the acceleration along slowly or rapidly varying $\phi(x)$. It may be that by the nature of $\phi(x)$, the gradient may have to be approximated by finite differences, an approach which offers a flexible recourse even when not required.

AD-A107 455

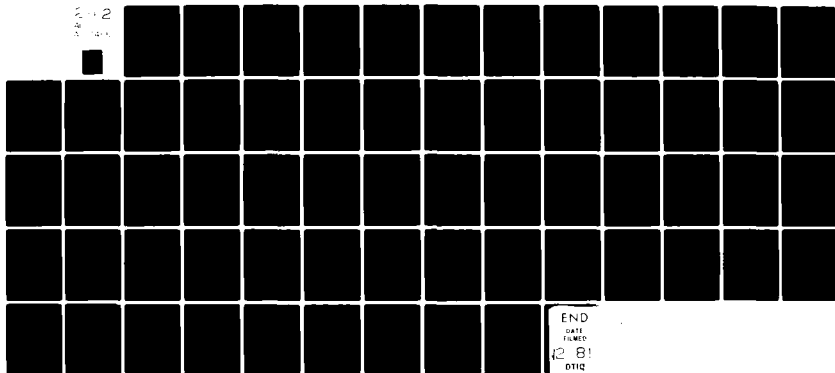
NAVAL POSTGRADUATE SCHOOL MONTEREY CA
A COMPUTER ANALYSIS OF THE PLASMA-BOUNDARY LAYER BEHAVIOR OVER --ETC(U)
JUN 81 S T VAN BROCKLIN

F/6 20/9

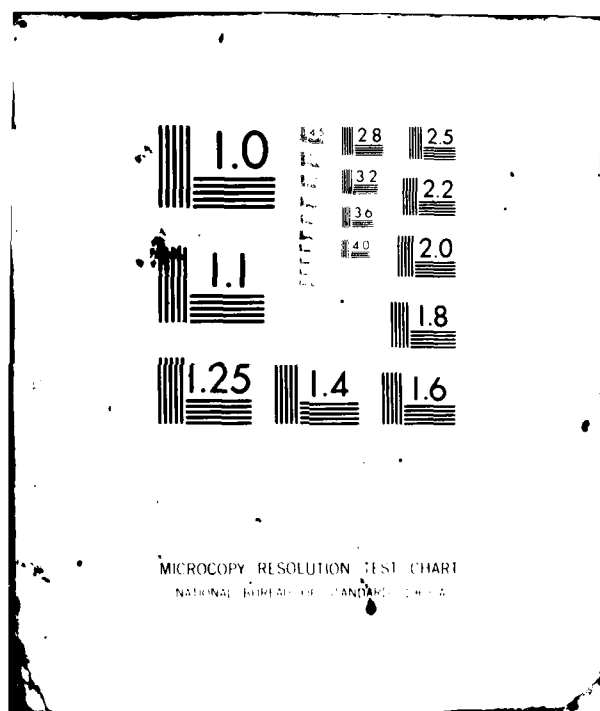
UNCLASSIFIED

NL

2-2
2-2
2-2



END
DATE
FILMED
12-81
DTIC



The Newton method involves approximating the nonlinear problem by a suitable linear problem involving derivatives of the nonlinear equations evaluated at $x^{(1)}$. The linearized problem is simply a set of linear algebraic equations, the solution to which furnishes an increment that when added to the solution $x^{(1)}$ will yield $x^{(2)}$. This method is a generalization to n-dimensions of Newton's method for evaluating the zeros of a function.

Each function $f_i(x)$ is approximated by the initial two terms of a Taylor series expansion about the solution vector $x^{(1)}$;

$$f_i(x) = f_i(x^{(1)}) + J(x^{(1)}) \cdot [x - x^{(1)}] \quad (C4)$$

where "J" is the familiar Jacobian matrix;

$$J = \sum_{j=1}^n \frac{\partial f_i(x^{(1)})}{\partial x_j} \quad (C5)$$

The right-hand-side of equation C4 is the linear vector function (tangent hyperplane) of x which best approximates the nonlinear function f evaluated at $x^{(1)}$. We set this right-hand-side equal to zero and solve for x , which is an improvement from $x^{(1)}$. We call this improved solution vector $x^{(2)}$, and from equation C4 we get;

$$x^{(2)} = x^{(1)} - J(x^{(1)})^{-1} \cdot f(x) \quad (C6)$$

The Jacobian need not be known very accurately, and often is left unchanged for several iterations since its evaluation often entails penalizing computer time. Thus the method (slightly modified as described briefly in section III.B) used by Dolson [Ref. 12], is referred to in many texts as the Newton method or as the Newton-Raphson method [Refs. 25, 26].

The Jacobian matrix of coefficients for elliptic problems is typically a sparse banded matrix, to which there are many computer subroutines available for solution.

B. MODIFIED NEWTON-RAPHSON METHOD

The particular solution technique employed in this study merits a detailed discussion, since it is not common in the literature. Bailey and Touryan [Ref. 27] use a similar method and provide some description of its development. The method is similar to other Newton methods however, the Jacobian matrix is replaced by a matrix of coefficients developed from a sequence of linear differential equations which approximate the system of nonlinear equations. This method will be referred to as a modified Newton-Raphson method or MNR method for short, and will be presented in general using a specific example.

Take Poisson's equation given earlier and repeated here for simplicity;

$$\nabla^2 \phi = c_1 (n_e - n_i) \quad (C7)$$

The known solution variables are;

$$\phi^{(1)}, n_e^{(1)}, \text{ and } n_i^{(1)}$$

In general the first step is linearization of the equation. In this case Eq. C7 is linear, but it will serve as an example. We assume that the succeeding solution variables at iteration-(2), namely $z^{(2)}$, can be approximated by the solution $z^{(1)}$ plus some small change $\Delta z^{(1)}$.

$$\Delta z^{(2)} = z^{(1)} + \Delta z^{(1)} \quad (C8)$$

where;

$$z^{(k)} = (\phi^{(k)}, n_e^{(k)}, n_i^{(k)})^T$$

It remains to determine $\Delta z^{(1)}$. Substitution of this relationship into the Poisson Equation is the second step:

$$\nabla^2 \phi^{(2)} = \nabla^2 \phi^{(1)} + \nabla^2 \Delta \phi^{(1)} = c_1 (n_e^{(1)} - n_i^{(1)}) + c_1 (\Delta n_e^{(1)} - \Delta n_i^{(1)})$$

rearranged;

$$\nabla^2 \Delta \phi^{(1)} - c_1 (\Delta n_e^{(1)} - \Delta n_i^{(1)}) = - [\nabla^2 \phi^{(1)} - c_1 (n_e^{(1)} - n_i^{(1)})] \quad (C9)$$

The right hand side of Eq. C9 is a function of the known solution vector $z^{(1)}$. We are applying this relationship at each computational node. A second order partial differential equation can be approximated by a second order difference equation or "3-point formula," so Eq. C9 will become a system of linear algebraic relationships involving near neighboring values of the solution vector $z^{(1)}$. The left side of Eq. C9 is composed of a system of coefficients expressible in terms of $z^{(1)}$ times the unknown (perturbation) vector $\Delta z^{(1)}$. So we now have;

$$A(z^{(1)}) \cdot \Delta z^{(1)} = -F(z^{(1)}) \quad (C10)$$

Here the matrix of coefficients "A" is a sparse matrix with a relatively narrow band of non-zero elements about the main diagonal, provided that the "natural" order of the resulting linearized equations is preserved. There are standard computer routines available which take advantage of this banded structure, such as LEQT1B, an IMSL routine.

It follows that since $\Delta z^{(1)} = z^{(2)} - z^{(1)}$;

$$z^{(2)} = z^{(1)} - [A(z^{(1)})]^{-1} \cdot F(z^{(1)}) \quad (C11)$$

For the case of a nonlinear term such as;

$$n_e \frac{\partial \phi}{\partial x}$$

there is no additional difficulty. When linearized this term becomes;

$$n_e \frac{\partial \phi}{\partial x} + \Delta n_e \frac{\partial \phi}{\partial x} + n_e \frac{\partial \Delta \phi}{\partial x} + \Delta n_e \frac{\partial \Delta \phi}{\partial x} \quad (C12)$$

We neglect high order terms created by the inner products of the elements of $\Delta z^{(1)}$, such as the last term in relation C12. The first term would be a part of the function $F(z^{(1)})$ in the right side of Equation C10, and the remaining two terms would be included as part of the expression:

$$\Lambda(z^{(1)}) \cdot \Delta z^{(1)}.$$

APPENDIX D

DESCRIPTION OF COMPUTER PROGRAMS

This appendix serves as a user oriented guide to the computer programs listed in App. E. The programs are listed in the order used to generate solutions to the problem formulated in this report. The output consists of printed results for each iteration and punched output to provide a permanent file copy, which is to be used as input to the three plotting programs also listed in App. E. These plotting programs use the Versatec plotter and associated software, and represent the only facility not commonly available elsewhere. The main program SHTH as presented, is configured to also produce output at a monitor terminal as used on CP/CMS (IBM 360) or MVS (IBM 370). The output in summary is via three devices;

- DEVICE 4 - typically a CRT
- DEVICE 6 - typically a printer
- DEVICE 7 - typically a punch or disk output

These can be manipulated in convenient configurations to give a full or partial (sampled) display of the solution at each iteration, or merely to display convergence information in a simple format.

The SHTH program is the main program which together with its 9 subroutines and 1 IMSL subroutine solves the non-dimensionalized forms of Eqs. 1 through 4. The input to the program consists of control cards and data cards, namely;

1 control card
3 or 104 initial solution data cards
1 control card

The control card is described here in terms of the Fortran variable names thereon.

ITMIN - is the iteration counter (ITER) starting value. If **ITMIN** = 1, then the program will read in the next 3 cards as data which contain the short form starter solutions. If **ITMIN** is greater than 1, then the program will read in the next 104 cards as data, representing a detailed starting solution. This detailed starting solution is typically the output of a previous run of the program. If **ITMIN** = 00, then the program will not read in any data, being thus informed that the problem is over.

ITMAX - is the last iteration value. The program ceases iterations at this point and outputs the solutions and auxillary information.

ITNDT - enables the employment of the net production term (RTSIDE) when ITER is greater than **ITNDT**, otherwise the net production is set to zero.

ITEMP - for ITER less than **ITEMP**, the electron temperature is isothermal, otherwise it is a function of E/n. (see SHTH statements 899-990).

ITBC - for ITER greater than 5 and less than **ITBC**, the wall boundary conditions for the species is floated.

LADJ - 1 electron temperature is calculated
- 0 electron temperature is isothermal.

LPUN - 1 output is punched on device 7. - 0 output is not punched.

H - sets the mesh spacing equal to H*LAMS (sheath length).

PKTR - is the adjustment factor to the temperature equation (see Sec. IV) and is used when **LADJ** = 1 and ITER is less than **ITEMP**. The adjustment factor is not used when **LADJ** is set to zero. When the temperature is coupled and **LADJ** = 1, then the program calculates its own adjustment factor.

NAME - is reserved for user labelling and identification which is used at output.

The solution set is;

PH voltage potential (volts) .

NE electron density (10^{18} m^{-3})

NI ion density (10^{18} m^{-3})

TH nondimensional electron temperature

The short form starter solution is illustrated in App. E. It consists of PH, NE and NI values at the anode, wall and equilibrium boundaries. The long form starting solution consists of PH, NE, NI, and TH distributions, each one represented by 25 data cards and a label card. Each card has 7 values. (see format-803).

A typical iteration series would start out for about ten iterations from the short form data with ten volts at the anode and other appropriate boundary conditions. The initial solution converges very well for $H = 0.5$, the net production term coupled after 2 or 3 iterations, and the wall conditions not floated. This output is then used as input. The voltage is amplified to say 25 or 35 volts and a new control card is structured to couple the temperature or whatever else is desired. The H value may also be changed to reflect a smaller mesh spacing. It must be kept in mind that too many changes in one solution run can be catastrophic.

Each iteration of the solution by the SHTH program accomplishes the following;

- (1) floats the NE, NI wall values
- (2) sweeps through the A-matrix and C-vector setting up the equations that satisfy the boundary conditions and the internal mesh conditions
- (3) couples the electron temperature equation
- (4) couples the net production term
- (5) calculates the anode electron density required to satisfy current matching between the anode and the free-stream.

The system of equations has the form presented in Eq. C10 in App. C, and is solved by use of the IMSL routine LEQT1B. The solution vector is then updated from the return information contained in vector C.

There are two solution convergence monitors. The first is the sum of the squares of the differences (spectral norm) of the $-F(z^{(1)})$ values from Eq. C10. The other is the spectral norm of the $\Delta z^{(1)}$ upon return from LEQT1B. Both of these are available at the video terminal (device 4) and printer (device 6).

After solution update, the electron temperature is calculated and adjusted per the control card options. It should

be pointed out that on the last iteration, the temperature distribution is automatically calculated for output, but is not used in the scheme, unless otherwise coupled per the control card.

The matching of the anode current to the free-stream current is accomplished by solving for the anode electron density using subroutine ANODE. The call to this subprogram will require a change to the SHTH program as it is presently overridden with a comment card, (prior to statement 9000).

The final outputs are straight-forward. Subroutines JWALL and JOULE are called in this phase of the program, in order to compute the current into the wall and the Joule heat distribution. The electric field, net production and space charge density distributions are also calculated and provided as punched and printed output.

The punched output is used as input for the STREAM, PICT and PLOT programs. These programs use the Versatec plotter to provide a presentation of the current stream lines, an oblique perspectives of the solutions and plots of the solutions as they vary normal to the wall extending from the anode site. The details of these programs are cumbersome, and it is wise to leave them to the user for inspection.

The first two distributions in the punched output are used in the **STREAM** program, requiring that the nonpertinent data be removed. The next 8 distributions are used for the **PLOT** and **PICT** programs. The **PICT** program has an option card filled with ones or zeros in the first eight positions. This option card enables the user to elect which distributions to plot. The plots provided in this report as Figs. 12 through 14, were produced using the **PICT** and **PLOT** programs. The programs are simple and speak for themselves.

APPENDIX E

COMPUTER PROGRAM LISTINGS

This appendix contains a listing of the programs used in the solution of the equations presented in this work (namely: Eqs. 9,10 and 11), and the auxiliary programs that provided the plots for the report.

SHTH (MAIN PROGRAM)-----	109
DELOP-----	127
GRDNT-----	129
TEMP-----	131
RTSIDE-----	132
PATCH-----	133
ANODE-----	134
JWALL-----	136
JOULE-----	137
OUTPUT-----	138
PLOT-----	139
PICT-----	141
STREAM-----	144
INITIAL INPUT (sample)-----	150

SHI02410
SHI02420
SHI02430
SHI02440
SHI02450
SHI02460
SHI02470
SHI02480
SHI02490
SHI02500
SHI02510
SHI02520
SHI02530
SHI02540
SHI02550
SHI02560
SHI02570
SHI02580
SHI02590
SHI02600
SHI02610
SHI02620
SHI02630
SHI02640
SHI02650
SHI02660
SHI02670
SHI02680
SHI02690
SHI02700
SHI02710
SHI02720
SHI02730
SHI02740
SHI02750
SHI02760
SHI02770
SHI02780
SHI02790
SHI02800
SHI02810
SHI02820
SHI02830
SHI02840
SHI02850
SHI02860
SHI02870
SHI02880

DENSE=1.D+18
DEO=6.65D-02
DID=8.00D-06
RECOM=ALFA1+ALFA3*DENS0
BETA=+38.5D0
TGAS=273.D0
TEINF=IGAS*BETA
UPH=BOLTZ*BETA*IGAS/COUL
1 CONTINUE
DT=0.D0
ITER=0
ADJ=1.D0

CC

DO 50 INC=1,NC
DO 50 JNC=1,NS
PH(INC,JNC)=0.D0
NE(INC,JNC)=1.D0
NI(INC,JNC)=1.D0
GRDX(INC,JNC)=0.D0
GRDY(INC,JNC)=0.D0
GRDZ(INC,JNC)=0.D0
NEDOT(INC,JNC)=0.D0
HEAT(INC,JNC)=0.D0
TH(INC,JNC)=1.D0
DO 51 JKL=1,NS
NE(1,JKL)=0.D0
NI(1,JKL)=0.D0
NE(INC,JKL)=0.D0
NI(INC,JKL)=0.D0

50

51 CONTINUE

READ(5,800) ITMIN,ITMAX,ITNDT,ITEMP,ITBC,LADJ,LPUN,H,FKTR,NAME
IF(ITMIN.LE.0) GO TO 9999

CC

SET THE TEMP ADJ FKTR

IF(LADJ.EQ.0) ADJ=FKTR
WRITE(4,847) ITMIN,ITMAX,ITNDT,ITEMP,ITBC,LADJ,LPUN,H,FKTR,NAME
WRITE(6,847) ITMIN,ITMAX,ITNDT,ITEMP,ITBC,LADJ,LPUN,H,FKTR,NAME
IF(ITMAX.LE.ITNDT) WRITE(6,850)
IF(ITMAX.GT.ITNDT) WRITE(6,851) ITNDT
IF(ITMAX.GT.0) WRITE(6,852) ITMP
IF(LADJ.EQ.0) WRITE(6,881)
IF(ITMAX.LE.ITMP) WRITE(6,852)

```

IF(IITMIN,GE,ITBC,OR,ITBC,LE,NBC) WRITE(6,854)
IF(ITBC,GT,IITMIN,AND,ITBC,GT,NBC) WRITE(6,855) NBC,ITBC
IF(IITMIN,GT,1) GO TO 10
READ(5,801) PHIZ,PHW,PHQ
READ(5,801) NED,NEW,NEQ
WRITE(6,811) PHIZ,PHW,PHQ
WRITE(6,812) NED,NEW,NEQ
WRITE(6,813) NID,NIW,NIQ
WRITE(6,812) NED,NEW,NEQ
WRITE(6,813) NID,NIW,NIQ
SNEW=NEW
SNEQ=NEQ
SNID=NID
SNIW=NIW
SNIQ=NIQ
SPHW=PHW
SPHQ=PHQ
GO TO 20
10 CONTINUE
READ(5,803) DUMMY
DO 11 I=1,NC
11 READ(5,804) (PH(I,J),J=1,NS)
DO 12 I=1,NC
12 READ(5,803) DUMMY
DO 13 I=1,NC
13 READ(5,804) (NE(I,J),J=1,NS)
DO 14 I=1,NC
14 READ(5,803) DUMMY
DO 15 I=1,NC
15 READ(5,804) (NI(I,J),J=1,NS)
DO 16 I=1,NC
16 READ(5,803) DUMMY
DO 17 I=1,NC
17 READ(5,804) (TH(I,J),J=1,NS)
SNEW=NE(1,1)
SNID=NI(1,1)
PHIZ=PH(1,1)
DO 18 J=1,NS
DO 18 J=1,NC
PH(I,J)=PH(I,J)/UPH
CALL PATCH(TH,1,DO,99,DO)
CALL OUTPUT(6,PH,UPH,VOLTAGE POTENTIAL)
CALL OUTPUT(6,NE,1,DO,ELECTRON DENSITY)
CALL OUTPUT(6,NI,1,DO,ION DENSITY)
CALL OUTPUT(6,TH,1,DO,TEMPERATURE DISTRIBUTION)
20 CONTINUE

```

SHT02890
 SHT02900
 SHT02910
 SHT02920
 SHT02930
 SHT02940
 SHT02950
 SHT02960
 SHT02970
 SHT02980
 SHT02990
 SHT03000
 SHT03010
 SHT03020
 SHT03030
 SHT03040
 SHT03050
 SHT03060
 SHT03070
 SHT03080
 SHT03090
 SHT03100
 SHT03110
 SHT03120
 SHT03130
 SHT03140
 SHT03150
 SHT03160
 SHT03170
 SHT03180
 SHT03190
 SHT03200
 SHT03210
 SHT03220
 SHT03230
 SHT03240
 SHT03250
 SHT03260
 SHT03270
 SHT03280
 SHT03290
 SHT03300
 SHT03310
 SHT03320
 SHT03330
 SHT03340
 SHT03350
 SHT03360

```

CC      SET UP NONDIMENSIONAL VALUES
-----
HH=H*H
PHIB=PHIZ/UPH
SPHIB=PHIB
LAM= (EPSO*PHIZ/(COUL*DENSE))**.5D0
CONJ=COUL*DENSE/LAM
EQP=COUL*PHIZ/(BOLTZ*BETA*TGAS)*HH
EQE=EQE*DEO/DIO
EQT=UPH/(LAM*DENSE)*1.D+20/H
-----
CC      BEGIN ITERATIONS
-----
DO 9000 ITER=ITMIN,ITMAX
WRITE(4,808)
WRITE(6,808)
IF(ITER.GT.1) NIW=0.D0
IF(ITER.GT.1) NEW=0.D0
IF(ITER.GT.1) NEQ=0.D0
IF(ITER.GT.1) NIQ=0.D0
IF(ITER.GT.1) NED=0.D0
IF(ITER.GT.1) NID=0.D0
IF(ITER.GT.1) PHIB=0.D0
IF(ITER.GT.1) PHW=0.D0
IF(ITER.GT.1) PHQ=0.D0
IF(ITER.GT.1) DT=1.D0
IF(ITER.GT.1) CALL RTSIDE(NE,NI,TH,NEDOT)
-----
CCCCC   FLOAT WALL NE,NI B.C.
CCCCC   NE,NI TAKE ON NEAREST NEIGHBOR MINIMUM VALUES
CCCCC   OUT TO 6 COMPUTATIONAL NODES FROM THE WALL.
CCCCC   FLOAT WALL B.C. FOR ITER.GT.NBC AND ITER.LT.ITBC
-----
NBC=5
IF(ITER.LT.NBC) GO TO 90
IF(ITER.GT.ITBC) GO TO 90
DO 88 JX=2,NS
XNEW=1.D0
XNIW=1.D0

```

```

SHT03370
SHT03380
SHT03390
SHT03400
SHT03410
SHT03420
SHT03430
SHT03440
SHT03450
SHT03460
SHT03470
SHT03480
SHT03490
SHT03500
SHT03510
SHT03520
SHT03530
SHT03540
SHT03550
SHT03560
SHT03570
SHT03580
SHT03590
SHT03600
SHT03610
SHT03620
SHT03630
SHT03640
SHT03650
SHT03660
SHT03670
SHT03680
SHT03690
SHT03700
SHT03710
SHT03720
SHT03730
SHT03740
SHT03750
SHT03760
SHT03770
SHT03780
SHT03790
SHT03800
SHT03810
SHT03820
SHT03830
SHT03840

```



```

CR      DO 85 IX=1,6
CR      DO 85 INX=1,5
CR      IF(X=7-IX,IX-1,JX).GT.NE(IX,JX)) NE(IX-1,JX)=NE(IX,JX)
CR      IF(NI(IX-1,JX).GT.NI(IX,JX)) NI(IX-1,JX)=NI(IX,JX)
CR      IF(NI(IX,JX).LE.XNEW) NEM=IX
CR      IF(NI(IX,JX).LE.XNEW) XNEW=NE(IX,JX)
CR      IF(NI(IX,JX).LE.XNIW) NIM=IX
CR      IF(NI(IX,JX).LE.XNIW) XNIW=NI(IX,JX)
CR      85 CONTINUE
CR      DO 86 IX=1,NEM
CR      NE(IX,JX)=XNEW
CR      86 CONTINUE
CR      DO 87 IX=1,NIM
CR      NI(IX,JX)=XNIW
CR      88 CONTINUE
CR      90 CALL PATCH(NE,0.00,1.00)
CR      CALL PATCH(NI,0.00,1.00)
CR      SET UP COEFFICIENTS FOR MATRIX...A
CR      AND VECTOR...C
CR      M.EQ.1 POISSON EQUATION
CR      M.EQ.2 ELECTRON CONCENTRATION
CR      M.EQ.3 ION CONCENTRATION
CR      I1=3
CR      I2=NSV3-3
CR      DO 100 INC=1,111
CR      C(INC)=0.00
CR      DO 100 JNC=1,111
CR      A(INC,JNC)=0.00
CR      100 DO 5000 M=1,3
CR      I1=I1+1
CR      I2=I2+1
CR      SET UP FIRST 21 ROWS (WALL B.C.)
CR      DO 200 IR=1,12,3
CR      IF(M.NE.1) GO TO 190
CR
SHI03850
SHI03860
SHI03870
SHI03880
SHI03890
SHI03900
SHI03910
SHI03920
SHI03930
SHI03940
SHI03950
SHI03960
SHI03970
SHI03980
SHI03990
SHI04000
SHI04010
SHI04020
SHI04030
SHI04040
SHI04050
SHI04060
SHI04070
SHI04080
SHI04090
SHI04100
SHI04110
SHI04120
SHI04130
SHI04140
SHI04150
SHI04160
SHI04170
SHI04180
SHI04190
SHI04200
SHI04210
SHI04220
SHI04230
SHI04240
SHI04250
SHI04260
SHI04270
SHI04280
SHI04290
SHI04300
SHI04310
SHI04320

```

```

C      ZERO CURRENT INTO WALL  FOR M.EQ.1
C-----
DFT=DEO/DIO
XIR=DFLOAT( IR+2 )
JB=XIR/3.D0
DPHDX={-3.D0*PH(1,JB)+4.D0*PH(2,JB)-PH(3,JB)}/2.D0
DNEDX={-3.D0*NE(1,JB)+4.D0*NE(2,JB)-NE(3,JB)}/2.D0
DNIDX={-3.D0*NI(1,JB)+4.D0*NI(2,JB)-NI(3,JB)}/2.D0
DPHDX=PH(2,JB)-PH(1,JB)
DNEDX=NE(2,JB)-NE(1,JB)
DNIDX=NI(2,JB)-NI(1,JB)
IF(ITER.EQ.1) DPHDX=0.D0
IF(ITER.EQ.1) DNEDX=0.D0
IF(ITER.EQ.1) DNIDX=0.D0
A( IIR,JD )=+NE(1,JB)/TH(1,JB)*DFT+BETA*NI(1,JB)
A( IIR,JD )=+NEW/TH(1,JB)*DFT+BETA*NIW
A( IIR,J5 )=-A( IIR,JD )
A( IIR,JD+1 )=-DFT*DPHDX/TH(1,JB)-DFT
A( IIR,J5+1 )=+DFT
A( IIR,JD+2 )=-BETA*DPHDX+1.D0
A( IIR,J5+2 )=-1.D0
C( IIR )=CIRCLE+DFT*( NE(1,JB)*DPHDX/TH(1,JB)-DNEDX )
WRITE( 6,753 ) DPHDX,DNEDX,DNIDX
753  FORMAT( 3X,3(D10.4,3X) )
A( IIR,JD )=+NE(1,JB)
IF(ITER.EQ.1) A( IIR,JD )=NEW
A( IIR,J5 )=-A( IIR,JD )
A( IIR,JD+1 )=-OPHDX-TH(1,JB)
A( IIR,J5+1 )=+TH(1,JB)
C( IIR )=NE(1,JB)*DPHDX-TH(1,JB)*DNEDX
190  IF( M.EQ.1 ) A( IIR,JD )=1.D0
IF( M.EQ.2 ) C( IIR )=NEW
IF( M.EQ.3 ) C( IIR )=NIW
200  CONTINUE
C-----
C      SET UP ROWS 22 THRU NXN-22  (FIELD AND SYMMETRY)
C-----
I START=NSY3+M
I END=NXNM-3+M
IC=1
JC=1
DO 500 IR=I START,I END,3
CALL DELOP( PH,NE,NI,TH )
THETA=TH( IC,JC )

```



```

C C C
      SET UP NODAL SYMMETRY B.C.
      IS=NSY3+M
      DO 540 IR=1S,NXNM,NSY3
      A(IR,J2)=+0.00
      A(IR,J4)=+2.00
      540 CONTINUE
C C C
      SET UP INTERNODAL SYMMETRY B.C.
      IS=2*NSY3-3+M
      DO 550 IR=1S,NXNM,NSY3
      A(IR,J4)=+0.00
      A(IR,J2)=+2.00
      550 CONTINUE
C C C
      NODE CONDITIONS SET
      A(M,JD)=1.00
      IF(M.EQ.1) C(1)=PHIB
      IF(M.EQ.2) C(M)=NED
      IF(M.EQ.3) C(M)=NID
      5000 CONTINUE
C C C C C C C
      MATRIX A IS NOW COMPLETE
      COMPUTE SPECTRAL NORM OF C
      FOR CONVERGENCE TEST
      -----
      NXM2=NXN-2
      CPH=0.00
      CNE=0.00
      CNI=0.00
      DO 605 K=1, NXM2, 3
      K1=K+1
      K2=K+2
      CPH=CPH+C(K)*C(K)
      CNE=CNE+C(K1)*C(K1)
      CNI=CNI+C(K2)*C(K2)
      CER=CPH+CNE+CNI
      WRITE(6,802) ITER,CER,CPH,CNE,CNI,ADJ
      605
      NSSS=NSY3+2
C C

```

```

SHT05770
SHT05780
SHT05790
SHT05800
SHT05810
SHT05820
SHT05830
SHT05840
SHT05850
SHT05860
SHT05870
SHT05880
SHT05890
SHT05900
SHT05910
SHT05920
SHT05930
SHT05940
SHT05950
SHT05960
SHT05970
SHT05980
SHT05990
SHT06000
SHT06010
SHT06020
SHT06030
SHT06040
SHT06050
SHT06060
SHT06070
SHT06080
SHT06090
SHT06100
SHT06110
SHT06120
SHT06130
SHT06140
SHT06150
SHT06160
SHT06170
SHT06180
SHT06190
SHT06200
SHT06210
SHT06220
SHT06230
SHT06240

```

```

C      CALL LEQ1B(A,NXN,NSS,NSY3+1,NXN,C,1,NXN,O,XL,IER)
C
C-----
C      UPDATE P,NE,NI FROM VECTOR C
C-----
C      CPH=0.00
C      CNE=0.00
C      CNI=0.00
C      CER=0.00
C      DO 7000 M=1,3
C      GO TO (710,720,730),M
C      CONTINUE
C      DO 711 I=1,NC
C      K=0
C      DO 711 J=1,NSY3,3
C      K=K+1
C      JJ=J+(I-1)*NSY3
C      CPH=CPH+C(JJ)*C(JJ)
C      PH(I,K)=C(JJ)+PH(I,K)
C      GO TO 7000
C      CONTINUE
C
C      DO 721 I=1,NC
C      K=0
C      DO 721 J=1,NSY3,3
C      K=K+1
C      JJ=J+(I-1)*NSY3+1
C      CNE=CNE+C(JJ)*C(JJ)
C      NE(I,K)=C(JJ)+NE(I,K)
C      GO TO 7000
C      CONTINUE
C
C      DO 731 I=1,NC
C      K=0
C      DO 731 J=1,NSY3,3
C      K=K+1
C      JJ=J+(I-1)*NSY3+2
C      CNI=CNI+C(JJ)*C(JJ)
C      NI(I,K)=C(JJ)+NI(I,K)

```

```

SHT06250
SHT06260
SHT06270
SHT06280
SHT06290
SHT06300
SHT06310
SHT06320
SHT06330
SHT06340
SHT06350
SHT06360
SHT06370
SHT06380
SHT06390
SHT06400
SHT06410
SHT06420
SHT06430
SHT06440
SHT06450
SHT06460
SHT06470
SHT06480
SHT06490
SHT06500
SHT06510
SHT06520
SHT06530
SHT06540
SHT06550
SHT06560
SHT06570
SHT06580
SHT06590
SHT06600
SHT06610
SHT06620
SHT06630
SHT06640
SHT06650
SHT06660
SHT06670
SHT06680
SHT06690
SHT06700
SHT06710
SHT06720

```


SHT07210
SHT07220
SHT07230
SHT07240
SHT07250
SHT07260
SHT07270
SHT07280
SHT07290
SHT07300
SHT07310
SHT07320
SHT07330
SHT07340
SHT07350
SHT07360
SHT07370
SHT07380
SHT07390
SHT07400
SHT07410
SHT07420
SHT07430
SHT07440
SHT07450
SHT07460
SHT07470
SHT07480
SHT07490
SHT07500
SHT07510
SHT07520
SHT07530
SHT07540
SHT07550
SHT07560
SHT07570
SHT07580
SHT07590
SHT07600
SHT07610
SHT07620
SHT07630
SHT07640
SHT07650
SHT07660
SHT07670
SHT07680

```

9100 DO 9100 J=1,NS
      GRDX(I,J)=NE(I,J)-NI(I,J)
      CALL RTSIDE(6,GRDX,1.0D0,SPACE CHARGE DENSITY)
      CALL OUTPUT(NE,NI,TH,NEDOT)
      CALL OUTPUT(6,NEDOT,1.0D0,NEDOT DISTRIBUTION)
      EFLD=EQT*DENSO*1.0D-20
      CALL OUTPUT(6,GRAD,EFLD,ELECTRIC FIELD)
      CALL TEMP(PH,TH,ADJ)
      CALL OUTPUT(6,TH,1.0D0,REAL TEMP PROFILE (ADJ))
      CALL PATCH(TH,1.0D0,99.0D0)
      CALL JOULE(PH,NE,NI,TH,HEAT)
      CALL PATCH(HEAT,1.0D0,1.0D+10)
      DO 9120 I=1,NC
        HEAT(I,J)=DLOG10(HEAT(I,J))
      CONTINUE
      CALL OUTPUT(6,HEAT,1.0D0,LOG10 JOULE HT (W/M**3))
      WRITE(6,805)
      WRITE(6,847) ITMIN,ITMAX,ITNDI,ITEMP,ITBC,LADJ,LPUN,H,FKTR,NAME
      IF(LPUN.EQ.0) WRITE(6,848)
      IF(LPUN.GT.0) WRITE(6,849)

9120 CC
      IF(LPUN.EQ.0) GO TO 9300
      WRITE(7,800) ITMIN,ITMAX,ITNDI,ITEMP,ITBC,LADJ,LPUN,H,FKTR,NAME
      CALL OUTPUT(7,PH,UPH,VOLTAGE POTENTIAL)
      CALL OUTPUT(7,NE,1.0D0,ELECTRON DENSITY)
      CALL OUTPUT(7,NI,1.0D0,ION DENSITY)
      CALL TEMP(PH,TH,ADJ)
      CALL PATCH(TH,1.0D0,99.0D0)
      CALL OUTPUT(7,TH,1.0D0,TEMP DIST (TRUNCATED))
      DO 9200 I=1,NC
        GRDX(I,J)=NE(I,J)-NI(I,J)
        CALL RTSIDE(TH,1.0D0,99.0D0)
        CALL OUTPUT(7,GRDX,1.0D0,SPACE CHARGE DENSITY)
        CALL PATCH(NE,NI,TH,NEDOT)
        CALL OUTPUT(7,NEDOT,1.0D0,NEDOT DISTRIBUTION)
        CALL GRDT(PH,GRDX,GRDY,GRAD)
        DO 9210 I=1,NC
          GRAD(I,J)=DLOG10(GRAD(I,J)*EFLD)
        CONTINUE
        CALL OUTPUT(7,GRAD,1.0D0,LOG10 E-FIELD (V/M))
        CALL OUTPUT(7,HEAT,1.0D0,LOG10 JOULE HT (W/M**3))
      CONTINUE

```


[illegible]

```

CCCCCCCCCCCCCCCCCCCCCCCCCCCCCCCCCCCCCCCCCCCCCCCCCCCCCCCCCCCC
SUBROUTINE DELOP
REDIMENSIONED
DELO0010
DELO0020
DELO0030
DELO0040
DELO0050
DELO0060
DELO0070
DELO0080
DELO0090
DELO0100
DELO0110
DELO0120
DELO0130
DELO0140
DELO0150
DELO0160
DELO0170
DELO0180
DELO0190
DELO0200
DELO0210
DELO0220
DELO0230
DELO0240
DELO0250
DELO0260
DELO0270
DELO0280
DELO0290
DELO0300
DELO0310
DELO0320
DELO0330
DELO0340
DELO0350
DELO0360
DELO0370
DELO0380
DELO0390
DELO0400
DELO0410
DELO0420
DELO0430
DELO0440
DELO0450
DELO0460
DELO0470
DELO0480

CCCCCCCCCCCCCCCCCCCCCCCCCCCCCCCCCCCCCCCCCCCCCCCCCCCCCCCCCCCC
SUBROUTINE DELOP(PH,NE,NI,TH)
IMPLICIT REAL*8 (A-H,O-S)
REAL*8 PH(NCOLS,1),NE(NCOLS,1),NI(NCOLS,1),TH(NCOLS,1)
COMMON /IPARM/ NCOLS, NSYM, ITER
COMMON /DIVER/ DPHDX, DPHDY, DNEDX, DNEDY, DNIDX, DNIDY, DTHDX, DTHDY
COMMON /DPARM/ M, IC, JC, ICM, ICP, JCM, JCP
REAL*8 NE, NI, NEDOT
DPHDX=0.00
DPHDY=0.00
DNEDX=0.00
DNEDY=0.00
DNIDX=0.00
DNIDY=0.00
DTHDX=0.00
DTHDY=0.00
ICP=IC+1
ICM=IC-1
JCP=JC+1
JCM=JC-1
IF(JC.EQ.1) JCM=JCP
IF(JC.EQ.NSYM) JCP=JCM
IF(JC.EQ.1) GO TO 310
IF(JC.EQ.NSYM) GO TO 320
OPHDX=PH(ICP,JC)-PH(ICM,JC)
DNEDX=NE(ICP,JC)-NE(ICM,JC)
DNIDX=NI(ICP,JC)-NI(ICM,JC)

```

00490
 DEL000500
 DEL000510
 DEL000520
 DEL000530
 DEL000540
 DEL000550
 DEL000560
 DEL000570
 DEL000580
 DEL000590
 DEL000600
 DEL000610
 DEL000620
 DEL000630
 DEL000640
 DEL000650
 DEL000660
 DEL000670
 DEL000680
 DEL000690
 DEL000700
 DEL000710
 DEL000720
 DEL000730
 DEL000740
 DEL000750
 DEL000760
 DEL000770
 DEL000780

```

    PHDY=PH(IC,JCP)-PH(IC,JCM)
    DNEDY=NE(IC,JCP)-NE(IC,JCM)
    DNIDY=NI(IC,JCP)-NI(IC,JCM)
    DTHDX=TH(IC,JCP)-TH(IC,JCM)
    GO TO 350
310  IC=IC+1
    ICP=IC-1
    ICM=IC-1
    OPHDX=PH(ICP,1)-PH(ICM,1)
    DNEDX=NE(ICP,1)-NE(ICM,1)
    DNIDX=NI(ICP,1)-NI(ICM,1)
    DTHDX=TH(ICP,1)-TH(ICM,1)
    GO TO 350
320  CONTINUE
    OPHDX=PH(ICP,NSYM)-PH(ICM,NSYM)
    DNEDX=NE(ICP,NSYM)-NE(ICM,NSYM)
    DNIDX=NI(ICP,NSYM)-NI(ICM,NSYM)
    DTHDX=TH(ICP,NSYM)-TH(ICM,NSYM)
    CONTINUE
350  OPHDX=OPHDX/2.00
    DNEDX=DNEDX/2.00
    DNIDX=DNIDX/2.00
    DTHDX=DTHDX/2.00
    PHDY=PHDY/2.00
    DNEDY=DNEDY/2.00
    DNIDY=DNIDY/2.00
    DTHDY=DTHDY/2.00
    RETURN
    END
  
```

GRD000010
GRD000020
GRD000030
GRD000040
GRD000050
GRD000060
GRD000070
GRD000080
GRD000090
GRD000100
GRD000110
GRD000120
GRD000130
GRD000140
GRD000150
GRD000160
GRD000170
GRD000180
GRD000190
GRD000200
GRD000210
GRD000220
GRD000230
GRD000240
GRD000250
GRD000260
GRD000270
GRD000280
GRD000290
GRD000300
GRD000310
GRD000320
GRD000330
GRD000340
GRD000350
GRD000360
GRD000370
GRD000380
GRD000390
GRD000400
GRD000410
GRD000420
GRD000430
GRD000440
GRD000450
GRD000460
GRD000470
GRD000480

```

CCCCCCCCCCCCCCCCCCCCCCCCCCCCCCCCCCCCCCCCCCCCCCCCCCCCCCCCCCCC
SUBROUTINE GRDNT
  COMPUTES THE GRADIENT OF THE INPUTED FIELD
  VALUE IN BOTH COORDS AND THE SCALAR

CCCCCCCCCCCCCCCCCCCCCCCCCCCCCCCCCCCCCCCCCCCCCCCCCCCCCCCCCCCC
SUBROUTINE GRDNT(PH,GX,GY,GRAD)
  IMPLICIT REAL*8 (A-H,O-S)
  REAL*8 PH(NC,1),GRAD(NC,1),GX(NC,1),GY(NC,1)
  COMMON /IPARM/ NC,NS,ITER
  NCM1=NC-1
  NCM2=NC-2
  DO 900 J=1,NS
    JP=J+1
    JM=J-1
    GX(1,J)={-3.DO*PH(1,J)+4.DO*PH(2,J)-PH(3,J)}/2.DO
    IF(J.EQ.1) JM=JP
    IF(J.EQ.NS) JP=JM
    GY(1,J)={PH(1,JP)-PH(1,JM)}/2.DO
  CONTINUE
  DO 910 J=1,NS
    JP=J+1
    JM=J-1
    GX(NC,J)={-3.DO*PH(NC,J)+4.DO*PH(NCM1,J)-PH(NCM2,J)}/2.DO
    IF(J.EQ.1) JM=JP
    IF(J.EQ.NS) JP=JM
    GY(NC,J)={PH(NC,JP)-PH(NC,JM)}/2.DO
  CONTINUE
  DO 920 I=1,NS
    IP=I+1
    IM=I-1
    JM=J-1
    JP=J+1
    IF(J.EQ.1) JM=JP
    IF(J.EQ.NS) JP=JM
    GX(I,J)={PH(IP,J)-PH(IM,J)}/2.DO
    GY(I,J)={PH(IP,JP)-PH(IP,JM)}/2.DO
  
```

GRD00490
GRD00500
GRD00510
GRD00520
GRD00530
GRD00540

920 CONTINUE
DO 950 I=1,NC
DO 950 J=1,N3
950 GRAD(I,J)=GX(I,J)*GX(I,J)+GY(I,J)*GY(I,J)**.5D0
RETURN
END


```

CCCCCCCCCCCCCCCCCCCCCCCCCCCCCCCCCCCCCCCCCCCCCCCCCCCCCCCCCCCC
SUBROUTINE RTSIDE
      USED TO CALCULATE THE NEDOT TERM OVER THE FIELD
      2 BODY (HEAVY)
      3 BODY (ELECT)..HIN & HIRSCH
CCCCCCCCCCCCCCCCCCCCCCCCCCCCCCCCCCCCCCCCCCCCCCCCCCCCCCCCCCCC
SUBROUTINE RTSIDE(NE,NI,TH,NEDOT)
      IMPLICIT REAL*8 (A-H,O-Z)
      REAL*8 NE(NCOLS,1),NI(NCOLS,1),TH(NCOLS,1),NEDOT(NCOLS,1)
      COMMON /IPARM/ NCOLS,NSYM,ITER
      COMMON /IONIZ/ RECON,A1,A2,A3,I
      DO 10 J=1,NSYM
      DO 10 I=1,NCOLS
      10 NEDOT(I,J)=NE(I,J)*(1.00-NI(I,J))*RECCM
      +2*(TH(I,J)*T)**(-4.50)*(1.00-NE(I,J))*NI(I,J)*NE(I,J)
      RETURN
      END

```

```

RTS00010
RTS00020
RTS00030
RTS00040
RTS00050
RTS00060
RTS00070
RTS00080
RTS00090
RTS00100
RTS00110
RTS00120
RTS00130
RTS00140
RTS00150
RTS00160
RTS00170
RTS00180
RTS00190
RTS00200
RTS00210
RTS00220
RTS00230
RTS00240
RTS00250
RTS00260
RTS00270

```


133


```

150 DEL=-.01D0
CONTINUE
NED=NED+DEL
DZEDX=NE(2,1)-NED
DZEDY=NE(1,2)-NED
JNSAV=JCALC
JX=.5D0*(-NED*DPHDX/TH(1,1)+DZEDX)
JY=-NED*DPHDY/TH(1,1)+DZEDY
JCALC=(JX+JY)**.5D0
IF(JCALC.GT.JEQUI.AND.JCALC.LE.JNSAV) GO TO 150
IF(JCALC.LE.JEQUI.AND.JCALC.GE.JNSAV) GO TO 150
DEL=-DEL*.1D0
IF(DABS(DEL).GE..0001D0) GO TO 150
JNODE=JNODE+CJ*DEQ
JEQUI=JEQUI+CJ*DEQ
RETURN
END

```

```

AN000490
AN000500
AN000510
AN000520
AN000530
AN000540
AN000550
AN000560
AN000570
AN000580
AN000590
AN000600
AN000610
AN000620
AN000630
AN000640
AN000650

```



```

CCCCCCCCCCCCCCCCCCCCCCCCCCCCCCCCCCCCCCCCCCCCCCCCCCCCCCCC
SUBROUTINE OUTPUT
OUTPUTS TO THE DESIGNATED DEVICE..IOD
THE Q-ARRAY PASSED AND LABELED
WITH THE LIST PASSED IN THE ARGUMENTS.
CCCCCCCCCCCCCCCCCCCCCCCCCCCCCCCCCCCCCCCCCCCCCCCCCCCCCCCC

```

138

[illegible]

```

EXTERNAL PLOT,PLT3D1,PATCH
REAL*8 T1(1,12),X(25),Y(19),F(2),SZ(2)
REAL*4 DD(25,19),WK(25,19,3)
INTEGER*4 KX(1400),KY(400)
INTEGER*4 KON(8)
DATA KON/8*1/
LOGICAL*1 IDN(25,19)
COMMON /IPARM/ NC,NS
NC=25
XNC=FLOAT(NC)
NS=7
LAST=8
DO 8 I=1,NC
  X(I)=FLOAT(I)/XNC
  NOFOLD=2
  JM=NS*NOFOLD-NOFOLD+1
  DO 9 J=1,JM
    Y(J)=FLOAT(J)/XNC
  READ(5,802)(KONT(I),I=1,8)

```

```

      READ(5,800) (TTL(KINK),KINK=7,12)
      DO 1000 KORK=1, LAST
      READ(5,800) (TTL(KINK),KINK=1,6)
      DO 10 I=1,NC
      IK=1
      IF(KORK.EQ.2.OR.KORK.EQ.3) IK=NC-I+1
      READ(5,801) (O(IK,J),J=1,NS)
      IF(KORK.EQ.4) CALL PATCH(D,I,99.)
      IF(KONT(KORK).GT.0) WRITE(6,806)
      IF(KONT(KORK).LE.0) WRITE(6,807)
      WRITE(6,808) (TTL(KINK),KINK=1,6), (NORK,NORK=1,NS)
      IF(KONT(KORK).LE.0) GO TO 1000
      XMAX=0.0
      DO 11 I=1,NC
      DO 11 J=1,NS
      IF(XMAX.LE.D(I,J)) XMAX=D(I,J)
      11 CONTINUE
      DO 12 I=1,NC
      DO 12 J=1,NS
      O(I,J)=O(I,J)/XMAX
      DD(I,J+6)=D(I,J)
      DD(I,8-J)=D(I,J)
      DD(I,20-J)=D(I,J)
      12 CONTINUE
      DO 20 I=1,NC
      WRITE(6,809) I,(D(I,J),J=1,NS)
      20 CONTINUE
      *****
      * BETA ROTATES FIRST ABOUT Z AXIS
      * ALPHA ROTATES SECOND AROUND Y AXIS
      *****
      BEIA=30.
      ALPHA=30.
      F(1)=1.E+06
      F(2)=F(1)
      SZ(1)=2
      SZ(2)=SZ(1)
      NK=400
      LNS=2
      CALL PLT3D1(X,NC,Y,JM,DD,ALPHA,BETA,F,TTL,SZ,WK,IDN,KX,KY,NK,LNS)
      CONTINUE
      1000 FORMAT(6A8)
      800 FORMAT(3X,7(1X,E10.4))
      801 FORMAT(8I1)
      802 FORMAT(1I1)
      806 FORMAT(1I1)
      807 FORMAT(.1)
      *** PLOTTED *** (/)
      *** NOT PLOTTED *** (/)

```

```

PIC00970
PIC00980
PIC00990
PIC01000
PIC01010
PIC01020
PIC01030
PIC01040
PIC01050
PIC01060
PIC01070
PIC01080
PIC01090
PIC01100
PIC01110
PIC01120
PIC01130

```

```

808 FORMAT('0',6A8,'.',7(9X,'( ',12,' ')),/)
809 FORMAT(' ',12,'.',7(3X,E10.4))
STOP 1
END

```

CC

```

SUBROUTINE PATCH(Q,XL,XU)
REAL*4 Q(NC,1),XU,XL
COMMON /IPARM/ NC,NS
DO 100 I=1,NC
  IF(Q(I,J).GT.XU) Q(I,J)=XU
  IF(Q(I,J).LT.XL) Q(I,J)=XL
100 CONTINUE
RETURN
END

```

STR00010
STR00020
STR00030
STR00040
STR00050
STR00060
STR00070
STR00080
STR00090
STR00100
STR00110
STR00120
STR00130
STR00140
STR00150
STR00160
STR00170
STR00180
STR00190
STR00200
STR00210
STR00220
STR00230
STR00240
STR00250
STR00260
STR00270
STR00280
STR00290
STR00300
STR00310
STR00320
STR00330
STR00340
STR00350
STR00360
STR00370
STR00380
STR00390
STR00400
STR00410
STR00420
STR00430
STR00440
STR00450
STR00460
STR00470
STR00480

* CURRENT STREAM PROFILE *

MAY 1981

PROGRAM TO GENERATE CURRENT STREAMLINES ON THE VERSATEC PLOTTER
FROM TWO DATA ARRAYS, WHICH CONTAIN THE X,Y MAGNITUDE COMPONENTS.

A VECTOR FIELD IS GENERATED AND USING A 'NEAREST NEIGHBOR'
PRINCIPLE (4 NEIGHBORS), A LOCAL DIRECTION IS DETERMINED,
WHICH IS SUCCESSIVELY USED TO 'MARCH OUT' A STREAMLINE.

INPUT: CONSISTS OF THE FIRST TWO SECTIONS OF PUNCHED OUTPUT
FROM PROGRAM 'SHTH'.

OUTPUT: PRINTOUT OF INPUTED ARRAYS.
MARCHING PATH OF A STREAMLINE
ONE VERSATEC PLOT.

REAL*4 JX(25,7),JY(25,7),DUMMY(20),X(25),Y(7),XP(300),YP(300)
REAL*4 VX(25,7),VY(25,7),XS(6),YS(6)
INTEGER INT(6)
COMMON /SET/ VX,VY,X,Y
UNITS=.40
NC=25
NS=7
READ(5,800) INT,H,(DUMMY(JKL),JKL=1,12)
WRITE(6,810) INT,H,(DUMMY(JKL),JKL=1,12)
DOV=H*7.43273E-03*35.**.5
READ(5,801) DUMMY
WRITE(6,801) DUMMY

SET UP STREAM STARTING COORDINATES

NSM1=NS-1
DO 8 J=1,NSM1
XS(J)=FLOAT(J-1)*.5
XS(J)=FLOAT(NC-1)*.5
DO 10 I=1,NC
READ(5,802) (JX(I,J),J=1,NS)
WRITE(6,802) (JX(I,J),J=1,NS)

8

CCCCCCCCCCCCCCCCCCCCCCCCCCCCCCCC

CC

STR00490
STR00500
STR00510
STR00520
STR00530
STR00540
STR00550
STR00560
STR00570
STR00580
STR00590
STR00600
STR00610
STR00620
STR00630
STR00640
STR00650
STR00660
STR00670
STR00680
STR00690
STR00700
STR00710
STR00720
STR00730
STR00740
STR00750
STR00760
STR00770
STR00780
STR00790
STR00800
STR00810
STR00820
STR00830
STR00840
STR00850
STR00860
STR00870
STR00880
STR00890
STR00900
STR00910
STR00920
STR00930
STR00940
STR00950
STR00960

```

10  CONTINUE
    READ(5,801) DUMMY
    WRITE(6,801) DUMMY
    DO 12 I=1,NC
12  READ(5,802) (JY(I,J),J=1,NS)
    WRITE(6,802) (JY(I,J),J=1,NS)
    CONTINUE
        COMPUTE VX AND VY
        DO 14 I=1,NC
        DO 14 J=1,NS
        HYP=(JX(I,J)*JX(I,J)+JY(I,J)*JY(I,J))**.5
        VX(I,J)=JX(I,J)/HYP
        VY(I,J)=JY(I,J)/HYP
        SETMSG AND FACTOR PLOT SIZE
        CALL SETMSG(2)
        CALL PLOTS(0,0,0)
        CALL FACTOR(UNIT)
        DRAW AXIS
        XOR=5.0
        YOR=10.0
        CALL NEWPEN(+4)
        CALL PLOT(XOR,YOR,+3)
        X1=XOR+12
        CALL PLOT(X1,YOR,+2)
        Y1=YOR+6.
        Y2=YOR-6.
        CALL PLOT(XOR,Y1,+3)
        CALL PLOT(XOR,Y2,+2)
        CALL PLOT(XOR,YOR,+3)
        COMPUTE NODE POSITIONS
        DO 20 I=1,NC
        X(I)=FLOAT(I-1)
20  DO 22 J=1,NS
        Y(J)=FLOAT(J-1)
        NEWPEN SETS LINE HEAVINESS (THICKNESS)
        CALL NEWPEN(+2)
        CALCULATE AND PLOT STREAM FUNCTION

```

```

C C C C
+ STEP ... FORWARD PROGRESSION (WITH DERIVATIVES)
- STEP ... BACKWARD PROGRESSION (AGAINST DERIVATIVES)

TOLER=.03
STEP=+.10
NEWT=NS-2
DO 500 J JNK=1,NEWT
  XLOC=XS(JJNK)
  YLOC=YS(JJNK)
  XPOS=XOR+XLOC
  YPOS=YOR+YLOC
  CALL PLOT(XPOS,YPOS,+3)
  IJK=0
400 CONTINUE
  IJK=IJK+1
  XP(IJK)=XLOC
  YP(IJK)=YLOC
  IF (JJK.EQ.1) WRITE(6,807) IJK,XLOC,YLOC

C C C
TEST FOR BOUNDARY
IF (XLOC.LT.X(1).OR.XLOC.GT.X(NC)) GO TO 450
IF (YLOC.LT.Y(1).OR.YLOC.GT.Y(NS)) GO TO 450
CALL MARCH(STEP,XLOC,YLOC,XNEW,YNEW,TOLER)
XPOS=XOR+XNEW
YPOS=YOR+YNEW
CALL PLOT(XPOS,YPOS,+2)
XLOC=XNEW
YLOC=YNEW
GO TO 400
CONTINUE

C C C
DRAW IMAGE STREAM LINE

XPOS=XOR+XP(1)
YPOS=YOR-YP(1)
CALL PLOT(XPOS,YPOS,+3)
DO 460 I=1,IJK
  XPOS=XOR+XP(I)
  YPOS=YOR-YP(I)
  CALL PLOT(XPOS,YPOS,+2)
CONTINUE
460 CONTINUE
CALL PLOT(0.,0.,+999)
800 FORMAT(6(I2,1X),F5-2,12A4)
810 FORMAT(16(I2,1X),F5-2,12A4,/)
801 FORMAT(20A4)

STR00970
STR00980
STR00990
STR01000
STR01010
STR01020
STR01030
STR01040
STR01050
STR01060
STR01070
STR01080
STR01090
STR01100
STR01110
STR01120
STR01130
STR01140
STR01150
STR01160
STR01170
STR01180
STR01190
STR01200
STR01210
STR01220
STR01230
STR01240
STR01250
STR01260
STR01270
STR01280
STR01290
STR01300
STR01310
STR01320
STR01330
STR01340
STR01350
STR01360
STR01370
STR01380
STR01390
STR01400
STR01410
STR01420
STR01430
STR01440

```


STR01930
STR01940
STR01950
STR01960
STR01970
STR01980
STR01990
STR02000
STR02010
STR02020
STR02030
STR02040
STR02050
STR02060
STR02070
STR02080
STR02090
STR02100
STR02110
STR02120
STR02130
STR02140
STR02150
STR02160
STR02170
STR02180
STR02190
STR02200
STR02210
STR02220
STR02230
STR02240
STR02250
STR02260
STR02270
STR02280
STR02290
STR02300
STR02310
STR02320
STR02330
STR02340
STR02350
STR02360
STR02370
STR02380
STR02390
STR02400

```

NC=25
IM=AIN(XLOC)+1
JM=AIN(X(YLOC)+1)
IF(ABS(X(IM)-XLOC).LT.TOLER) LOGIC(1)=.TRUE.
IF(ABS(X(JM)-YLOC).LT.TOLER) LOGIC(2)=.TRUE.
IF(ABS(Y(JM)-YLOC).LT.TOLER) LOGIC(3)=.TRUE.
IF(ABS(Y(IM)-YLOC).LT.TOLER) LOGIC(4)=.TRUE.
IF(LOGIC(1).AND.LOGIC(2)) GO TO 350
IF(LOGIC(2).AND.LOGIC(3)) GO TO 360
IF(LOGIC(3).AND.LOGIC(4)) GO TO 370
IF(LOGIC(4).AND.LOGIC(1)) GO TO 380

C
IP=IM+1
JP=JM+1
IF(LOGIC(1)) GO TO 310
IF(LOGIC(2)) GO TO 320
IF(LOGIC(3)) GO TO 330
IF(LOGIC(4)) GO TO 340

C
CONTINUE
CX 300 WRITE(6,730)
730 FORMAT(1,300.1)
IP=IM+1
JP=JM+1
D1=DIST(IM,JM,XLOC,YLOC)
D2=DIST(IP,JM,XLOC,YLOC)
D3=DIST(IP,JP,XLOC,YLOC)
D4=DIST(IM,JP,XLOC,YLOC)
DFX=VX(IM,JM)/D1+VX(IP,JM)/D2+VX(IP,JP)/D3+VX(IM,JP)/D4
DFY=VY(IM,JM)/D1+VY(IP,JM)/D2+VY(IP,JP)/D3+VY(IM,JP)/D4
GO TO 400

310 IP=IM
CX 731 WRITE(6,731)
731 FORMAT(1,310.1)
GO TO 303

320 JP=JM
CX 732 WRITE(6,732)
732 FORMAT(1,320.1)
GO TO 303

330 IM=IP
CX 733 WRITE(6,733)
733 FORMAT(1,330.1)
GO TO 303

340 JM=JP
CX 734 WRITE(6,734)
734 FORMAT(1,340.1)
GO TO 303

350 DFX=VX(IM,JM)

```



```
CX      WRITE(6,735)
   735  FORMAT(' ',350')
        DFY=VY(IM,JM)
        GO TO 400
   360  DFX=VX(IP,JM)
        DFY=VY(IP,JM)
        WRITE(6,736)
   CX    736  FORMAT(' ',360')
        GO TO 400
   370  DFX=VX(IP,JP)
        DFY=VY(IP,JP)
        WRITE(6,737)
   CX    737  FORMAT(' ',370')
        GO TO 400
   380  DFX=VX(IM,JP)
        DFY=VY(IM,JP)
        WRITE(6,738)
   CX    738  FORMAT(' ',380')
C
C
C          NORMALIZE DIRECTIONAL DERIVATIVES
   400  CONTINUE
        DER=(DFX*DFX+DFY*DFY)**.5
        DFX=DFX/DER
        DFY=DFY/DER
   CX    700  WRITE(6,700) IM,JM,IP,JP,DFX,DFY
       700 $  FORMAT(' ',IM='.',I2,' ',JM='.',I2,' ',IP='.',I2,' ',JP='.',I2,' ',
                ' DFX=',E10.4,' ',DFY=',E10.4')
        XNEW=XLOC+STEP*DFX
        YNEW=YLOC+STEP*DFY
        RETURN
END

*****
*
*          FUNCTION DIST
*
*****
*****
COMMON /SET/ VX(25,7),VY(25,7),X(25),Y(7)
D1=X(I)-XL
D2=Y(J)-YL
DIST=(D1*D1+D2*D2)**.5
RETURN
END
```

01 10 03 10 01 01 00.50 01.00 F414A
 PHD 10.00 00.00 00.00
 MED 00.30 01.00 01.00
 NID 00.00 00.00 01.00
 00 00 00 00 00 00.00 00.00 STOP

153

LIST OF REFERENCES

1. Chung, P.M., Talbot, L., and Touryan, K.J., Electric Probes in Stationary And Flowing Plasmas, Springer-Verlag, 1975.
2. Schuöcker, D., "Improved Model For Anode Spot Formation in Vacuum Arcs," IEEE Transactions in Plasma Science, PS-7, p. 209, 1979.
3. Biblarz, O., Dolson, R.L., and Shorb, A.M., "Anode Phenomena in a Collision Dominated Plasma", Journal of Applied Physics, vol 46, p. 3342, 1975.
4. Davydov, D. and Zmanovskaja, L. Zh. Tekh. Fiz., vol. 3, p. 715, 1936.
5. Schulz, G.J. and Brown, S.C., "Microwave Study of Positive Ion Collection by Probes," Physical Review, vol. 98, p. 1642, 15 June 1955.
6. Cohen, I.M., "Asymptotic Theory of Spherical Electrostatic Probes in a Slightly Ionized, Collision-Dominated Gas," The Physics of Fluids, vol. 6, no. 10, p. 1492, 1963.
7. Su, C.H. and Lam, S.H., "Continuum Theory of Spherical Probes," The Physics of Fluids, vol. 6, no. 10, p. 1479, 1968.
8. Radbill, J.R., "Computation of Electrostatic Probe Characteristics," American Institute of Aeronautics and Astronautics, vol. 4, p. 1195, 1966.
9. Sutton, G.W. and Sherman, A., Engineering Magnetohydrodynamics, p. 168, McGraw-Hill, 1965.
10. Delcroix, J.L., Introduction to the Theory of Ionized Gases, p. 39, Interscience, 1960.
11. Barad, M.S. and Cohen, I.M., "Continuum Theory of Spherical Electrostatic Probes in a Stationary, Moderately Ionized Plasma," The Physics of Fluids, vol. 4, p. 724, 4 April 1974.
12. Dolson, R.C., A Computer Analysis for the Determination of Electrode Voltage Losses in Magnetohydrodynamic Generator Plasmas, Ph.D. Thesis, Naval Postgraduate School, Monterey, California, December 1975.
...see also...
Dolson, R.C. and Biblarz, O., "Analysis of the Voltage Drop Arising From a Collision Dominated Sheath," Journal of Applied Physics, vol. 47, p. 5280, 1976.

13. Argyropoulos, G.S., and others, "Results of Numerical Modeling of Some Recent MHD Generator Channel Designs," paper presented at the Thirteenth Symposium on Engineering Aspects of MHD, Stanford, March 1973.
14. Air Force Wright Aeronautical Laboratories Report TR-74-47, Experimental and Analytical Research on a Two Megawatt, High Performance MHD Generator, by O.K. Sonju and J. Reno, pp. 61-94, June 1974.
15. Air Force Wright Aeronautical Laboratories Report TR-80-2088, Electrode Boundary Layers in Dense Diffuse Plasmas, by J. Biblarz, R.E. Ball and S.T. Van Brocklin, October 1980.
16. Feldman, L.A., A Numerical Schema for Predicting Transient Shock, and Magnetohydrodynamic Phenomena, Ph.D. Thesis, Auburn University, Auburn Alabama, 6 June 1978.
17. Persson, K.B., "Inertia-Controlled Ambipolar Diffusion," The Physics of Fluids, vol 5, number 21, pp. 1625-1632, December 1962.
18. Brown, S.C. Basic Data of Plasma Physics, chap. 3, Wiley, 1959.
19. Engelhardt, A.G., Phelps, A.V., and Risk, C.G., "Determination of Momentum Transfer and Inelastic Collision Cross Sections for Electrons in Nitrogen Using Transport Coefficients," Physical Review vol 135, number 6A, p. A1566, 14 September 1964.
20. Air Force Wright Laboratories Report TR-74-216, Carbon Dioxide Electric Discharge Laser Kinetics Handbook, by Douglas-Hamilton, D.H., and Lowder, R.S., 1975.
21. Chatterton, P.A., Vacuum Breakdown, Electrical Breakdown of Gases, Eds. J.M. Meek and J.D. Craggs, Wiley-Interscience, p. 143, 1978.
22. Mitchner, M. and Kruger, C.H., Partially Ionized Gases, Wiley-Interscience, 1973.
23. Hinnov, E. and Hirschberg, J.G., "Electron-Ion Recombination in Dense Plasmas," Physical Review vol. 125, pp. 795-801, 1 February 1962.
24. Gurevich, A.V., and Pitaenskii, L.P., "Recombination Coefficients in a Dense Low-Temperature Plasma," Soviet Physics JETP, vol. 19, p. 870, 1964.
25. Ketter, R.L. and Prawel, S.P.Jr., Modern Methods of Engineering Computation, McGraw-Hill, 1969.

26. Kelly, L.G., Handbook of Numerical Methods and Applications, Addison-Wesley, 1967
27. Sandia Laboratories Report SC-RR-72 0827, "Continuum Electrostatic Probes in the Presence of Negative Ions. Numerical Computation," by B.B. Bailey, and K.T. Touryan, December 1972.

INITIAL DISTRIBUTION LIST

	COPIES
1. Defense Technical Information Center Cameron Station Alexandria, Virginia 22314	2
2. Library Code 0142 Naval Postgraduate School Monterey, California 93940	2
3. Office of Research Administration Code 012A Naval Postgraduate School Monterey, California 93940	2
4. Chairman Department of Aeronautics Code 67 Naval Postgraduate School Monterey, California 93940	2
5. Professor J. Biblarz Department of Aeronautics Code 67Bi Naval Postgraduate School Monterey, California 93940	6
6. Chairman Department of Physics and Chemistry Code 61 Naval Postgraduate School Monterey, California 93940	1
7. LCDR S.T. Van Brocklin Department of Aeronautics c/o Code 67Bi Naval Postgraduate School Monterey, California 93940	5
8. LCDR J. Wainionpaa Department of Aeronautics c/o Code 67Bi Naval Postgraduate School Monterey, California 93940	1
9. LCDR Jon Barto Department of Aeronautics c/o Code 67Bi Naval Postgraduate School Monterey, California 93940	1
10. Professor A. W. Cooper Department of Physics and Chemistry Code 61Cr Naval Postgraduate School Monterey, California 93940	1
11. Professor F. R. Schwirzke Department of Physics and Chemistry Code 61Sw Naval Postgraduate School Monterey, California 93940	2

12. Professor R. E. Ball 1
 Department of Aeronautics
 Code 67Bp
 Naval Postgraduate School
 Monterey, California 93940
13. Professor A. E. Fuhs 1
 Department of Aeronautics
 Code 67Fu
 Naval Postgraduate School
 Monterey, California 93940
14. Professor F. D. Faulkner 1
 Department of Mathematics
 Code 53Fa
 Naval Postgraduate School
 Monterey, California 93940
15. Commander 1
 Naval Air Systems Command
 Department of the Navy
 ATTN: Dr. H.R. Rosenwasser, Code AIR 310C
 Washington, D.C. 20360
16. Dr. John A. Satkowski 1
 Office of Naval Research
 Power Program, Code 473
 Washington, D.C. 20360
17. Dr. William L. Nigham 1
 United Aircraft Research Laboratory
 East Hartford, Connecticut 06108
18. Dr. B.N. Srivastava 1
 AVCO Everett Research Laboratory
 2385 Revere Beach Parkway
 Everett, Massachusetts 02149
19. Dr. J. Schwartz 1
 TRW Systems
 Redondo Beach, California 90276
20. Dr. Alan Garscadden 2
 AFAPL/POD
 Bldg. 450/ Room D101
 Wright-Patterson AFB, Ohio 45433
21. Dr. J. Stricker 1
 Department of Aeronautics
 Technion, Haifa 32000
 ISRAEL
22. Dr. Y.L. Khait 1
 Department of Physics
 Ben Gurion University
 P.O. Box 653
 Beer Sheva 84120
 ISRAEL
23. Dr. Robert R. Mitchell 1
 Westinghouse R&D Center
 1370 Beulah Road
 Pittsburgh, Pennsylvania 15235
24. Dr. Richard J. Rosa 1
 Montana State University
 Bozeman, Montana 59707

25. Professor H. W. Liepmann 1
Division of Engineering and
Applied Science
California Institute of Technology
Pasadena, California 91125
26. Capt. T. A. Filcoff 1
AFWL-AREP
Kirtland Air Force Base
Albuquerque, New Mexico 87117

**DAT
FILM**